



uOttawa

L'Université canadienne
Canada's university

**FACULTÉ DES ÉTUDES SUPÉRIEURES
ET POSTDOCTORALES**



uOttawa

L'Université canadienne
Canada's university

**FACULTY OF GRADUATE AND
POSTDOCTORAL STUDIES**

Véronique Millette

AUTEUR DE LA THÈSE / AUTHOR OF THESIS

M.A.Sc. (Biomedical Engineering)

GRADE / DEGREE

School of Information Technology and Engineering

FACULTÉ, ÉCOLE, DÉPARTEMENT / FACULTY, SCHOOL, DEPARTMENT

Signal Processing of Heart Signals for the Quantification of Non-Deterministic Events

TITRE DE LA THÈSE / TITLE OF THESIS

Michel Labrosse

DIRECTEUR (DIRECTRICE) DE LA THÈSE / THESIS SUPERVISOR

Natalie Baddour

CO-DIRECTEUR (CO-DIRECTRICE) DE LA THÈSE / THESIS CO-SUPERVISOR

Hilmi Dajani

Richar Dansereau

Gary W. Slater

Le Doyen de la Faculté des études supérieures et postdoctorales / Dean of the Faculty of Graduate and Postdoctoral Studies

SIGNAL PROCESSING OF HEART SIGNALS FOR THE QUANTIFICATION OF NON- DETERMINISTIC EVENTS

Véronique Millette

A thesis submitted to the Faculty of Graduate and Postdoctoral Studies
in partial fulfillment of the requirements for the degree of

MASTER OF APPLIED SCIENCE

in Biomedical Engineering

Ottawa-Carleton Institute for Biomedical Engineering
University of Ottawa
Ottawa, Canada

December 2009

©2009 Véronique Millette



Library and Archives
Canada

Published Heritage
Branch

395 Wellington Street
Ottawa ON K1A 0N4
Canada

Bibliothèque et
Archives Canada

Direction du
Patrimoine de l'édition

395, rue Wellington
Ottawa ON K1A 0N4
Canada

Your file *Votre référence*
ISBN: 978-0-494-66226-7
Our file *Notre référence*
ISBN: 978-0-494-66226-7

NOTICE:

The author has granted a non-exclusive license allowing Library and Archives Canada to reproduce, publish, archive, preserve, conserve, communicate to the public by telecommunication or on the Internet, loan, distribute and sell theses worldwide, for commercial or non-commercial purposes, in microform, paper, electronic and/or any other formats.

The author retains copyright ownership and moral rights in this thesis. Neither the thesis nor substantial extracts from it may be printed or otherwise reproduced without the author's permission.

In compliance with the Canadian Privacy Act some supporting forms may have been removed from this thesis.

While these forms may be included in the document page count, their removal does not represent any loss of content from the thesis.

AVIS:

L'auteur a accordé une licence non exclusive permettant à la Bibliothèque et Archives Canada de reproduire, publier, archiver, sauvegarder, conserver, transmettre au public par télécommunication ou par l'Internet, prêter, distribuer et vendre des thèses partout dans le monde, à des fins commerciales ou autres, sur support microforme, papier, électronique et/ou autres formats.

L'auteur conserve la propriété du droit d'auteur et des droits moraux qui protègent cette thèse. Ni la thèse ni des extraits substantiels de celle-ci ne doivent être imprimés ou autrement reproduits sans son autorisation.

Conformément à la loi canadienne sur la protection de la vie privée, quelques formulaires secondaires ont été enlevés de cette thèse.

Bien que ces formulaires aient inclus dans la pagination, il n'y aura aucun contenu manquant.

■♦■
Canada

Abstract

The issue of cavitation in mechanical heart valve (MHV) patients was first recognized when damaged mechanical heart valves were observed. Cavitation bubble implosion can cause mechanical damage to the valve structure and blood elements, when it occurs near the surface of the MHV. Some methods have been suggested to quantify the level of cavitation present in MHV patients. Two algorithms from the literature were selected for implementation and comparison. These algorithms were selected as they have been previously proposed and implemented for in vivo heart signals. In this thesis, a rigorous closed-form mathematical analysis of the algorithms is presented with the aim of improving robustness, reliability and accuracy. Improvements are made to the selected algorithms, including a new improved segmentation algorithm, alignment of the S1 and S2 peaks in the signal, and the implementation of the Short-Time Fourier Transform to study the time evolution of the energy in the signal. In vitro measurements were made using a left-heart simulator to test the new improved algorithm. The improvements result in better heart beat alignment and better detection and measurement of the random events in the heart signals, so that they may provide a method to analyze cavitation in MHV patients. The use of the Short-Time Fourier Transform allows the examination of the random events in both time and frequency allowing for further investigation and interpretation of the signal. Cavitation results from the physiologically realistic left-heart simulator indicate that cavitation may not occur under normal physiological heart conditions.

Acknowledgements

I am very thankful to my supervisors, Dr. Natalie Baddour and Dr. Michel Labrosse, whose encouragement, guidance and support enabled me to develop an understanding of the subject and successfully write my thesis. Thank you for the help you provided throughout my Master's degree. You were always accessible and were always ready to give a helping hand.

I would like to thank the Department of Mechanical Engineering at the University of Ottawa and my supervisors for the funding.

I would like to thank the University of Ottawa Heart Institute for the laboratory space that allowed me to perform the experiments. I would also like to thank Dr. Rosendo A. Rodriguez from the Heart Institute for explaining the medical side of the problem and for providing answers to my questions.

Last but not least, I would like to thank my parents, my fiancé Ryan, my family and my friends for their love and support. You have always encouraged me to succeed, and were there for me when I needed a break from my thesis. Finally, I would like to thank the friends with whom I spent over two years in the CBY office; it would not have been the same without you. You have made this experience very enjoyable.

Table of Contents

Abstract.....	i
Acknowledgements.....	ii
Acronyms.....	xiii
Chapter 1: Introduction.....	1
1.1 Motivation.....	1
1.2 Objectives	2
1.3 Thesis Organisation	2
Chapter 2: Literature Review.....	4
2.1 Mechanical heart valve cavitation	4
2.2 In vitro visualisation of cavitation near MHVs.....	5
2.3 In vivo assessment of cavitation	7
Chapter 3: Background: algorithms, hardware and heart signals	14
3.1 Algorithms	14
3.1.1 Johansen’s algorithms.....	14
3.1.1.1 Johansen’s 2004 algorithm	15
3.1.1.2 Johansen’s 2003 algorithm	17
3.1.2 Segmentation algorithm.....	18
3.2 Experimental setup.....	19
3.3 Heart signals.....	20
Chapter 4: Investigation of Johansen’s algorithms.....	21
4.1 Implementation of the algorithms.....	21

4.2	Closed-form mathematical analysis of the algorithms.....	31
4.2.1	Calculations with a continuous signal $x(t)$ using Johansen’s 2004 algorithm.....	32
4.2.1.1	Deterministic energy.....	32
4.2.1.2	Total energy.....	39
4.2.1.3	Non-deterministic energy.....	42
4.2.2	Calculations with a continuous sine signal using Johansen’s 2004 algorithm.....	47
4.2.2.1	Deterministic energy.....	48
4.2.2.2	Total energy.....	51
4.2.2.3	Non-deterministic energy.....	52
4.2.2.4	Superposition problem.....	52
4.2.3	Calculations using Johansen’s 2003 algorithm.....	59
4.2.3.1	Signal with no “tails”.....	59
4.2.3.2	Signal with “tails”.....	64
4.3	Discussion of the results in terms of the analysis.....	67
Chapter 5:	Improvements and new algorithm.....	70
5.1	Improvements to Johansen’s algorithm.....	70
5.1.1	Segmentation algorithm.....	70
5.1.2	Energy in the “tails”.....	73
5.1.3	Calculation of the energy in the time domain.....	76
5.1.4	Aligning the S1 peaks in the signal.....	77
5.1.5	Aligning the S2 peaks in the signal.....	88

5.2	New algorithm using the Short-Time Fourier Transform.....	95
5.2.1	The Short-Time Fourier Transform (STFT)	95
5.2.2	Using the STFT in the algorithm	97
5.2.3	Results.....	98
5.3	Summary of the new algorithm.....	105
Chapter 6:	Experimental testing.....	108
6.1	Description of the experimental setup	108
6.1.1	Left-heart simulator	108
6.1.2	Materials and signal acquisition.....	111
6.2	Experiment.....	115
6.2.1	Experimental trials	116
6.2.2	Discussion	118
6.3	Results and discussion	123
Chapter 7:	Conclusions and Future Work	146
7.1	Conclusions.....	146
7.2	Future Work.....	149
References	150
Appendix A:	Conference paper	153

List of Figures

Figure 1: The tilting disk MHV on the left and the bileaflet MHV on the right [1].....	4
Figure 2: Illustration of the possible overlap between the lower frequency cavitation signal and the higher frequency valve resonance signal [1]	10
Figure 3: Flow chart of the experimental setup for the data gathering.....	20
Figure 4: Block diagram summarizing Johansen's 2004 algorithm.....	23
Figure 5: Block diagram summarizing Johansen's 2003 algorithm.....	24
Figure 6: Normalized stethoscope signal (Pre-recorded PCG 1).....	26
Figure 7: Normalized stethoscope signal with segmentation points.....	27
Figure 8: Superimposed and truncated heart beats of the signal (Pre-recorded PCG 1) ..	28
Figure 9: Ensemble average of the superimposed heart beats	29
Figure 10: Segmented continuous signal $x(t)$	33
Figure 11: Rectangular window $w(t)$	33
Figure 12: Plot of $W(j\omega)$ for $T=6$ (sinc function).....	35
Figure 13: Shifted rectangular window $w_l(t)$	36
Figure 14: n th window $w_n(t)$	36
Figure 15: Plot of $y_1(t) = \sin(t)$	53
Figure 16: Plot of $y_2(t) = y_1(t - 0.5) u(t - 0.5)$	54
Figure 17: Plot of $y_1(t) = \sin(t)$	55
Figure 18: Plot of $y_2(t) = y_1(t - 0.5)$	56
Figure 19: Signal with no "tails".....	60

Figure 20: Signal with "tails"	64
Figure 21: Zoomed in view of the superimposed heart beats in Figure 8.....	68
Figure 22: S1 peaks are identified and marked as 'x'	72
Figure 23: Pre-recorded stethoscope test signal with segmentation points	72
Figure 24: Superimposed heart beats of the pre-recorded stethoscope test signal	78
Figure 25: Superimposed heart beats of the pre-recorded stethoscope test signal before the S1's were aligned.....	79
Figure 26: Ensemble average of the heart beats without the S1's aligned.....	80
Figure 27: Superimposed heart beats of the pre-recorded stethoscope test signal after the S1's were aligned	81
Figure 28: Ensemble average of the heart beats with the S1's aligned.....	82
Figure 29: Superimposed heart beats of the pre-recorded stethoscope test signal before the S2's were aligned.....	89
Figure 30: Ensemble average of the heart beats without the S2's aligned.....	90
Figure 31: Superimposed heart beats of the pre-recorded stethoscope test signal after the S2's were aligned	91
Figure 32: Ensemble average of the heart beats with the S2's aligned.....	92
Figure 33: 3D representation of the spectrogram of the ensemble averaged heart beat for the first pre-recorded stethoscope test signal.....	99
Figure 34: The time evolution of the deterministic energy.....	100
Figure 35: 3D representation of the spectrogram for the first heart beat of the first pre- recorded stethoscope test signal.....	101
Figure 36: The time evolution of the total energy	102

Figure 37: The time evolution of the non-deterministic energy	103
Figure 38: The time evolution of the total, deterministic, and non-deterministic energy	104
Figure 39: Top part of the left-heart simulator [24].....	110
Figure 40: Front view of the left-heart simulator.....	111
Figure 41: Bioprosthetic valve, Magna 27mm	112
Figure 42: St. Jude Medical bileaflet mechanical heart valve	112
Figure 43: High-speed camera setup to observe the aortic valve	113
Figure 44: High-speed camera setup to observe the mitral valve.....	113
Figure 45: Electronic stethoscope.....	114
Figure 46: Hydrophone and amplifier.....	114
Figure 47: Stethoscope and hydrophone setup	115
Figure 48: Setup used by Chandran and Aluri, and Lee <i>et al.</i> [30, 31]	119
Figure 49: Setup used by Garrison <i>et al.</i> [6].....	121
Figure 50: Setup used by Zapanta <i>et al.</i> [4].....	123
Figure 51: 3D representation of the spectrogram of the ensemble average of the signal MHV recording 1 (70 beats/min).....	125
Figure 52: Rotated 3D representation of the spectrogram of the ensemble average of the signal MHV recording 1 (70 beats/min).....	126
Figure 53: Time evolution of the deterministic energy	127
Figure 54: 3D representation of the spectrogram for the first heart beat of the signal MHV recording 1 (70 beats/min).....	128

Figure 55: Rotated 3D representation of the spectrogram for the signal MHV recording 1 (70beats/min)	129
Figure 56: The time evolution of the total energy	130
Figure 57: The time evolution of the non-deterministic energy	131
Figure 58: The time evolution of the deterministic, total, and non-deterministic energy	132
Figure 59: 3D representation of the spectrogram of the ensemble averaged heart beat for the signal MHV recording 3 (100 beats/min)	133
Figure 60: Rotated 3D representation of the spectrogram of the ensemble averaged heart beat for the signal MHV recording 3 (100 beats/min).....	134
Figure 61: 3D representation of the spectrogram of the first heart beat for the signal MHV recording 3 (100 beats/min).....	135
Figure 62: Rotated 3D representation of the spectrogram of the first heart beat for the signal MHV recording 3 (100 beats/min)	136
Figure 63: The time evolution of the deterministic, total, and non-deterministic energy	137
Figure 64: 3D representation of the spectrogram of the ensemble averaged heart beat for the signal Bioprosthetic valve recording 1.....	138
Figure 65: Rotated 3D representation of the spectrogram of the ensemble averaged heart beat for the signal Bioprosthetic valve recording	139
Figure 66: 3D representation of the spectrogram of the first heart beat for the signal Bioprosthetic valve recording 1	140

Figure 67: Rotated 3D representation of the spectrogram of the first heart beat for the
signal Bioprosthetic valve recording 141

Figure 68: The time evolution of the deterministic, total, and non-deterministic energy
..... 142

List of Tables

Table 1: Results of the energy obtained with Johansen's 2004 and 2003 algorithms.....	30
Table 2: Segmentation and truncation steps	32
Table 3: Shifting step.....	35
Table 4: Beat superimposition, ensemble average and energy calculation steps	37
Table 5: Segmentation, truncation and shifting steps	40
Table 6: Beat superimposition and energy calculation steps	41
Table 7: Energy density spectrum and energy calculation steps	61
Table 8: Results of the energy obtained with Johansen's two algorithms using the stethoscope signal	74
Table 9: Results of the energy obtained with Johansen's two algorithms using the hydrophone signal.....	75
Table 10: Comparison of the results obtained with Johansen's 2004 algorithm in both the time and frequency domain.....	77
Table 11: Comparison of the results obtained with and without the S1's aligned	83
Table 12: Shifts for the signal Pre-recorded PCG 1	85
Table 13: Energy results for the Pre-recorded PCG 1 signal with all beats and with three beats removed	86
Table 14: Results obtained with all beats and with some beats removed.....	87
Table 15: Comparison of the energy results obtained with and without the S2's aligned	93
Table 16: Comparison of the percentage results obtained with the S1 peaks and with the S2 peaks aligned	94

Table 17: Comparison of the percentage results obtained with the STFT and with the FT	105
Table 18: Comparison of the energy results obtained using the STFT.....	143
Table 19: Comparison of the percentage results obtained with the FT and with the STFT	144

Acronyms

Ave: Average

Det: Deterministic

DWT: Discrete Wavelet Transform

FT: Fourier Transform

FFT: Fast Fourier Transform

HB: Number of heart beats measured

HFPF: High-Frequency Pressure Fluctuations

MFCC: Mel-Frequency Cepstral Coefficient

MHV: Mechanical Heart Valves

MSWT: Mel-Scaled Wavelet Transform

Non-det: Non-deterministic

PCG: Phonocardiogram

RMS: Root Mean Square

S1: First heart sound

S2: Second heart sound

STD: Standard deviation

STFT: Short-Time Fourier Transform

Chapter 1: Introduction

1.1 Motivation

Mechanical heart valves are used throughout the world to replace native valves in patients with heart valve dysfunctions. However, the patients remain at risk of blood cell damage, thromboembolic events and material failure of the mechanical heart valve [1]. The issue of cavitation was first recognized when damaged mechanical heart valves were observed, as the damage on the valves was consistent with the occurrence of cavitation near the valves. It is known that cavitation bubble implosion produces high-speed micro jets and high-pressure shock waves. It was suspected that this could cause mechanical damage to the valve structure and blood elements, when it occurs near the surface of the mechanical heart valve. It is thought that this could damage blood components, leading to both clot formation and possibly cerebral embolization in mechanical heart valve patients. This problem motivated the research to find an in vivo technique to quantify the level of cavitation present in mechanical heart valve patients which could be useful to help cardiologists determine the amount of anticoagulant medication to prescribe for their patients.

A few techniques have been suggested previously in the literature; however, there has not been a rigorous analysis done on these algorithms to ensure that they are robust and reliable. Additionally, the proposed algorithms need improvement to eventually accurately quantify noninvasively in vivo levels of cavitation present in MHV patients.

1.2 Objectives

The objective of the thesis is to investigate and improve heart signal processing algorithms for robustness and reliability. The first step towards this objective is to perform a rigorous closed-form mathematical analysis of two of the most ‘promising’ cavitation-quantification algorithms from the literature with the aim of improving robustness, reliability, accuracy, usability, repeatability, and ease of implementation of the algorithms. Based on the shortcomings in the algorithms made apparent by the initial implementation and subsequent mathematical analysis, the second step of the thesis is to propose improvements to the selected algorithms so that they may accurately detect and quantify random events in a heart signal. This is done with the goal that the algorithms may eventually provide a method to accurately analyze cavitation in MHV patients. The final step is to test the new algorithm by applying it to heart signals obtained from a physiologically realistic heart simulator.

1.3 Thesis Organisation

This thesis has seven chapters, including an introduction (Chapter 1) and conclusions (Chapter 7). Chapter 2 consists of the literature review. It provides a description of the previous studies that visualised cavitation in vitro near mechanical heart valves, as well as the studies that assessed cavitation in vivo. Chapter 3 explains the selected algorithms, the new segmentation algorithm, and the experimental setup. Then, the selected algorithms are implemented and the results are presented in Chapter 4. Chapter 4 also includes the closed-form mathematical analysis of the algorithms and a discussion of the results in terms of the analysis. Then, Chapter 5 discusses the proposed

improvements made to the selected algorithm and provides a summary of the new algorithm. Finally, the experiment conducted at the University of Ottawa Heart Institute is described in Chapter 6 along with the results obtained with the new algorithm. Chapter 7 concludes the thesis.

Chapter 2: Literature Review

2.1 Mechanical heart valve cavitation

Mechanical heart valves (MHV) have been used for many years to replace the native heart valves in patients with various heart valve diseases. There are approximately 175,000 MHVs that are implanted every year throughout the world. Currently, most of the implanted mechanical heart valves are based on the tilting disk (A) or bileaflet (B) concept as shown in Figure 1. Even though this surgery is usually successful, the patients remain at risk of blood cell damage, thromboembolic events, and material failure of the MHV [1].

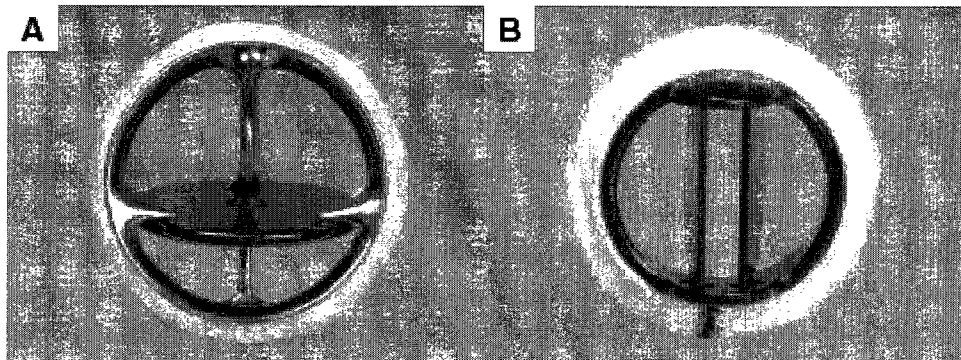


Figure 1: The tilting disk MHV on the left and the bileaflet MHV on the right [1]

In the mid 1980s, a phenomenon known as cavitation was identified as a potential likely cause of a series of MHV failures [1]. Cavitation is the rapid formation and collapse of vaporous bubbles in a fluid in a region where the pressure of the fluid is lower than its vapour pressure. Cavitation in MHVs is thought to occur during valve closure and during occluder rebounds, and has been shown in vitro to occur near the valve [2].

The bubbles' growth and collapse typically has a duration of a few milliseconds, and their characteristic size is in the range of tens to hundreds of microns [1].

The fluid's boiling point is reached by decreasing the pressure and not by increasing the temperature. When the pressure decreases lower than the vapour pressure, micro-bubbles form and grow. Once the pressure recovers (increases above the vapour pressure), the micro-bubbles implode, producing high-speed micro jets and high-pressure shock waves that can cause mechanical damage to the valve structure and blood elements, when it occurs near the surface of a MHV [1, 3]. It is thought that this damages blood components, leading to both clot formation and possibly cerebral embolization in MHV patients.

2.2 In vitro visualisation of cavitation near MHVs

One of the first groups to visualize cavitation bubble formation and collapse near MHVs was Graf *et al.* [1]. It was visualized using a strobe light and a video camera. They observed that cavitation appeared at the impact between the occluder and valve housing. They investigated ten different types of commercial MHVs in the mitral position of a pulsatile mock loop. In vivo, the mitral position has been assumed to create the harshest valve closing conditions, which might have influenced the choice of the valve position. In their experiment, they evaluated the dP/dt which represents the temporal rate of change of the left ventricular pressure, measured as the slope of the ventricular pressure curve. They found that almost all the investigated MHVs generated cavitation when dP/dt was well above the physiological range. They also found that the bileaflet valves such as the St. Jude Medical and CarboMedics valve required a higher dP/dt in order to cavitate

than tilting disc valves such as the Medtronic Hall and the Omnicarbon valve. They also observed that only three tilting disc valves and a bileaflet valve in their experiment generated cavitation at a dP/dt within the physiological range.

Kafesjian *et al.* observed that the areas on the MHVs where microscopic pitting and erosion was found corresponded to the locations where cavitation was demonstrated on the valves by Graf *et al.* Additionally, they observed that highly polished surfaces reduced the risk of such erosion [1].

As for when the cavitation occurs in the heart cycle, Graf *et al.* visualised that cavitation could occur at valve closure, and Wu *et al.* demonstrated that the disc could rebound during valve closure which could cause repetitive inception of cavitation [1].

Later, Zapanta *et al.* did a study that compares the cavitation potential of MHVs based on valve closing dynamics. They examined six different MHVs; the selection incorporated three different valve parameters in order to determine their effect on valve dynamics and cavitation. The parameters were valve geometry, occluder material, and gap width between the occluder and the valve housing. The results they obtained demonstrated that valve geometry and occluder material have significant effects on valve closing dynamics and cavitation, and that the gap width had no significant effect on cavitation but may affect closing dynamics. Additionally, they observed that for all the valves they examined, the root mean square (RMS) pressure increased (signifying potentially an increase in cavitation) as the average closing velocity and deceleration increased [4].

2.3 In vivo assessment of cavitation

Cavitation in a fluid can be detected acoustically or visually. But since blood is not a transparent fluid, the cavitation near a MHV has to be detected acoustically for in vivo studies. The acoustic evidence of cavitation is defined by the high-frequency pressure fluctuations (HFPPs) associated with transient bubble collapse [1]. These HFPPs can be detected acoustically with the use of a high sensitivity hydrophone by applying it on the patient's chest since a hydrophone can record high frequency sounds [5]. It is thought that the HFPPs may provide information regarding the intensity and duration of cavitation [1].

The sound measured at valve closure includes a mechanical resonance component coming from the MHV and a cavitation component. To obtain the part of the signal that characterizes the cavitation, the mechanical resonance component has to be removed from the signal [1]. Garrison *et al.* proposed a method to remove this component from the signal. They measured the pressure on the atrial side of a Björk-Shiley monostrut mitral valve in vitro with a high fidelity piezo-electric transducer, and could only observe cavitation with a camera when pressure signals at frequencies above 35 kHz were present. Therefore, the mechanical resonance of the valve they used did not have components above 35 kHz [1, 6]. Garrison *et al.* proposed to remove the valve mechanical resonance components from the pressure signal using a high-pass filter with a cut-off frequency of 35 kHz. After high-pass filtering, their results showed that only the high frequency cavitation oscillations remained in the pressure signal. Then, they defined a cavitation intensity parameter as the root mean square (RMS) of the high-pass filtered pressure trace [6]. This was the first method they developed; it was to quantify cavitation

intensity in the time domain. The second method (frequency domain method) used the power spectrum to characterize cavitation. They proposed to perform a Fast Fourier Transform (FFT) on the pressure signal and calculating a power spectrum. They derived three cavitation quantification parameters from this analysis. The first one is simply the maximum value of the power spectrum in the range of 100 kHz to 200 kHz. The second one is the area under the power vs. frequency curve between 35 kHz and 350 kHz. Finally, the third parameter is the volume under the 3D power vs. frequency vs. time surface between 35 kHz and 350 kHz. In their study, they found that several parameters could be extracted from the resulting pressure traces which quantify cavitation intensity [6].

Zapanta *et al.* and Dexter *et al.* both measured HFPPs in vivo in animals with MHV implants and detected cavitation [7, 8]. Zapanta *et al.* used a high fidelity, piezoelectric pressure transducer to measure the HFPPs in calves caused by cavitation bubble formation and collapse after valve closure. The calves had undergone implantation of a left ventricular assist device equipped with MHVs. The RMS value of the mitral pressure signal after valve closure was used as a measure of cavitation intensity. The pressure signals they observed in vivo were similar to those observed in vitro in previous studies [8]. Dexter *et al.* looked for the presence of transient negative pressure spikes that are conducive to cavitation in vivo. Half of the goats had their mitral valve replaced with a bioprosthetic valve, and the other half with a bileaflet pyrolytic carbon valve. The pressure was recorded from a high frequency atrial transducer; they found that no transient negative pressure spikes occurred in the goats with bioprosthetic

valves whereas transient negative pressure spikes below the vapour pressure of blood were recorded in the majority of the goats with bileaflet pyrolytic carbon valves [7].

Using a hydrophone, Paulsen *et al.* measured HFPPs in the first intraoperative study of patients. For patients with MHVs, they observed HFPPs above 35kHz, but not for patients with native or bioprosthetic heart valves [1]. Later, Andersen *et al.* came up with a technique to measure cavitation noninvasively postoperatively. They measured HFPPs intraoperatively using a hydrophone and postoperatively using the same hydrophone mounted in a specially designed water-filled sound chamber. Their data supported the data obtained intraoperatively that the MHVs generate HFPPs above 50 kHz whereas the native and bioprosthetic heart valves do not [1].

Depending on the MHV design, Johansen *et al.* determined that the valves had different closing-sound characteristics. The material, geometrical structures, and dimensions of the MHV determine its resonance mode and frequency content of the closing sound. They found that the mechanical resonance of the valves induces maximum frequencies between 40.9 kHz and 65.9 kHz [1, 5]. The cut-off frequency of 35 kHz previously suggested by Garrison *et al.* to remove the valve mechanical resonance components was for one particular MHV design only. However, some valve designs have frequencies above 35 kHz which require a different cut-off frequency. Therefore, *a priori* knowledge of the valve mechanical resonance is required to choose the cut-off frequency of the high-pass filter. Another drawback of this method is the possibility of frequency overlap between the cavitation and valve resonance signal components. Some important information may be removed from the cavitation signal by the high-pass filter [1, 9].

Figure 2 illustrates the possible frequency overlap between the lower frequency cavitation signal and the higher frequency valve resonance signal.

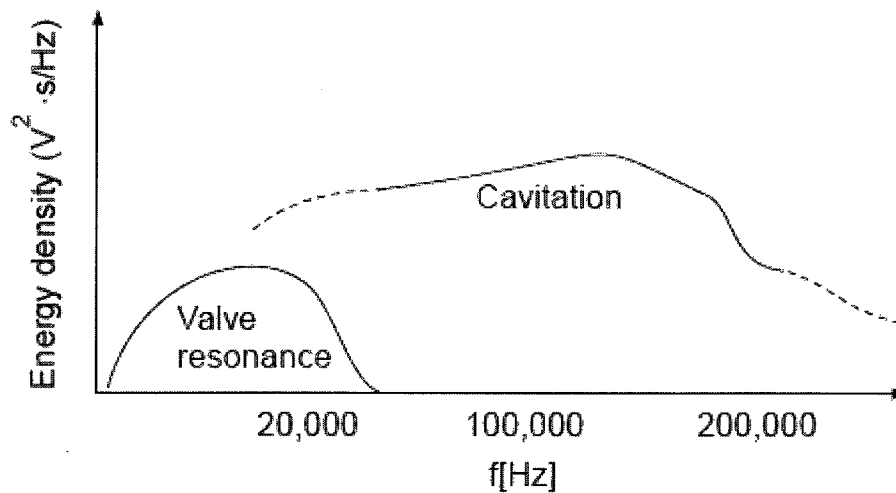


Figure 2: Illustration of the possible overlap between the lower frequency cavitation signal and the higher frequency valve resonance signal [1]

A different approach was then proposed by Johansen *et al.* to evaluate the cavitation in vivo which does not require *a priori* knowledge of the valve mechanical resonance and is not limited in bandwidth as a consequence of filtering [1]. It is suggested that the cavitation bubble implosion creates random (non-deterministic) pressure fluctuations since the number and size of the bubbles varies from beat to beat. On the other hand, the mechanical resonance occurring at valve closure is assumed to be deterministic since valve closure is cyclic. Therefore, they proposed to decompose the cavitation and valve mechanical resonance components by separating the HFPP into deterministic and non-deterministic parts [1, 9, 10]. In their experiment, three different 29 mm mitral valves were used: the Björk-Shiley monostrut, the Medtronic Hall and the CarboMedics CPHV standard mitral bileaflet valve. They were operated in vitro in a custom-made single-shot valve-closing model. The HFPPs were detected with the use of

a pressure transducer positioned in the atrial chamber. They observed that as the cavitation intensity increases, both the non-deterministic energy and dP/dt tend to increase for all three valves [9]. Their results showed that the non-deterministic energy correlated well with the RMS value of the HFPP after appropriate filtering for the three valves used in this experiment [1]. Later, Johansen *et al.* applied this method in vivo. They implanted a Medtronic Hall tilting disc valve in pigs in the mitral position. Different hemodynamic conditions were established by infusion of dobutamine and by blood volume regulation, which led to different levels of cavitation created by the MHV. For each hemodynamic setting, they detected HFPPs which indicated the presence of cavitation both in terms of an RMS measure and in terms of a non-deterministic signal energy parameter. For the RMS measure, the appropriate filter cut-off frequency was chosen [10].

The use of Johansen *et al.*'s method may be limited when it comes to evaluating bileaflet valves due to the asynchronous closure of the valve [1]. Additionally, they assume that all random events in the signal are due to cavitation, when in fact, noise is also a random event in the signal. Finally, the non-deterministic energy obtained in Johansen *et al.*'s method does not retain time information, which would be useful in order to know when the cavitation occurs in the heart cycle and also to know the duration of the cavitation event.

Sohn *et al.* later proposed another method to quantify cavitation near MHVs. In their study, they investigated both visual and acoustic cavitation characteristics. They installed a Björk-Shiley Convex-Concave valve in a single-shot valve chamber filled with water. They evaluated two different occluder materials, and water with two different air

contents. Both air content and load (dP/dt) were controlled to set the cavitation level [11]. Their results showed that a distinctive peak pressure accompanied the synchronous collapse of cavitation bubbles which they thought might be a useful signature for detecting and quantifying cavitation. The high-speed photography was used to correlate the degree of cavitation to the acoustic measurements (done with a hydrophone). Their in vitro tests indicated that it might be a more reliable method than the RMS pressure method. They also concluded that the use of the peak pressure method might be preferred for correlating cavitation intensity in structures for which the separation of valve closure noise and cavitation signal as suggested by Johansen *et al.* is difficult [11].

Sohn *et al.*'s study has not been done in vivo; therefore, it is not known if it would be successful in measuring cavitation intensity. Additionally, high-speed photography could not be used in vivo to correlate the degree of cavitation to the acoustic measurements since the latter are done noninvasively outside the body. Their method could be misleading if changes in signal-to-noise ratios are not accounted for when determining the peak pressure value. Finally, the individual cavitation events of each heart cycle cannot be distinguished.

Later, Herbertson *et al.* suggested the use of wavelet transforms to denoise and then isolate the desired cavitation signal during MHV closure. They explored a wavelet denoising method since the analytical techniques currently used fail to suitably isolate the cavitation signal from other valve closing sounds and noise detected with a hydrophone. They applied the wavelet technique to the signal produced by the closure of a 29 mm Medtronic Hall MHV in the mitral position in degassed water. The MHV was implanted in a single-shot chamber driven by a pneumatic pump. A Millar microtip catheter

pressure transducer was used to measure the pressure in the ventricular chamber [2]. The general denoising procedure they used involved the decomposition of the recorded signal, thresholding the signal at the various decomposition levels, and reconstructing the signal after eliminating the thresholded components. The decomposition was done by splitting the signal into a high-scale, low-frequency component and the low-scale, high-frequency components. Once the procedure was complete, the denoised signal theoretically contained only the cavitation events and a greatly decreased mechanical closure signal. Additionally, individual events were now more discernible. They observed that compared to the previous methods, a wavelet analysis of the cavitation signal provides more information about the cavitation events, and allows the examination of cavitation as it pertains to time which allows further investigation and interpretation of the waveform [2].

Herbertson *et al.*'s study has not been tried in vivo; therefore, it is not known if it would successfully isolate the desired cavitation signal. Additionally, they created a method which obtains a "noncavitating" signal that is assumed to contain all valve closing signals except those pertaining to cavitation [2]. However, the "noncavitating" data were not measured experimentally; therefore, this calculation has not been verified. Finally, they assumed in their method that the entire cavitation signal is found above 35 kHz, which might not be the case.

In the literature, many algorithms were proposed but no rigorous analysis has been done on these algorithms to ensure that they are robust and reliable. Furthermore, the algorithms need improvement to eventually accurately quantify noninvasively in vivo the level of cavitation present in MHV patients.

Chapter 3: Background: algorithms, hardware and heart signals

The cavitation near MHVs has to be detected acoustically for in vivo studies since it can not be detected visually due to the non-transparency of blood. When a cavitation bubble implodes, it creates high frequency pressure fluctuations (HFPP). These HFPPs can be detected acoustically with the use of a high sensitivity hydrophone by applying it on the patient's chest. The sound measured at valve closure includes a mechanical resonance component coming from the MHV and a cavitation component. To obtain the part of the signal that characterizes cavitation, the mechanical resonance component has to be removed from the signal [1]. This chapter presents different cavitation detection and quantification techniques as well as the experimental setup.

3.1 Algorithms

3.1.1 Johansen's algorithms

It has been suggested in [9] and [10] by Johansen *et al.* that the cavitation near MHVs can be quantified by separating the acoustic pressure signal into deterministic and non-deterministic components. The deterministic component represents the valve closing sound. They assumed that the mechanical resonance occurring at valve closure is deterministic since valve closure is cyclic. The non-deterministic component is the information of interest since it contains the signal information originating from cavitation. It also contains random noise from various sources such as the detection equipment used. They suggested that the cavitation bubble implosion creates random

(non-deterministic) pressure fluctuations since the number and size of bubbles varies from beat to beat.

Johansen's algorithms suggested that the non-deterministic energy can be obtained by subtracting the deterministic energy from the total energy [9, 10].

$$E_{\text{non-det}} = E_{\text{total}} - E_{\text{det}} \quad (3.1)$$

where $E_{\text{non-det}}$ represents the non-deterministic signal energy, E_{total} represents the total signal energy and E_{det} represents the deterministic signal energy. Johansen suggested two different algorithms to determine the non-deterministic energy. They appear to be the same, but from an analytical point of view, they are different. The following two subsections describe the two versions of the algorithm.

3.1.1.1 Johansen's 2004 algorithm

The equations presented herein differ slightly from the equations in Johansen's paper [10] since the notation employed in Johansen's paper was for the continuous Fourier Transform whereas the notation employed in this thesis is for the Discrete Fourier Transform.

The first step in this algorithm consists of finding the deterministic energy. It is found in the same way in both Johansen's 2004 algorithm [10] and Johansen's 2003 algorithm [9]. It is defined as

$$E_{\text{det}} = \frac{1}{N} \sum_{n=1}^N |\mathbb{F}(p_{ea}[n])|^2 \quad (3.2)$$

where N is the number of samples, $p_{ea}[n]$ is the ensemble average of the heart beats, and \mathbb{F} is the Fourier Transform.

The ensemble average is calculated according to

$$p_{ea}[n] = \frac{1}{HB} \sum_{m=1}^{HB} p_{xy}[n, m] \quad (3.3)$$

where HB is the number of heart beats measured, and $p_{xy}[n, m]$ represents the n^{th} sample of the m^{th} heart beat of the pressure signal.

Prior to calculating the ensemble average of the heart beats, the total signal is segmented into individual heart beats and all the heart beats are lined up in time. The temporal alignment of the heart beats of the pressure signal was done by cross-correlating each heart beat with a chosen template. The time delay calculated in the cross-correlation was said to enable alignment with reference to a chosen reference template heart beat. After the cross-correlation, the pressure signals of each beat were ensemble averaged, and the energy density spectrum of the averaged signal was obtained. Finally, the energy was calculated from the energy density spectrum to obtain the deterministic energy [10].

The second step in this algorithm consists of determining the total energy. This is where Johansen's 2004 and 2003 algorithms are different. The following presents the method of obtaining the total energy in Johansen's 2004 algorithm. The total energy is calculated according to

$$E_{\text{total}} = \frac{1}{HB} \sum_{i=1}^{HB} \left(\frac{1}{N} \sum_{n=1}^N A_i[n] \right) \quad (3.4)$$

where $A_i[n]$ is the amplitude spectrum squared of the i^{th} heart beat such that

$$A_i[n] = \left| \mathbb{F}(p_{xy}[:, i]) \right|^2 \text{ and } N \text{ in equation (3.4) is the number of points in each heart beat.}$$

To obtain the total energy, the energy density spectrum is determined for each heart beat,

followed by the calculation of the average of these energy density spectra. From that, the total energy is obtained [10].

The final step consists of subtracting the deterministic energy from the total energy to obtain the non-deterministic energy.

3.1.1.2 Johansen's 2003 algorithm

The first step in this algorithm consists of finding the deterministic energy. It is found in the exact same way as Johansen's 2004 algorithm. The deterministic energy is determined using equation (3.2).

The second step in this algorithm consists of determining the total energy. It was suggested in [9] that the total energy of the signal can be calculated from the energy density spectrum of the raw data. The total energy is calculated according to

$$E_{\text{total}} = \frac{1}{N} \sum_{n=1}^N |\mathbb{F}(x[n])|^2 \quad (3.5)$$

where $x[n]$ is the raw data (complete acoustic heart signal output of the hydrophone), and N in equation (3.5) is the number of samples in the raw signal (complete acoustic heart signal with no segmentation). Again, equation (3.5) differs slightly from the equation in Johansen's paper [9] since the notation employed in the paper was for the continuous Fourier Transform whereas the notation employed in this thesis is for the Discrete Fourier Transform.

The final step consists of subtracting the deterministic energy from the total energy to obtain the non-deterministic energy, as before.

3.1.2 Segmentation algorithm

The segmentation algorithm used in this thesis was the method suggested in [12], which was developed by Karim Courtemanche. The full paper is provided in Appendix A. This algorithm was used instead of Johansen's cross-correlation method since the results obtained by Johansen could not be reproduced. Note that segmentation was not the focus of this thesis. Other researchers are doing work on segmentation exclusively.

The Courtemanche segmentation algorithm proposed the use of an adaptive threshold wavelet transform filtering technique used with Shannon energy, physiological factors and heart rate approximation to properly identify the first heart sounds (S1) and segment the heart signal. However, this method can still present some errors when faced with complex signals. Therefore, the addition of a Mel-Scaled Wavelet Transform (MSWT) validation step was proposed. The MSWT is a modified Mel-Frequency Cepstral Coefficient (MFCC) algorithm with the Discrete Wavelet Transform (DWT), and it was used to reduce the impact of noise on the coefficients. The preliminary results obtained in the paper indicated that the MSWT is less prone to noise than the MFCC and can distinguish S1 sounds from others when faced with complex signals [12].

The segmentation points obtained using the Courtemanche segmentation algorithm [12] were compared with those obtained using the segmentation algorithm suggested in [13]. The stethoscope signals used in this thesis were independently simulated by Sankua Chao, the first author of [13], and it was found that the segmentation points obtained were very similar to the ones obtained using the Courtemanche algorithm.

3.2 Experimental setup

In this research, the high-frequency pressure fluctuations were measured using a miniature hydrophone. The hydrophone used for this research is the 8103 miniature hydrophone by Brüel & Kjaer, Naerum, Denmark. Its frequency range is 0.1 Hz to 180 kHz. The hydrophone was connected to the Nexus Conditioning Amplifier by Brüel & Kjaer. To help segment the hydrophone signal, an electronic stethoscope was positioned beside the hydrophone, and the stethoscope recording was done simultaneously with the hydrophone recording. The electronic stethoscope used was the Welch Allyn Elite Electronic Stethoscope, New York, USA. Its frequency range is 20 Hz to 20 kHz.

The stethoscope and hydrophone were connected to a Y-adapter, which was connected to the sound card. The Y-adapter used was a dual mono jack to stereo plug adapter. The sound card used in this research was the Creative Sound Blaster Audigy 2 ZS Notebook sound card. It was capable of recording with a sampling rate of up to 96 kHz. To maintain a manageable data set, a sampling rate of 44.1 kHz was used for healthy subjects since no cavitation was expected. The sampling rate could be changed to 96 kHz when cavitation was expected. Finally, the sound card was plugged into the laptop (ASUS A3E) where the data were stored. The data was recorded with a software called Creative Smart Recorder which came with the sound card. Figure 3 illustrates the equipment used and the experimental setup.

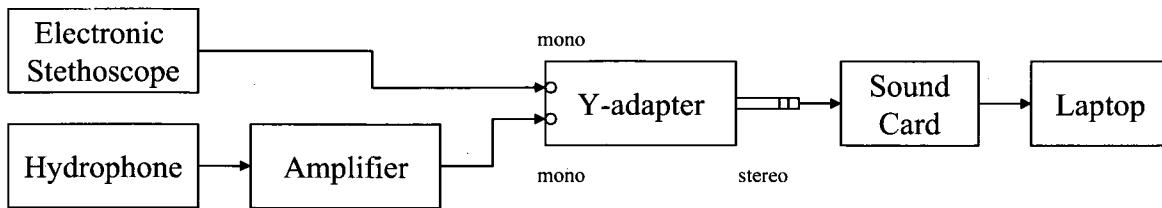


Figure 3: Flow chart of the experimental setup for the data gathering

3.3 Heart signals

For implementation of the algorithms, both stethoscope and hydrophone signals were used. The stethoscope signals were mostly used in chapters 4 and 5, and the hydrophone signals were mostly used in chapter 6. Explanations regarding the method of recording the hydrophone signals are provided in chapter 6.

Many of the stethoscope signals that were used in the algorithms were pre-recorded stethoscope test signals that were obtained from a CD provided with the Littmann stethoscope. That CD contained twenty examples of cardiac and pulmonary auscultation. The cardiac auscultation signals were used in this thesis.

The other stethoscope signal that was used in the algorithms is an in vivo stethoscope signal recorded by Karim Courtemanche, the first author of the paper in [12]. That recording was executed with the same electronic stethoscope, sound card, and laptop described in section 3.2.

Chapter 4: Investigation of Johansen's algorithms

The previous chapter described the experimental setup as well as different algorithms to detect and quantify cavitation in mechanical heart valve patients. This chapter presents the results obtained by implementing these algorithms. It also presents a mathematical analysis of the algorithms and a discussion of the results.

4.1 Implementation of the algorithms

In this section, Johansen's 2004 and 2003 algorithms are implemented in MATLAB and the results are discussed. When Johansen's algorithms were implemented, one of the important steps from his algorithms was modified. That is, the segmentation algorithm that was implemented is different from the one used in Johansen's algorithm. Instead, the Courtemanche segmentation algorithm as presented in section 3.1.2 was used.

In Johansen's 2004 algorithm, the first step consists of finding the deterministic energy. Equations (3.2) and (3.3) from chapter 3 are used for this purpose. In order to obtain the ensemble average of the heart beats, the starting point of each heart beat needs to be known. To obtain this value, the original signal is segmented at the beginning of each heart beat using the segmentation method explained in section 3.1.2. Then, each heart beat is truncated for all beats to have the same length. The end part of the beats is truncated since no important information is located there. The truncated heart beats are then superimposed one over the other and ensemble averaged to obtain an average heart

beat signal. This eliminates unwanted noise as well as reduces the signal parts that do not repeat from beat to beat. Finally, the energy is calculated from the energy density spectrum of the ensemble averaged heart beat to obtain the deterministic energy [14].

The second step in Johansen's 2004 algorithm consists of determining the total energy. Equation (3.4) from chapter 3 is used for that purpose. As for the deterministic energy, the signal is segmented at the beginning of each heart beat followed by the truncation of each beat to make them the same length. Then, the energy density spectrum is determined from each heart beat. Finally, the energy in each heart beat is calculated from each energy density spectrum signal of that heart beat. This is followed by a calculation of the average of these energies and this final value represents the total energy [14].

The final step consists of subtracting the deterministic energy from the total energy to obtain the non-deterministic energy. Figure 4 is a block diagram summarizing Johansen's 2004 algorithm with the segmentation algorithm modification.

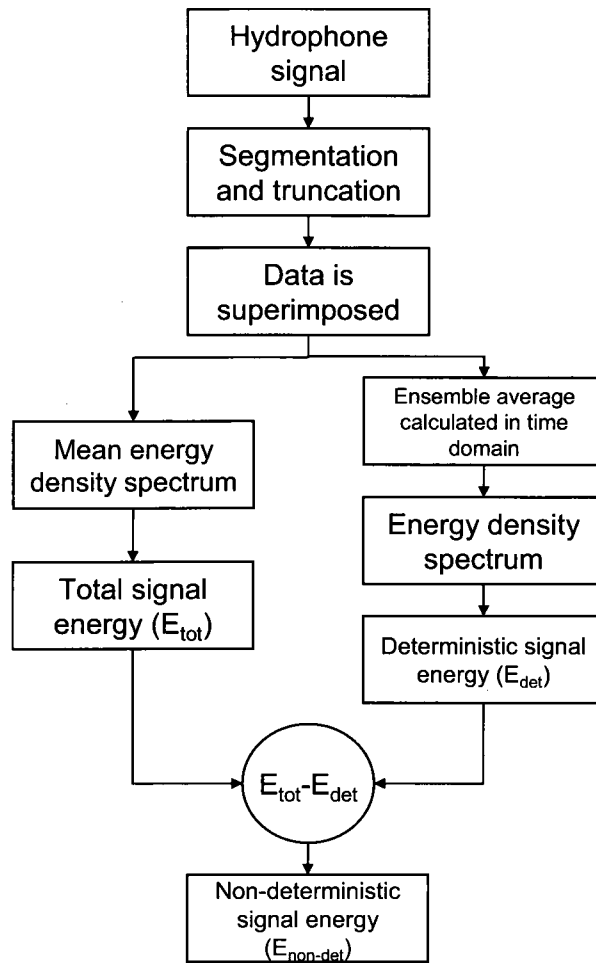


Figure 4: Block diagram summarizing Johansen's 2004 algorithm

In Johansen's 2003 algorithm, the first step consists of finding the deterministic energy. It is found in the exact same way as Johansen's 2004 algorithm. Therefore, equations (3.2) and (3.3) from chapter 3 are used for this purpose.

The second step in Johansen's 2003 algorithm consists of determining the total energy. Equation (3.5) from chapter 3 is used for this purpose. In this algorithm, the total energy of the signal is calculated from the energy density spectrum of the total signal instead of from the individual heart beats [14].

The final step consists of subtracting the deterministic energy from the total energy to obtain the non-deterministic energy. Figure 5 represents the block diagram summarizing Johansen's 2003 algorithm with the segmentation algorithm modification.

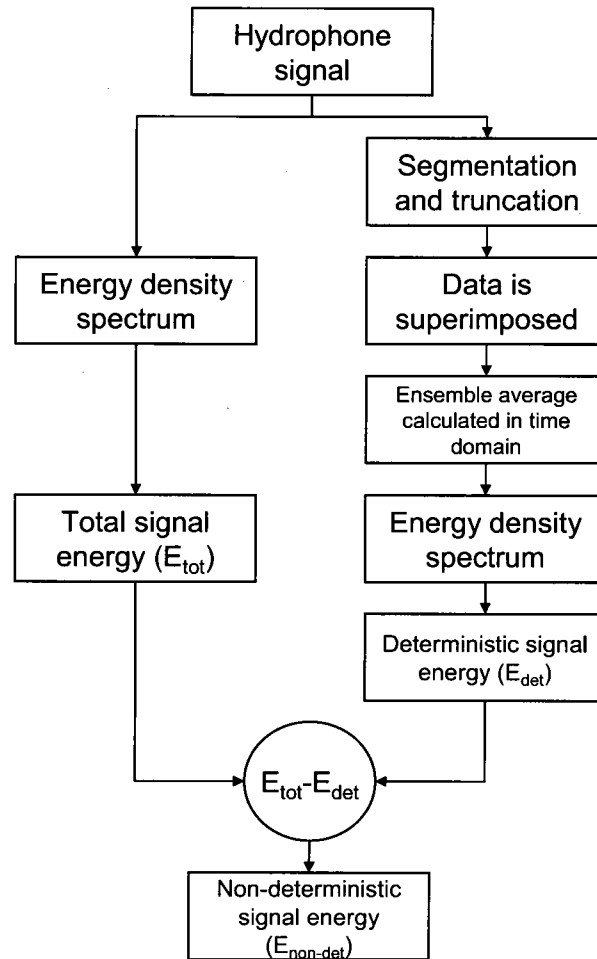


Figure 5: Block diagram summarizing Johansen's 2003 algorithm

The results in this section were obtained by testing the algorithms on some pre-recorded stethoscope test signals, and on an in vivo stethoscope signal that was recorded by Karim Courtemanche (Karim stethoscope signal 1). Stethoscope signals were tested prior to the hydrophone signals since they are less noisy and because a stethoscope signal should not contain a cavitation component since it records only low frequency sounds. This means that the non-deterministic energy result for stethoscope signals should

theoretically be near zero. Therefore, the use of stethoscope signals is a great way to test the robustness and accuracy of the algorithms. A sampling frequency of 44.1 kHz was used.

The first step in both algorithms was to segment the signal. The results of this first step are illustrated below with the signal Pre-recorded PCG 1. Figure 6 illustrates the stethoscope signal Pre-recorded PCG 1 and Figure 7 illustrates the same signal with its segmentation points marked with 'x'. The stethoscope signals were normalized at the beginning of the algorithm to allow for the comparison of signals from different patients if needed. Some patients have quiet heart beats, while others have louder beats. By normalizing, the data of different patients can be compared no matter what the signal amplitude is. That is why the figures and energy results are dimensionless.

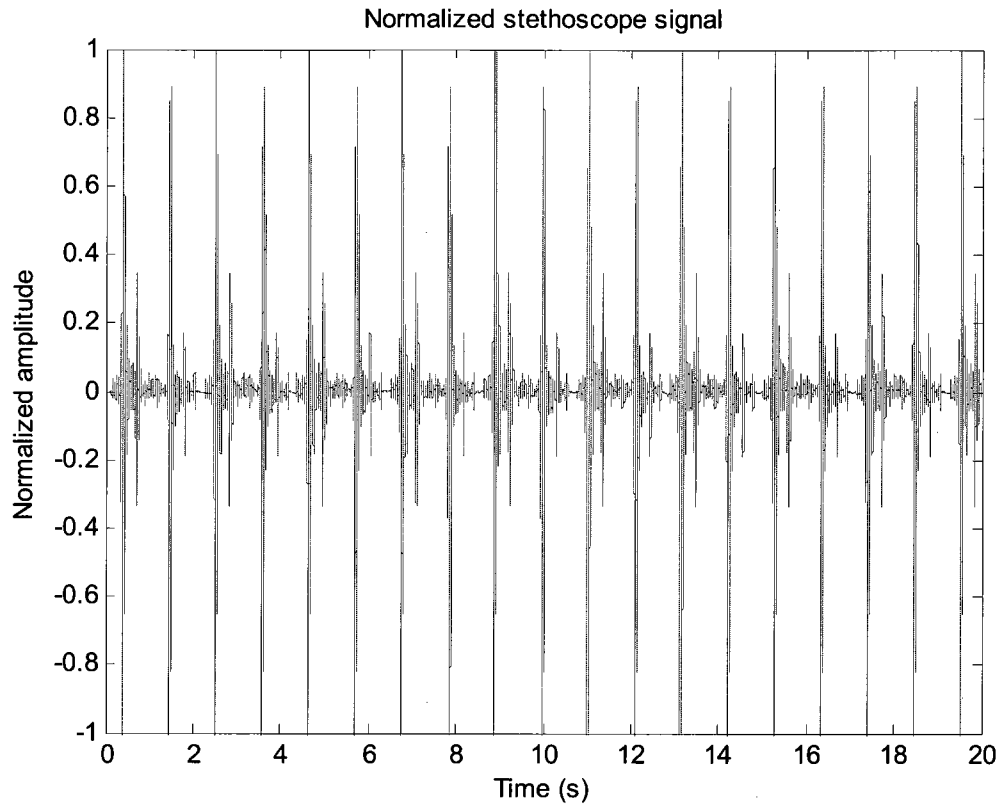


Figure 6: Normalized stethoscope signal (Pre-recorded PCG 1)

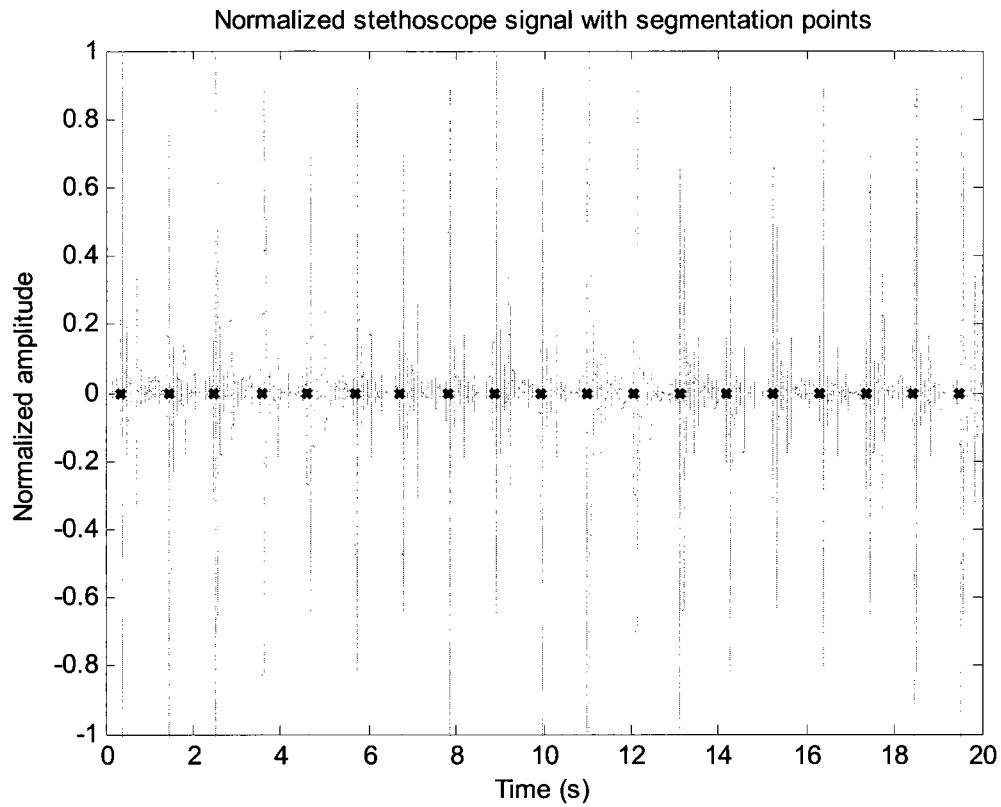


Figure 7: Normalized stethoscope signal with segmentation points

The next step was to truncate the heart beats and superimpose them one over the other as shown in Figure 8.

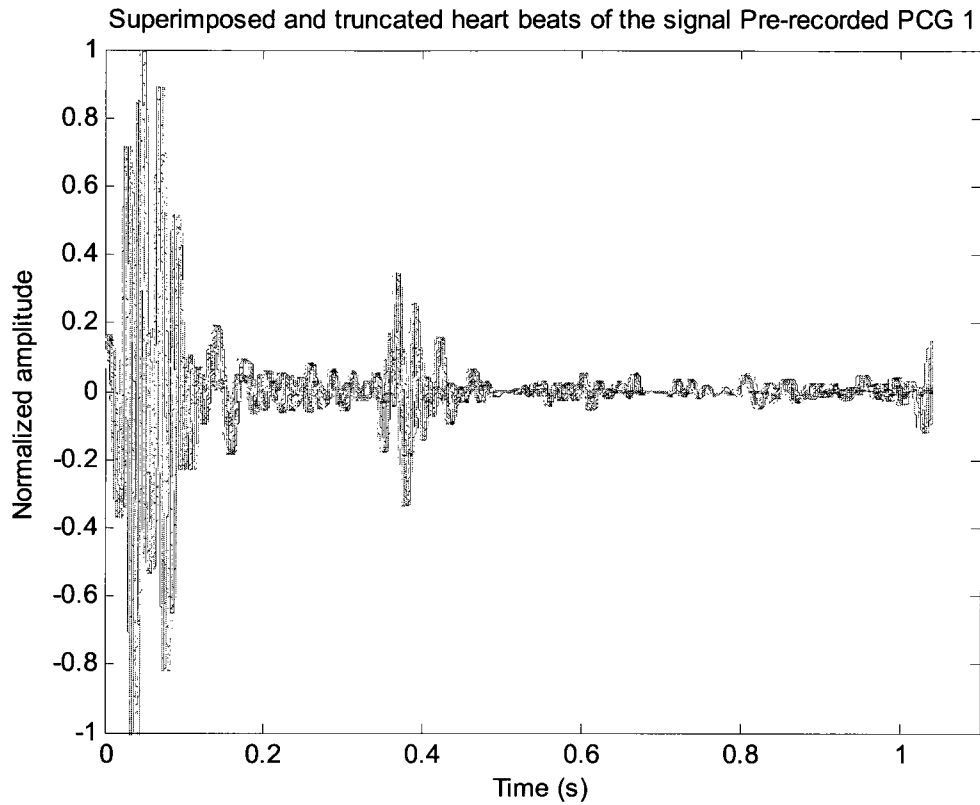


Figure 8: Superimposed and truncated heart beats of the signal (Pre-recorded PCG 1)

Then, to obtain the deterministic energy, the superimposed heart beats are ensemble averaged as shown in Figure 9.

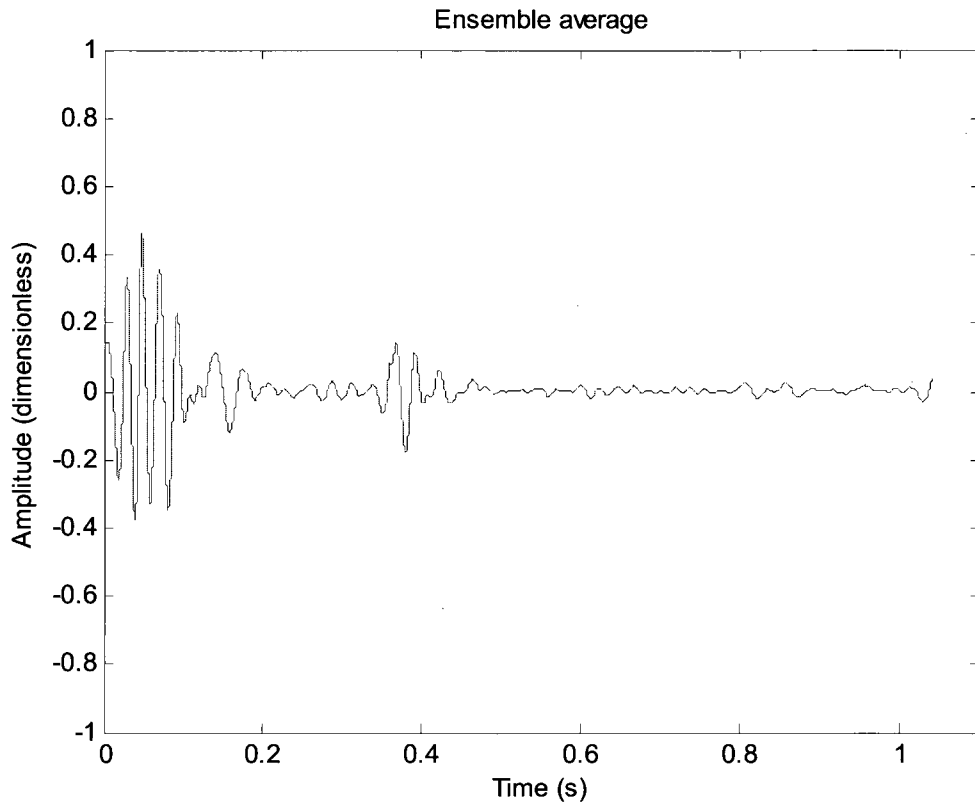


Figure 9: Ensemble average of the superimposed heart beats

The energy results obtained with a few signals including Pre-recorded PCG 1 using Johansen's 2004 and 2003 algorithms are compared in Table 1.

Table 1: Results of the energy obtained with Johansen's 2004 and 2003 algorithms

Signal used	Johansen's algorithm used	% of non-deterministic energy	Energy		
			Deterministic energy	Total energy	Non-deterministic energy
Pre-recorded PCG 1	2004	73.20 %	266.42	994.00	727.5855
	2003	98.60 %	266.42	1.90×10^4	1.88×10^4
Pre-recorded PCG 2	2004	88.17 %	106.21	898.09	791.88
	2003	99.37 %	106.21	1.68×10^4	1.67×10^4
Karim stethoscope signal 1	2004	51.29 %	229.67	471.52	241.85
	2003	97.84 %	229.67	1.06×10^4	1.04×10^4

The results in Table 1 show that the non-deterministic energy is not zero. This is due in part to the signal noise which is random and thus contributes to the non-deterministic energy. Some other factors making the non-deterministic energy non-zero come into play and are investigated in section 4.2. Then, a discussion of the results in terms of the analysis is provided in section 4.3.

4.2 Closed-form mathematical analysis of the algorithms

In this section, a closed form mathematical analysis of Johansen's algorithms is accomplished. Johansen's algorithms have, to date, not been subject to such rigorous analysis. Firstly, Johansen's 2004 algorithm is investigated. The analysis is first executed with a continuous signal $x(t)$ that represents the heart signal over several heart beats. Subsequently, it is executed with a continuous sine signal chosen to represent the heart signal since it is a simple periodic signal. For each signal, the analysis is done for two and three heart beats to search for patterns. Additionally, the analysis is accomplished for a signal with perfectly superimposed heart beats, for a signal with misplaced heart beats, and for a signal with cavitation/noise. Finally, Johansen's 2003 algorithm is investigated. The analysis is executed for a signal with "tails", and one without "tails". The analysis is also considered for a signal with perfectly superimposed heart beats and for a signal with cavitation/noise.

To analyse the theory in the algorithm used to quantify the amount of cavitation written by Johansen *et al.* in 2004 [10], Johansen's algorithm was implemented analytically. The calculations are done in both the time domain and frequency domain. In order to obtain the non-deterministic energy, the deterministic energy and the total energy need to be calculated.

4.2.1 Calculations with a continuous signal $x(t)$ using Johansen's 2004 algorithm

4.2.1.1 Deterministic energy

The first step in Johansen's algorithm consists of finding the deterministic energy. To obtain the deterministic energy, the original signal is first segmented at the beginning of each heart beat using the method suggested in [12]. Then, each heart beat is truncated for all beats to have the same length. In the analytical calculations, these two steps are accomplished by multiplying a continuous signal $x(t)$ by a rectangular window $w(t)$ having a length of one truncated heart beat.

Table 2: Segmentation and truncation steps

	Time	Frequency
Original signal	$x(t)$	$X(j\omega)$
Segmented and truncated signal	$x(t) \cdot w(t)$	$X(j\omega) * W(j\omega)$

The continuous signal $x(t)$ in the time domain could be, for example, the heart signal shown in Figure 10.

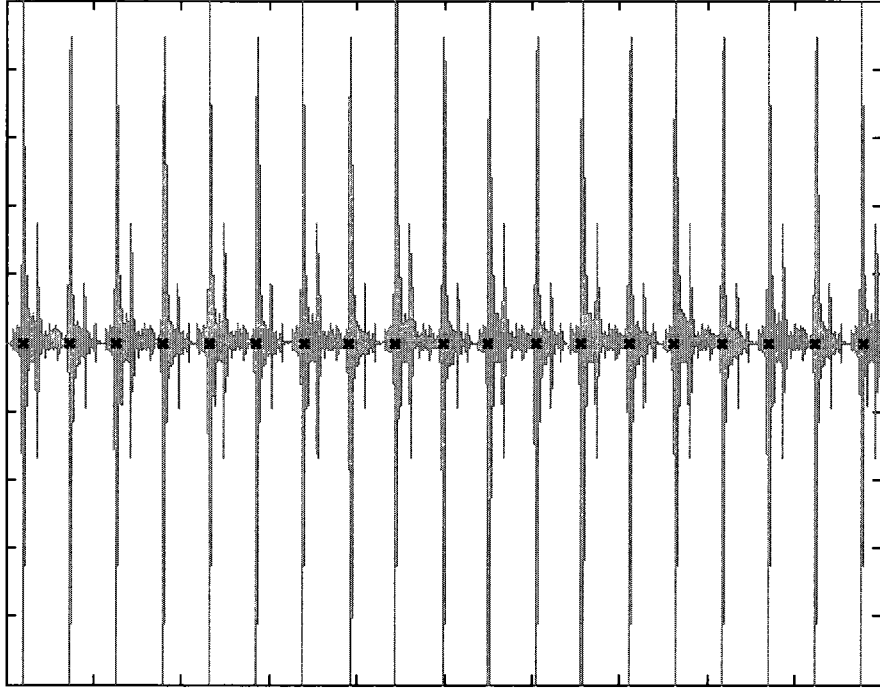


Figure 10: Segmented continuous signal $x(t)$

In Figure 10, the first black 'x' represents the segmentation point t_1 , the second one represents the segmentation point t_2 , the third one represents t_3 , and so on. The rectangular window in the time domain is shown in Figure 11 and given by,

$$w(t) = \begin{cases} 1 & \text{for } |t| \leq \frac{T}{2} \\ 0 & \text{otherwise} \end{cases} \quad (4.1)$$

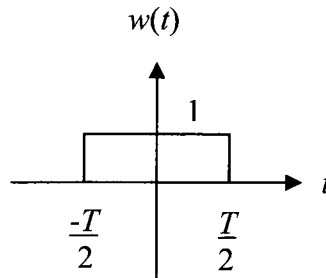


Figure 11: Rectangular window $w(t)$

In equation (4.1), T is the length of each heart beat after truncation. From there, the rectangular window in the frequency domain $W(j\omega)$ can be obtained by calculating the Fourier Transform of $w(t)$. The Fourier Transform of $w(t)$ can be calculated using the Fourier transform equation [15],

$$W(j\omega) = \int_{-\infty}^{+\infty} w(t)e^{-j\omega t} dt. \quad (4.2)$$

With the information given in Figure 11, equation (4.2) gives

$$W(j\omega) = \int_{-\frac{T}{2}}^{\frac{T}{2}} 1 \cdot e^{-j\omega t} dt = \frac{e^{-j\omega t}}{-j\omega} \Big|_{-\frac{T}{2}}^{\frac{T}{2}} = \frac{e^{-j\omega \frac{T}{2}} - e^{+j\omega \frac{T}{2}}}{-j\omega} = \frac{2 \cdot \sin\left(\omega \frac{T}{2}\right)}{\omega} = T \cdot \text{sinc}\left(\frac{\omega \frac{T}{2}}{\pi}\right) \quad (4.3)$$

where $\text{sinc}(x) = \frac{\sin(\pi x)}{\pi x}$. The result of $W(j\omega)$ for $T=6$ is plotted in Figure 12. It was

plotted using the software Maple.

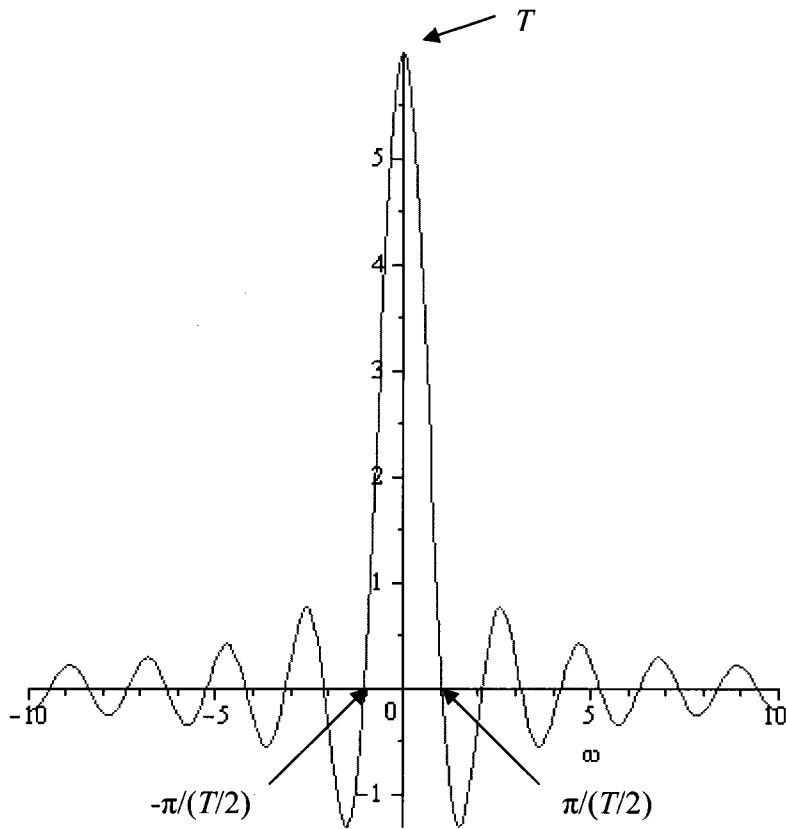


Figure 12: Plot of $W(j\omega)$ for $T=6$ (sinc function)

The rectangular window needs to be positioned from 0 to T since the first heart beat starts at zero. Therefore, the rectangular window $w(t)$ is shifted to the right by $T/2$.

Table 3: Shifting step

	Time	Frequency
Shifted rectangular window $w_i(t)$	$w_i(t) = w\left(t - \frac{T}{2}\right)$	$W_i(j\omega) = e^{-j\omega\frac{T}{2}}W(j\omega)$

The shifted rectangular window is illustrated in Figure 13.

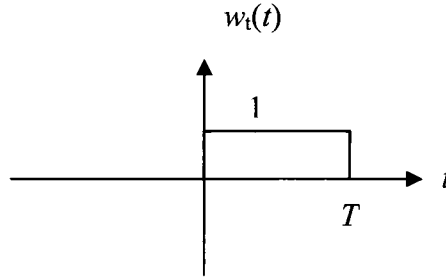


Figure 13: Shifted rectangular window $w_i(t)$

The rectangular window illustrated in Figure 13 applies to one heart beat only. There are many heart beats in one heart signal; therefore a general rectangular window equation is needed. The general rectangular window equation is

$$w_n(t) = \begin{cases} 1 & \text{for } t_n \leq t \leq t_n + T \\ 0 & \text{otherwise} \end{cases} \quad (4.4)$$

where t_n is the time at the n th heart beat as illustrated in Figure 10, and T is the length of each heart beat after truncation.

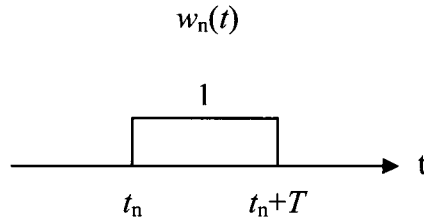


Figure 14: n th window $w_n(t)$

The next step in Johansen's algorithm is to obtain the deterministic energy. To do this, the truncated heart beats are superimposed one over the other and then averaged (ensemble average) to obtain an average heart beat signal. To perform the same step analytically, the window $w_i(t)$ is shifted to the right at the n th heart beat, and it is multiplied by the signal $x(t)$ to extract only that heart beat. Then, that heart beat is

shifted to the left to time zero. This is done for all heart beats. Therefore, all heart beats are positioned at time zero and can then be ensemble averaged. Finally, the energy is calculated from the energy density spectrum to obtain the deterministic energy. These steps are summarized in Table 4.

Table 4: Beat superimposition, ensemble average and energy calculation steps

		Time	Frequency
Beat superimposition	Shift window $w_i(t)$ to the right at the n th heart beat	$w_n(t) = w_i(t - t_n)$	$W_n(j\omega) = e^{-j\omega t_n} W_i(j\omega)$ $W_n(j\omega) = e^{-j\omega t_n} e^{-j\omega \frac{T}{2}} W(j\omega)$
	Multiply the signal $x(t)$ with the window $w_n(t)$	$y(t) = x(t) \cdot w_n(t)$	$Y(j\omega) = X(j\omega) * W_n(j\omega)$
	Shift the signal and window to the left to zero	$y_n(t) = y(t + t_n)$	$Y_n(j\omega) = e^{+j\omega t_n} \cdot Y(j\omega)$ $Y_n(j\omega) = e^{+j\omega t_n} \cdot (X(j\omega) * W_n(j\omega))$
Ensemble average		$z(t) = \frac{1}{HB} \sum_{n=1}^{HB} y_n(t)$	$Z(j\omega) = \frac{1}{HB} \sum_{n=1}^{HB} Y_n(j\omega)$
Energy calculation	Using Parseval's Relation [15]	$E_{\text{det}} = \int_{-\infty}^{+\infty} z(t) ^2 dt$	$E_{\text{det}} = \frac{1}{2\pi} \int_{-\infty}^{+\infty} Z(j\omega) ^2 d\omega$

In Table 4, HB is the number of heart beats measured, $|Z(j\omega)|^2$ is the energy density spectrum and E_{det} is the deterministic energy. It is important to note that $y_n(t)$ represents $y(t)$ shifted to the left by t_n , since this notation will be used throughout section 4.2. This step is done in order to superimpose all the heart beats in the heart signal at time zero. To illustrate these same steps analytically, the deterministic energy is first calculated for two

heart beats and then for three heart beats in the following calculations. These calculations are done in the time domain since the analytical calculation is simpler to perform in the time domain.

Two heart beats: For two heart beats, it follows that

$$z(t) = \frac{1}{2} \sum_{n=1}^2 y_n(t) = \frac{1}{2} y_1(t) + \frac{1}{2} y_2(t) \quad (4.5)$$

$$|z(t)|^2 = \frac{1}{4} y_1^2(t) + \frac{1}{4} y_2^2(t) + \frac{1}{2} |y_1(t)y_2(t)|$$

Hence the deterministic energy is given by

$$E_{\text{det}} = \int_{-\infty}^{+\infty} |z(t)|^2 dt = \frac{1}{4} \int_{-\infty}^{+\infty} y_1^2(t) dt + \frac{1}{4} \int_{-\infty}^{+\infty} y_2^2(t) dt + \underbrace{\frac{1}{2} \int_{-\infty}^{+\infty} |y_1(t)y_2(t)| dt}_{\text{Cross term (like cross correlation)}} \quad (4.6)$$

If $y_1(t) = y_2(t)$, implying that the heart beats are identical and perfectly superimposed as a result of a perfect segmentation process, then

$$E_{\text{det}} = \frac{1}{2} \int_{-\infty}^{+\infty} y_1^2(t) dt + \frac{1}{2} \int_{-\infty}^{+\infty} y_1^2(t) dt = \int_{-\infty}^{+\infty} y_1^2(t) dt \quad (4.7)$$

Three heart beats: For three heart beats, we have that

$$z(t) = \frac{1}{3} \sum_{n=1}^3 y_n(t) = \frac{1}{3} y_1(t) + \frac{1}{3} y_2(t) + \frac{1}{3} y_3(t) \quad (4.8)$$

so that

$$|z(t)|^2 = \left(\frac{1}{3} y_1(t) + \frac{1}{3} y_2(t) + \frac{1}{3} y_3(t) \right) \cdot \left(\frac{1}{3} y_1(t) + \frac{1}{3} y_2(t) + \frac{1}{3} y_3(t) \right) \quad (4.9)$$

$$= \frac{1}{9} y_1^2(t) + \frac{2}{9} y_1(t)y_2(t) + \frac{2}{9} y_1(t)y_3(t) + \frac{1}{9} y_2^2(t) + \frac{2}{9} y_2(t)y_3(t) + \frac{1}{9} y_3^2(t)$$

Hence the deterministic energy is given by

$$\begin{aligned}
E_{det} = \int_{-\infty}^{+\infty} |z(t)|^2 dt &= \frac{1}{9} \int_{-\infty}^{+\infty} y_1^2(t) dt + \frac{1}{9} \int_{-\infty}^{+\infty} y_2^2(t) dt + \frac{1}{9} \int_{-\infty}^{+\infty} y_3^2(t) dt \\
&+ \underbrace{\frac{2}{9} \int_{-\infty}^{+\infty} y_1(t)y_2(t) dt + \frac{2}{9} \int_{-\infty}^{+\infty} y_1(t)y_3(t) dt + \frac{2}{9} \int_{-\infty}^{+\infty} y_2(t)y_3(t) dt}_{\text{Cross terms}}
\end{aligned} \tag{4.10}$$

If $y_1(t) = y_2(t) = y_3(t)$, implying that the three heart beats are identical and perfectly superimposed, then

$$E_{det} = \int_{-\infty}^{+\infty} y_1^2(t) dt \tag{4.11}$$

As observed in (4.7) and (4.11), the result for the deterministic energy using two or three heart beats when they are perfectly superimposed is the same. The result is also the same using four, five, or more heart beats. However, once the heart beats are not perfectly superimposed, cross-terms will appear in the deterministic energy result, having an impact on both the deterministic and non-deterministic energy results. This demonstrates the importance of the correct segmentation of the original heartbeat signal. Imperfect segmentation and superimposition of the heartbeats leads to additional terms in the deterministic energy calculation, and the source of these terms is entirely from the imperfect segmentation and not noise or cavitation. This would, in turn, affect the non-deterministic energy not because of any true additional nondeterministic energy in the signal but rather through imperfect processing of the signal.

4.2.1.2 Total energy

The second step in Johansen's algorithm consists of finding the total energy. To obtain the total energy, the original signal is first segmented at the beginning of each heart beat using the same method used for the deterministic energy. Then, each heart beat

is truncated for all beats to have the same length. Then, the energy density spectrum is determined for each heart beat. Finally, the total energy is calculated from each energy density spectrum signal followed by a calculation of the mean of these individual heart beat energies. The mean of the individual heart beat energies represents the total signal energy.

In the analytical calculations, these two steps were accomplished by multiplying a continuous signal $x(t)$ by a rectangular window $w(t)$ having a length of one truncated heart beat. The signal $x(t)$ and the window $w(t)$ used to calculate the total energy are the same ones that were used previously in the deterministic energy calculation. Then, the rectangular window $w(t)$ is shifted to the right by $T/2$ since it needs to be positioned from 0 to T . This is illustrated in Table 5.

Table 5: Segmentation, truncation and shifting steps

	Time	Frequency
Original signal	$x(t)$	$X(j\omega)$
Segmented and truncation signal	$x(t) \cdot w(t)$	$X(j\omega) * W(j\omega)$
Shifted rectangular window $w_i(t)$	$w_i(t) = w\left(t - \frac{T}{2}\right)$	$W_i(j\omega) = e^{-j\omega \frac{T}{2}} W(j\omega)$

Then, the energy density spectrum is determined for each heart beat. The energy for each heart beat is calculated from each energy density spectrum signal. The total energy is then calculated as the average of the energies of each heart beat. This is illustrated in Table 6.

Table 6: Beat superimposition and energy calculation steps

		Time	Frequency
Beat superimposition	Shift window $w_t(t)$ to the right at the n th heart beat	$w_n(t) = w_t(t - t_n)$	$W_n(j\omega) = e^{-j\omega t_n} W_t(j\omega)$ $W_n(j\omega) = e^{-j\omega t_n} e^{-j\omega \frac{T}{2}} W(j\omega)$
	Multiply the signal $x(t)$ with the window $w_n(t)$	$y(t) = x(t) \cdot w_n(t)$	$Y(j\omega) = X(j\omega) * W_n(j\omega)$
	Shift the signal and window to the left to zero	$y_n(t) = y(t + t_n)$	$Y_n(j\omega) = e^{+j\omega t_n} \cdot Y(j\omega)$ $Y_n(j\omega) = e^{+j\omega t_n} \cdot (X(j\omega) * W_n(j\omega))$
Energy calculation for each heart beat	Using Parseval's Relation [15]	$e_n = \int_{-\infty}^{+\infty} y_n(t) ^2 dt$	$e_n = \frac{1}{2\pi} \int_{-\infty}^{+\infty} Y_n(j\omega) ^2 d\omega$
Total energy		$E_{total} = \frac{1}{HB} \sum_{n=1}^{HB} e_n$	$E_{total} = \frac{1}{HB} \sum_{n=1}^{HB} e_n$

In the table above, e_n represents the energy at the n th heart beat and E_{total} represents the total energy. In the following, the total energy calculation is demonstrated for two heart beats and then for three heart beats. These calculations were done in the time domain as for the deterministic energy calculations.

Two heart beats:

Starting with two heart beats, the total energy can be written as

$$E_{total} = \frac{1}{2} \sum_{n=1}^2 \int_{-\infty}^{+\infty} |y_n(t)|^2 dt = \frac{1}{2} \left(\int_{-\infty}^{+\infty} y_1^2(t) dt + \int_{-\infty}^{+\infty} y_2^2(t) dt \right) \quad (4.12)$$

Then if $y_1(t) = y_2(t)$ so that the heartbeats are identical and perfectly superimposed (i.e. perfect segmentation), then

$$E_{total} = \int_{-\infty}^{+\infty} y_1^2(t) dt \quad (4.13)$$

Three heart beats:

Similarly for three heart beats, the total energy is given by

$$E_{total} = \frac{1}{3} \sum_{n=1}^3 \int_{-\infty}^{+\infty} |y_n(t)|^2 dt = \frac{1}{3} \left(\int_{-\infty}^{+\infty} y_1^2(t) dt + \int_{-\infty}^{+\infty} y_2^2(t) dt + \int_{-\infty}^{+\infty} y_3^2(t) dt \right) \quad (4.14)$$

Then if the heartbeats are identical and perfectly superimposed so that

$y_1(t) = y_2(t) = y_3(t)$, then it follows that

$$E_{total} = \int_{-\infty}^{+\infty} y_1^2(t) dt \quad (4.15)$$

As observed in (4.13) and (4.15), the result for the total energy using two or three heart beats when they are perfectly superimposed is the same. The result is also the same using four, five or more heart beats.

4.2.1.3 Non-deterministic energy

The final step in Johansen's algorithm consists of finding the non-deterministic energy. To obtain the non-deterministic energy, the deterministic energy is subtracted from the total energy. The procedure is demonstrated with two and three heart beats in the following.

Two heart beats:

For two heartbeats, it follows that

$$\begin{aligned}
E_{non-det} &= E_{total} - E_{det} \\
&= \frac{1}{2} \int_{-\infty}^{+\infty} y_1^2(t) dt + \frac{1}{2} \int_{-\infty}^{+\infty} y_2^2(t) dt - \left(\frac{1}{4} \int_{-\infty}^{+\infty} y_1^2(t) dt + \frac{1}{2} \int_{-\infty}^{+\infty} y_1(t)y_2(t) dt + \frac{1}{4} \int_{-\infty}^{+\infty} y_2^2(t) dt \right) \quad (4.16)
\end{aligned}$$

which becomes

$$\begin{aligned}
E_{non-det} &= \frac{1}{2^2} \int_{-\infty}^{+\infty} (y_1^2(t) - 2y_1(t)y_2(t) + y_2^2(t)) dt \\
&= \frac{1}{2^2} \int_{-\infty}^{+\infty} (y_1(t) - y_2(t))^2 dt \quad (4.17)
\end{aligned}$$

Now clearly if the heart beats are identical and perfectly superimposed so that

$y_1(t) = y_2(t)$, then this yields

$$E_{non-det} = 0 \quad (4.18)$$

The preceding equation clearly demonstrates that Johansen's algorithm, in theory, works perfectly. Namely, if a signal consists of heart beats that repeat perfectly and can be segmented perfectly, then his algorithm will calculate the energies in the non-repeating components.

Now suppose that an additional component is added to the signal so that the beats are not perfectly superimposed but are 'similar'. This is done by considering one beat to be fundamentally the same as another but with the addition of an extra signal, which may be cavitation or noise, etc. This is modelled mathematically as

$$y_2(t) = y_1(t) + \underbrace{\eta(t)}_{\text{Cavitation/noise}} \quad (4.19)$$

In this case, the non-deterministic energy is given by

$$\begin{aligned}
E_{non-det} &= \frac{1}{4} \int_{-\infty}^{+\infty} y_1^2(t) dt + \frac{1}{4} \int_{-\infty}^{+\infty} (y_1(t) + \eta(t))^2 dt - \frac{1}{2} \int_{-\infty}^{+\infty} y_1(t)(y_1(t) + \eta(t)) dt \\
&= \frac{1}{4} \int_{-\infty}^{+\infty} y_1^2(t) dt + \frac{1}{4} \int_{-\infty}^{+\infty} (y_1^2(t) + 2y_1(t)\eta(t) + \eta^2(t)) dt - \frac{1}{2} \int_{-\infty}^{+\infty} (y_1^2(t) + y_1(t)\eta(t)) dt \quad (4.20)
\end{aligned}$$

which yields

$$E_{non-det} = \underbrace{\frac{1}{4} \int_{-\infty}^{+\infty} \eta^2(t) dt}_{\text{Represents cavitation/noise}} \quad (4.21)$$

Again, it has been shown analytically and in closed form that Johansen's algorithm is successful and the calculation of non-deterministic energy does in fact capture the contribution to the energy of the non-repeating portions of the input signal.

Three heart beats:

Repeating the above procedure with three heart beats,

$$\begin{aligned} E_{non-det} &= E_{total} - E_{det} \\ &= \frac{2}{9} \int_{-\infty}^{+\infty} y_1^2(t) dt + \frac{2}{9} \int_{-\infty}^{+\infty} y_2^2(t) dt + \frac{2}{9} \int_{-\infty}^{+\infty} y_3^2(t) dt - \frac{2}{9} \int_{-\infty}^{+\infty} y_1(t)y_2(t) dt - \frac{2}{9} \int_{-\infty}^{+\infty} y_1(t)y_3(t) dt - \frac{2}{9} \int_{-\infty}^{+\infty} y_2(t)y_3(t) dt \end{aligned}$$

which gives

$$E_{non-det} = \frac{1}{3^2} \int_{-\infty}^{+\infty} \left[(y_1(t) - y_2(t))^2 + (y_1(t) - y_3(t))^2 + (y_2(t) - y_3(t))^2 \right] dt \quad (4.22)$$

Again, for beats that are identical, then $E_{non-det} = 0$. As for the two-beat case, the case where the second and third beats are identical to the first but with the addition of noise or cavitation is also considered. This implies that the beats are modelled as

$$\begin{aligned} y_2(t) &= y_1(t) + \eta_1(t) \\ y_3(t) &= y_1(t) + \eta_2(t) \end{aligned} \quad (4.23)$$

Then the non-deterministic energy calculation is given by

$$\begin{aligned}
E_{non-det} &= \frac{2}{9} \int_{-\infty}^{+\infty} y_1^2(t) dt + \frac{2}{9} \int_{-\infty}^{+\infty} (y_1^2(t) + 2y_1(t)\eta_1(t) + \eta_1^2(t)) dt + \frac{2}{9} \int_{-\infty}^{+\infty} (y_1^2(t) + 2y_1(t)\eta_2(t) + \eta_2^2(t)) dt \\
&\quad - \frac{2}{9} \int_{-\infty}^{+\infty} (y_1^2(t) + y_1(t)\eta_1(t)) dt - \frac{2}{9} \int_{-\infty}^{+\infty} (y_1^2(t) + y_1(t)\eta_2(t)) dt \\
&\quad - \frac{2}{9} \int_{-\infty}^{+\infty} (y_1^2(t) + y_1(t)\eta_2(t) + y_1(t)\eta_1(t) + \eta_1(t)\eta_2(t)) dt
\end{aligned} \tag{4.24}$$

which simplifies to

$$E_{non-det} = \underbrace{\frac{2}{9} \int_{-\infty}^{+\infty} \eta_1^2(t) dt + \frac{2}{9} \int_{-\infty}^{+\infty} \eta_2^2(t) dt - \frac{2}{9} \int_{-\infty}^{+\infty} \eta_1(t)\eta_2(t) dt}_{\text{Represents cavitation/noise}} \tag{4.25}$$

The previous equation again demonstrates analytically that Johansen's algorithm is successful at capturing the non-repeating elements of a signal.

The non-deterministic energy for four or more heart beats can be predicted by looking at the pattern in equations (4.21) and (4.25). The calculations accomplished above confirm that the algorithm can be used to determine the level of cavitation in a heart signal. It clearly demonstrates that the non-deterministic energy does indeed represent the cavitation in the signal if the heart beats $y_1(t)$, $y_2(t)$, ... are well aligned at the beat superimposition step, and if there is no random noise in the signal. Therefore, the theory behind the algorithm is sound.

In the case when the heart beats are not perfectly superimposed, the non-deterministic energy result is affected. The impact is demonstrated below for two heart beats.

$$\begin{aligned}
E_{non-det} &= E_{total} - E_{det} \\
&= \frac{1}{2} \int_{-\infty}^{+\infty} y_1^2(t) dt + \frac{1}{2} \int_{-\infty}^{+\infty} y_2^2(t) dt - \left(\frac{1}{4} \int_{-\infty}^{+\infty} y_1^2(t) dt + \frac{1}{4} \int_{-\infty}^{+\infty} y_2^2(t) dt + \frac{1}{2} \int_{-\infty}^{+\infty} y_1(t) y_2(t) dt \right) \quad (4.26)
\end{aligned}$$

which becomes

$$E_{non-det} = \frac{1}{2^2} \int_{-\infty}^{+\infty} (y_1(t) - y_2(t))^2 dt \quad (4.27)$$

The non-deterministic energy equation in (4.27) is identical to the one in (4.17). In the following calculations, ε represents the factor by which a heart beat is misplaced. It means that $y_1(t)$ is shifted to the left by ε compared to $y_2(t)$, so that $y_2(t) = y_1(t + \varepsilon)$.

This gives

$$\begin{aligned}
E_{non-det} &= \frac{1}{4} \int_{-\infty}^{+\infty} y_1^2(t) dt + \frac{1}{4} \int_{-\infty}^{+\infty} y_1^2(t + \varepsilon) dt - \underbrace{\frac{1}{2} \int_{-\infty}^{+\infty} y_1(t) y_1(t + \varepsilon) dt}_{\text{Autocorrelation}} \quad (4.28)
\end{aligned}$$

Cavitation $\eta(t)$ is then added to the heart signal so that $y_2(t) = y_1(t + \varepsilon) + \underbrace{\eta(t)}_{\text{Cav./noise}}$. This

gives

$$\begin{aligned}
E_{non-det} &= \frac{1}{4} \int_{-\infty}^{+\infty} y_1^2(t) dt + \frac{1}{4} \int_{-\infty}^{+\infty} (y_1(t + \varepsilon) + \eta(t))^2 dt - \frac{1}{2} \int_{-\infty}^{+\infty} y_1(t) [y_1(t + \varepsilon) + \eta(t)] dt \\
&= \frac{1}{4} \int_{-\infty}^{+\infty} y_1^2(t) dt + \frac{1}{4} \int_{-\infty}^{+\infty} (y_1^2(t + \varepsilon) + 2y_1(t + \varepsilon)\eta(t) + \eta^2(t)) dt \\
&\quad - \frac{1}{2} \int_{-\infty}^{+\infty} (y_1(t)y_1(t + \varepsilon) + y_1(t)\eta(t)) dt \quad (4.29)
\end{aligned}$$

This becomes

$$\begin{aligned}
E_{non-det} &= \overbrace{\frac{1}{4} \int_{-\infty}^{+\infty} y_1^2(t) dt + \frac{1}{4} \int_{-\infty}^{+\infty} y_1^2(t + \varepsilon) dt - \frac{1}{2} \int_{-\infty}^{+\infty} y_1(t) y_1(t + \varepsilon) dt}^{\text{Identical result as in (4.28)}} \\
&+ \frac{1}{4} (2) \int_{-\infty}^{+\infty} y_1(t + \varepsilon) \eta(t) dt - \frac{1}{2} \int_{-\infty}^{+\infty} y_1(t) \eta(t) dt + \underbrace{\frac{1}{4} \int_{-\infty}^{+\infty} \eta^2(t) dt}_{\text{Cavitation/noise}}
\end{aligned} \tag{4.30}$$

From the non-deterministic energy result obtained in (4.30), one can observe that if

$$\varepsilon = 0, \text{ then } E_{non-det} = \frac{1}{4} \int_{-\infty}^{+\infty} \eta^2(t) dt \text{ which implies that the non-deterministic energy}$$

represents cavitation only. However, if $\varepsilon \neq 0$, then ε appears in the non-deterministic energy result as shown in (4.30), meaning that the non-deterministic energy is *not* a measure of cavitation alone. Therefore, if the beats are not properly superimposed, the beats that are not lined up will have an impact on the non-deterministic result, which might be falsely interpreted as a greater level of cavitation in the signal.

In conclusion, it has been shown in closed-form analytical form that Johansen's algorithm as proposed heuristically in his papers, can work as being an effective representation of the measure of cavitation in a signal that essentially repeats. However, it was also shown that any error in perfectly lining up the repeating heartbeats will also lead to another additional contribution to the non-deterministic energy which could lead to a false interpretation of the presence of additional cavitation in the signal.

4.2.2 Calculations with a continuous sine signal using Johansen's 2004 algorithm

In the following, the closed-form expressions derived in the previous sections are used with a simple test signal in order to calculate the relative sizes of contributions to the energies from the heartbeat portion of the signal compared with the cavitation portion of

the signal. The following test signal was constructed to represent a simple low-frequency sine signal which represents the heartbeat along with a higher frequency sine signal which would represent an extremely simple cavitation signal.

$$\begin{aligned}
 y_1(t) &= \underbrace{A_1 \sin(\Omega t)}_{\text{Heart beat}} + \underbrace{C_1 \sin(\omega_1 t + \phi_1)}_{\text{Cavitation}} \\
 y_2(t) &= \underbrace{A_2 \sin(\Omega t)}_{\text{Heart beat}} + \underbrace{C_2 \sin(\omega_2 t + \phi_2)}_{\text{Cavitation}}
 \end{aligned} \tag{4.31}$$

In the previous equation $y_1(t)$ and $y_2(t)$ are the two first heart beats in the test signal, A_i is the amplitude of the i th heart beat signal, C_i is the amplitude of the i th cavitation signal, Ω is the frequency of the heart signal, ω_1 and ω_2 are the (higher) frequencies of the cavitation signal, and ϕ_i is the phase shift for each cavitation signal. In general, the cavitation signal is assumed to be a non-periodic high-frequency signal. However, in order to calculate energies in closed form, the cavitation signal modelled above has been modelled with a sine signal for the sake of simplicity. A phase shift is required to ensure the cavitation signal will not be in-phase with the heartbeat. The heart signal is assumed to be periodic with a frequency much lower than that of the cavitation signal. The test signal was constructed with sinusoidal signals since they are periodic and easy to manipulate in calculations. They also make it possible to solve the calculations in closed form and analyse the results.

4.2.2.1 Deterministic energy

Once again, the first step consists of finding the deterministic energy. The same steps as section 4.2.1.1 are followed and identical formulas for the ensemble average and

energy calculation are obtained. The deterministic energy is calculated in the time domain for two heart beats as:

$$\begin{aligned}
z(t) &= \frac{1}{HB} \sum_{n=1}^{HB} y_n(t) = \frac{1}{2} y_1(t) + \frac{1}{2} y_2(t) \\
&= \frac{1}{2} \left[(A_1 \sin(\Omega t) + C_1 \sin(\omega_1 t + \phi_1)) \cdot w_1(t) \right] + \frac{1}{2} \left[(A_2 \sin(\Omega t) + C_2 \sin(\omega_2 t + \phi_2)) \cdot w_1(t) \right]
\end{aligned} \tag{4.32}$$

where $w_1(t)$ is the rectangular window in equation (4.4) and Figure 14 when $n = 1$. At this point in the calculations, $y_1(t)$ and $y_2(t)$ have already been superimposed and positioned from 0 to T , which is why they are both multiplied by $w_1(t)$, the window positioned from 0 to T . The following calculations are a continuation of (4.32). For $0 \leq t \leq T$, then

$$\begin{aligned}
|z(t)|^2 &= \frac{1}{4} \left[A_1^2 \sin^2(\Omega t) + C_1^2 \sin^2(\omega_1 t + \phi_1) + 2A_1C_1 \sin(\Omega t) \sin(\omega_1 t + \phi_1) \right] \\
&\quad + \frac{1}{4} \left[A_2^2 \sin^2(\Omega t) + C_2^2 \sin^2(\omega_2 t + \phi_2) + 2A_2C_2 \sin(\Omega t) \sin(\omega_2 t + \phi_2) \right] \\
&\quad + \frac{1}{2} \left[A_1A_2 \sin^2(\Omega t) + A_1C_2 \sin(\Omega t) \sin(\omega_2 t + \phi_2) \right] + \\
&\quad + \frac{1}{2} \left[A_2C_1 \sin(\Omega t) \sin(\omega_1 t + \phi_1) + C_1C_2 \sin(\omega_1 t + \phi_1) \sin(\omega_2 t + \phi_2) \right]
\end{aligned} \tag{4.33}$$

Note that $|z(t)| = 0$ for $t \notin [0, T]$. It then follows that the energy can be calculated from

$$E_{\text{det}} = \int_{-\infty}^{+\infty} |z(t)|^2 dt \tag{4.34}$$

which yields

$$\begin{aligned}
E_{\text{det}} = & \frac{1}{4} A_1^2 \int_0^T \sin^2(\Omega t) dt + \frac{1}{4} C_1^2 \int_0^T \sin^2(\omega_1 t + \phi_1) dt + \frac{1}{2} A_1 C_1 \int_0^T \sin(\Omega t) \sin(\omega_1 t + \phi_1) dt \\
& + \frac{1}{4} A_2^2 \int_0^T \sin^2(\Omega t) dt + \frac{1}{4} C_2^2 \int_0^T \sin^2(\omega_2 t + \phi_2) dt + \frac{1}{2} A_2 C_2 \int_0^T \sin(\Omega t) \sin(\omega_2 t + \phi_2) dt \\
& + \frac{1}{2} A_1 A_2 \int_0^T \sin^2(\Omega t) dt + \frac{1}{2} A_1 C_2 \int_0^T \sin(\Omega t) \sin(\omega_2 t + \phi_2) dt \\
& + \frac{1}{2} A_2 C_1 \int_0^T \sin(\Omega t) \sin(\omega_1 t + \phi_1) dt + \frac{1}{2} C_1 C_2 \int_0^T \sin(\omega_1 t + \phi_1) \sin(\omega_2 t + \phi_2) dt
\end{aligned} \tag{4.35}$$

where $T = 2\pi/\Omega$. Using the parameters $\omega_1 = 35000\Omega$ Hz, $\omega_2 = 36000\Omega$ Hz so that the

cavitation has a much higher frequency than the heartbeat, and also

$A_1 = A_2 = A$, $C_1 = C_2 = C$, $\phi_1 = \phi_2 = 0$, $y_1(t) \neq y_2(t)$, the software Maple can calculate the

energy as

$$\begin{aligned}
E_{\text{det}} = & \int_0^{2\pi/\Omega} \left[\frac{1}{2} \left(\underbrace{A \sin(\Omega t) + C \sin(35000\Omega t + 0)}_{y_1(t)} \right) + \frac{1}{2} \left(\underbrace{A \sin(\Omega t) + C \sin(36000\Omega t + 0)}_{y_2(t)} \right) \right]^2 dt \\
= & \frac{1}{2} \frac{\pi (C^2 + 2A^2)}{\Omega}
\end{aligned} \tag{4.36}$$

The software Maple was used to solve the last part of (4.36). The value of ω_1 was chosen as 35 kHz times the value of Ω since the high frequency pressure fluctuations due to cavitation occur in the frequency range of 35 kHz to 350 kHz [6]. The frequency ω_2 was assigned a different value than ω_1 to account for possible variations in frequency between heart beats. The value of Ω is approximately 1 Hz since the duration of a heart beat is approximately 1 second. If the value of ω_1 and ω_2 is changed to any integer between the frequency range mentioned previously, the deterministic energy equation in (4.36) will remain the same.

4.2.2.2 Total energy

Once again, the second step consists of finding the total energy. To obtain the total energy, the same steps as in section 4.2.1.2 are followed and an identical formula for the average energy is obtained. The total energy is calculated in the time domain for two heart beats as

$$E_{total} = \frac{1}{HB} \sum_{n=1}^{HB} \int_{-\infty}^{+\infty} |y_n(t)|^2 dt = \frac{1}{2} \left(\int_{-\infty}^{+\infty} y_1^2(t) dt + \int_{-\infty}^{+\infty} y_2^2(t) dt \right) \quad (4.37)$$

which becomes

$$E_{total} = \frac{1}{2} \int_{-\infty}^{+\infty} \left[(A_1 \sin(\Omega t) + C_1 \sin(\omega_1 t + \phi_1)) \cdot w_1(t) \right]^2 dt \\ + \frac{1}{2} \int_{-\infty}^{+\infty} \left[(A_2 \sin(\Omega t) + C_2 \sin(\omega_2 t + \phi_2)) \cdot w_1(t) \right]^2 dt \quad (4.38)$$

where $w_1(t)$ is the rectangular window in equation (4.4) and Figure 14 when $n = 1$. This gives

$$E_{total} = \frac{1}{2} \int_0^T \left(A_1^2 \sin^2(\Omega t) + C_1^2 \sin^2(\omega_1 t + \phi_1) + 2A_1C_1 \sin(\Omega t) \sin(\omega_1 t + \phi_1) \right) dt \\ + \frac{1}{2} \int_0^T \left(A_2^2 \sin^2(\Omega t) + C_2^2 \sin^2(\omega_2 t + \phi_2) + 2A_2C_2 \sin(\Omega t) \sin(\omega_2 t + \phi_2) \right) dt \quad (4.39)$$

where $T = 2\pi/\Omega$. Using Maple along with the parameters

$$\omega_1 = 35000\Omega \text{ Hz}, \omega_2 = 36000\Omega \text{ Hz}, A_1 = A_2 = A, C_1 = C_2 = C, \phi_1 = \phi_2 = 0, y_1(t) \neq y_2(t),$$

we obtain

$$\begin{aligned}
E_{total} &= \frac{1}{2} \int_0^{2\pi/\Omega} \left(\underbrace{A \sin(\Omega t) + C \sin(35000\Omega t + 0)}_{y_1(t)} \right)^2 dt + \frac{1}{2} \int_0^{2\pi/\Omega} \left(\underbrace{A \sin(\Omega t) + C \sin(36000\Omega t + 0)}_{y_2(t)} \right)^2 dt \\
&= \frac{\pi(A^2 + C^2)}{\Omega}
\end{aligned}
\tag{4.40}$$

4.2.2.3 Non-deterministic energy

The final step consists of finding the non-deterministic energy. To obtain the non-deterministic energy, the deterministic energy is subtracted from the total energy. It is calculated in the time domain for two heart beats in the following calculations.

$$\begin{aligned}
E_{non-det} &= E_{total} - E_{det} \\
&= \frac{\pi(A^2 + C^2)}{\Omega} - \frac{1}{2} \frac{\pi(C^2 + 2A^2)}{\Omega}
\end{aligned}
\tag{4.41}$$

which simplifies to give

$$E_{non-det} = \frac{1}{2} \frac{\pi C^2}{\Omega}
\tag{4.42}$$

It is observed in (4.42) that $E_{non-det}$ does *not* depend on A , the amplitude of the heart signal. It depends on C , the amplitude of the cavitation signal. Therefore, for perfectly aligned heart beats, the non-deterministic energy represents the cavitation in the signal which confirms that the algorithm can be used to determine the level of cavitation in a measured signal.

4.2.2.4 Superposition problem

When heart beats are not perfectly superimposed, there are two different possibilities after truncation:

1. The first possibility is that $y_2(t)$, the second heart beat, will be zero for the first few points since it is slightly shifted to the right due to its misalignment. This will resemble a misplaced heart beat since the value before the S1 in a heart beat should be near zero. Figure 15 and Figure 16 demonstrate the first possibility with the two first heart beats $y_1(t)$ and $y_2(t)$.

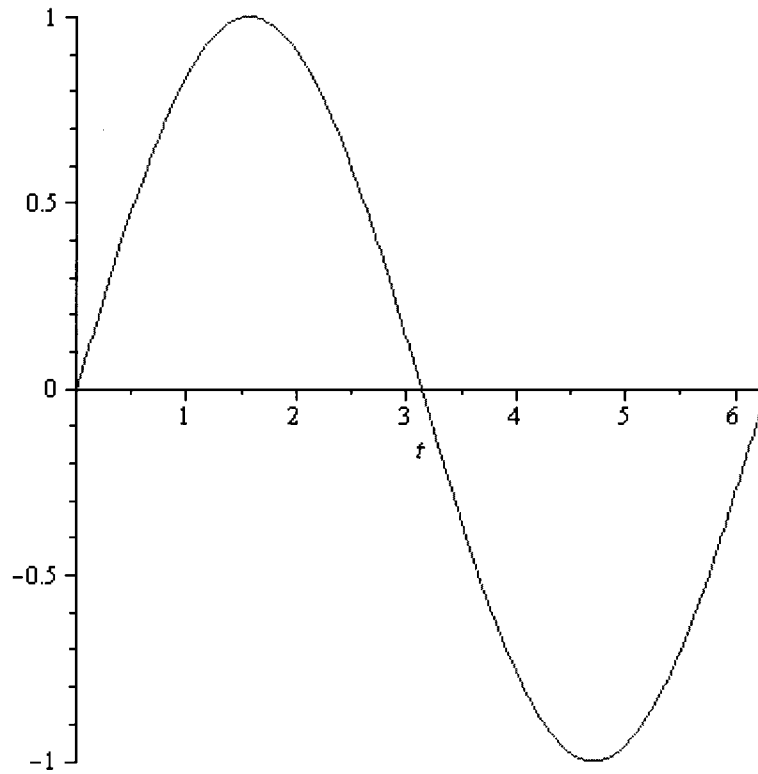


Figure 15: Plot of $y_1(t) = \sin(t)$

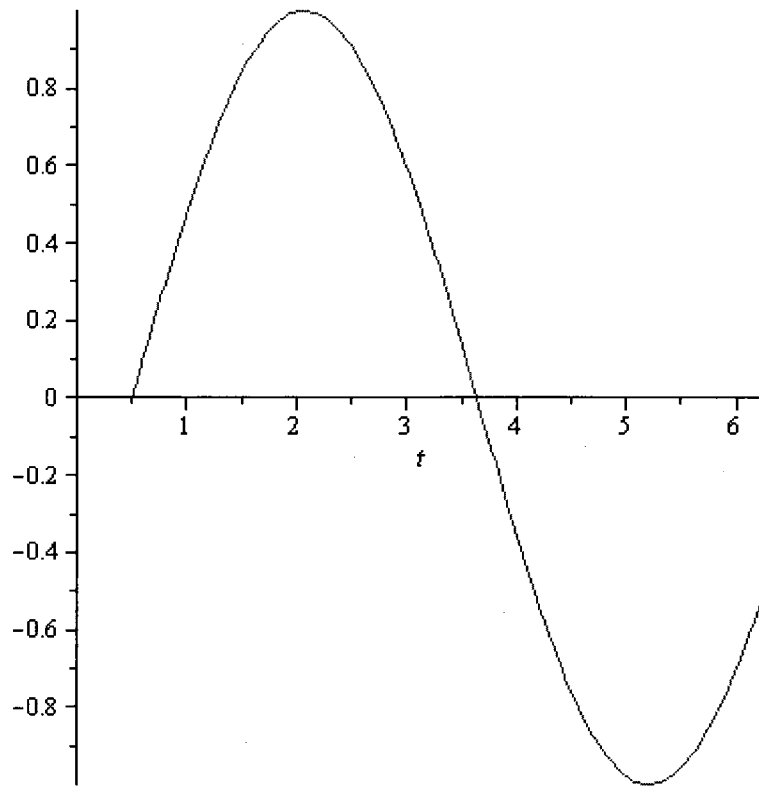


Figure 16: Plot of $y_2(t) = y_1(t-0.5)u(t-0.5)$

2. The second possibility is that the beginning of $y_2(t)$ will be the part of the beat that was cut off at the end by the truncation, since it is slightly shifted to the right. Figure 17 and Figure 18 demonstrate the second possibility with the two first heart beats $y_1(t)$ and $y_2(t)$.

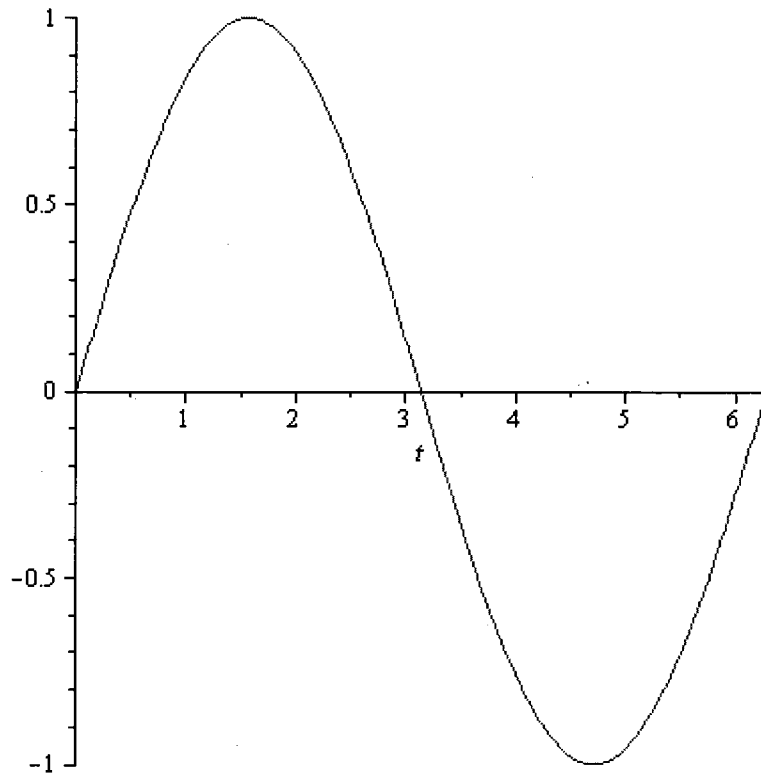


Figure 17: Plot of $y_1(t) = \sin(t)$

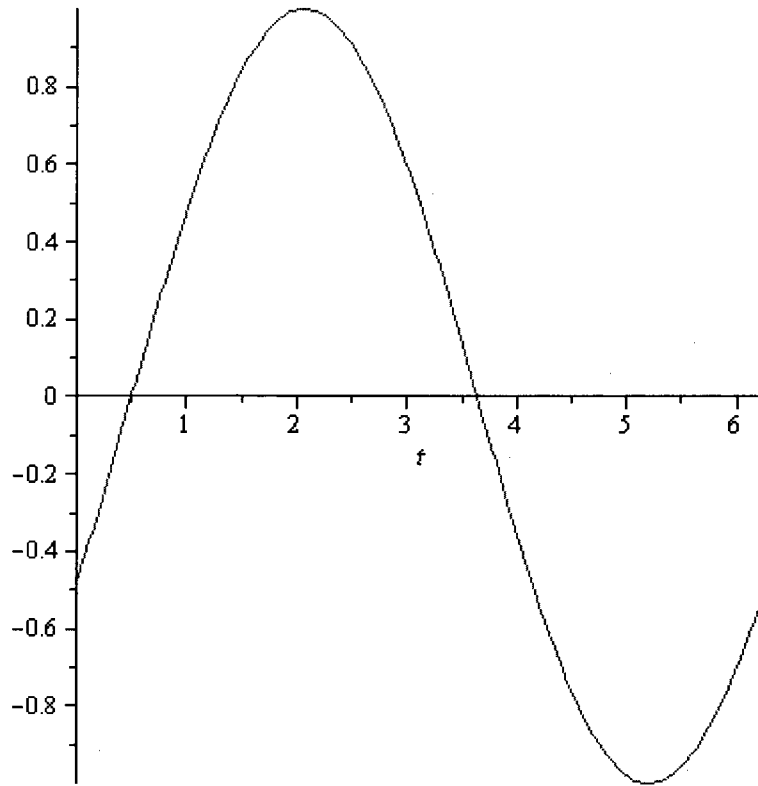


Figure 18: Plot of $y_2(t) = y_1(t - 0.5)$

Some calculations were executed below to compare the results obtained with the two possibilities mentioned previously. The calculations are done using two heart beats.

1st case:

The test signal used is identical to the one used in (4.31):

$$\begin{aligned} y_1(t) &= A_1 \sin(\Omega t) + C_1 \sin(\omega_1 t + \phi_1) \\ y_2(t) &= A_2 \sin(\Omega t) + C_2 \sin(\omega_2 t + \phi_2) \end{aligned} \quad (4.43)$$

The non-deterministic energy is given by

$$E_{non-det} = \frac{1}{4} \int_{-\infty}^{+\infty} y_1^2(t) dt + \frac{1}{4} \int_{-\infty}^{+\infty} y_2^2(t) dt - \frac{1}{2} \int_{-\infty}^{+\infty} y_1(t) y_2(t) dt \quad (4.44)$$

Now if the second heart beat is “misaligned” so that $y_2(t) = y_1(t - \varepsilon)u(t - \varepsilon)$, it follows

that

$$E_{non-det} = \frac{1}{4} \int_{-\infty}^{+\infty} y_1^2(t) dt + \frac{1}{4} \int_{-\infty}^{+\infty} (y_1(t-\varepsilon)u(t-\varepsilon))^2 dt - \frac{1}{2} \int_{-\infty}^{+\infty} y_1(t)y_1(t-\varepsilon)u(t-\varepsilon) dt \quad (4.45)$$

The heartbeats are truncated to have a length of T so that

$$E_{non-det} = \frac{1}{4} \int_0^T y_1^2(t) dt + \frac{1}{4} \int_0^T (y_1(t-\varepsilon)u(t-\varepsilon))^2 dt - \frac{1}{2} \int_0^T y_1(t)y_1(t-\varepsilon)u(t-\varepsilon) dt \quad (4.46)$$

which becomes

$$\begin{aligned} E_{non-det} &= \frac{1}{4} \int_0^T (A_1 \sin(\Omega t) + C_1 \sin(\omega_1 t + \phi_1))^2 dt + \frac{1}{4} \int_0^T [(A_1 \sin(\Omega(t-\varepsilon)) + C_1 \sin(\omega_1(t-\varepsilon) + \phi_1)) \cdot u(t-\varepsilon)]^2 dt \\ &\quad - \frac{1}{2} \int_0^T [(A_1 \sin(\Omega t) + C_1 \sin(\omega_1 t + \phi_1)) \cdot (A_1 \sin(\Omega(t-\varepsilon)) + C_1 \sin(\omega_1(t-\varepsilon) + \phi_1)) \cdot u(t-\varepsilon)] dt \end{aligned} \quad (4.47)$$

Using Maple along with the parameters $\omega_1 = 35000\text{Hz}$, $\Omega = 1$, $\phi_1 = 0$, $\varepsilon = 10\text{ms}$, then

$$\begin{aligned} E_{non-det} &= \frac{1}{4} \int_0^{2\pi/\Omega} (A_1 \sin(1 \cdot t) + C_1 \sin(35000 \cdot t + 0))^2 dt \\ &\quad + \frac{1}{4} \int_0^{2\pi/\Omega} [(A_1 \sin(t-10) + C_1 \sin(35000(t-10) + 0)) \cdot u(t-10)]^2 dt \\ &\quad - \frac{1}{2} \int_0^{2\pi/\Omega} [(A_1 \sin(1 \cdot t) + C_1 \sin(35000 \cdot t + 0)) \cdot (A_1 \sin(t-10) + C_1 \sin(35000(t-10) + 0)) \cdot u(t-10)] dt \end{aligned} \quad (4.48)$$

which becomes

$$E_{non-det} = \frac{1}{4} A^2 \pi + \frac{1}{4} C^2 \pi = 0.7854 A^2 + 0.7854 C^2 \quad (4.49)$$

Note that with misalignment of the beats explicitly modelled as a shift in one of the heart beats, the nondeterministic energy now depends on the magnitude of the cavitation signal *as well as* the magnitude of the heart beats themselves and the dependence on both is about the same, with both factors having a $\pi/4$ dependence.

2nd case:

The non-deterministic energy is still given by equation (4.44).

If we assume that $y_2(t) = y_1(t - \varepsilon)$, then the non-deterministic energy becomes

$$E_{non-det} = \frac{1}{4} \int_{-\infty}^{+\infty} y_1^2(t) dt + \frac{1}{4} \int_{-\infty}^{+\infty} y_1^2(t - \varepsilon) dt - \frac{1}{2} \int_{-\infty}^{+\infty} y_1(t) y_1(t - \varepsilon) dt \quad (4.50)$$

The heart beats are truncated to have a length of T . This gives

$$\begin{aligned} E_{non-det} &= \frac{1}{4} \int_0^T y_1^2(t) dt + \frac{1}{4} \int_0^T y_1^2(t - \varepsilon) dt - \frac{1}{2} \int_0^T y_1(t) y_1(t - \varepsilon) dt \\ &= \frac{1}{4} \int_0^T (A_1 \sin(\Omega t) + C_1 \sin(\omega_1 t + \phi_1))^2 dt + \frac{1}{4} \int_0^T (A_1 \sin(\Omega(t - \varepsilon)) + C_1 \sin(\omega_1(t - \varepsilon) + \phi_1))^2 dt \\ &\quad - \frac{1}{2} \int_0^T [(A_1 \sin(\Omega t) + C_1 \sin(\omega_1 t + \phi_1)) \cdot (A_1 \sin(\Omega(t - \varepsilon)) + C_1 \sin(\omega_1(t - \varepsilon) + \phi_1))] dt \end{aligned} \quad (4.51)$$

Using Maple with the parameters $\omega_1 = 35000\text{Hz}$, $\Omega = 1$, $\phi_1 = 0$, $\varepsilon = 10$, then the integrations yields

$$\begin{aligned} E_{non-det} &= \frac{1}{4} \int_0^{2\pi/\Omega} (A_1 \sin(1 \cdot t) + C_1 \sin(35000 \cdot t + 0))^2 dt \\ &\quad + \frac{1}{4} \int_0^{2\pi/\Omega} (A_1 \sin(t - 10) + C_1 \sin(35000(t - 10) + 0))^2 dt \\ &\quad - \frac{1}{2} \int_0^{2\pi/\Omega} [(A_1 \sin(1 \cdot t) + C_1 \sin(35000 \cdot t + 0)) \cdot (A_1 \sin(t - 10) + C_1 \sin(35000(t - 10) + 0))] dt \end{aligned} \quad (4.52)$$

which simplifies to

$$\begin{aligned} E_{non-det} &= \frac{1}{2} A^2 \pi + \frac{1}{2} C^2 \pi - \frac{1}{2} C^2 \pi \cos(350000) - \frac{1}{2} A^2 \pi \cos(10) \\ &= 2.8888A^2 + 1.3747C^2 \end{aligned} \quad (4.53)$$

Once again, with the effect of the misalignment of the beats accounted for, it can be seen that the nondeterministic energy depends on the magnitudes of *both* the cavitation and heart beat signals. The result obtained with the first possibility in (4.49) seems better than the result obtained with the second possibility in (4.53) since A , the amplitude of the heart beat signal, contributes less to the non-deterministic energy ($0.7854A^2$ vs. $2.8888A^2$). Ideally, the component coming from the heart beat should not be present in the non-deterministic energy since the latter is supposed to represent the cavitation only.

4.2.3 Calculations using Johansen’s 2003 algorithm

As previously discussed, Johansen *et al.* had suggested another algorithm for quantifying the cavitation in mechanical heart valve patients prior to the 2004 algorithm. It will be referred to as the 2003 algorithm in this thesis. It was demonstrated previously that the algorithm suggested by Johansen *et al.* in 2003 [9] was less accurate and less robust than the algorithm suggested in 2004. The calculations done below demonstrate why this algorithm is not accurate and robust for the quantification of cavitation in mechanical heart valve patients.

4.2.3.1 Signal with no “tails”

The term “tail” refers to the end part of the heart beat that would be truncated by the truncation algorithm to make it the same length as the shortest heart beat of the signal. A heart beat does not have a “tail” if it is the same length as the shortest heart beat. Therefore, a signal with no “tails” means that all the heart beats in the signal have the same length.

For example, the figure below is a continuous signal with no “tails”:

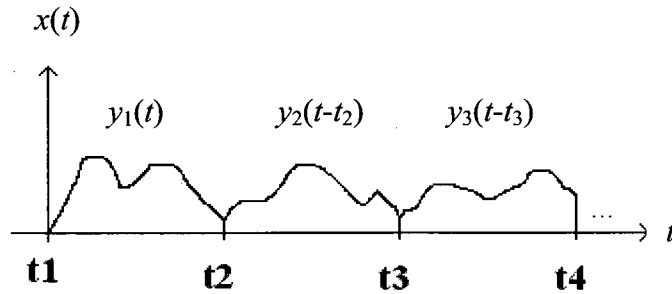


Figure 19: Signal with no "tails"

As mentioned previously, $y_n(t)$ represents a heart beat shifted to the left by t_n . The graph in Figure 19 represents the original signal; therefore, it is not of interest to have all heart beats superimposed one over the other. Hence, the heart beats are shifted back to their original position. That is why $y_2(t)$ is shifted to the right by t_2 , $y_3(t)$ is shifted to the right by t_3 , and so on. The heart beat $y_1(t)$ does not need to be shifted since it is already at the right position.

In order to obtain the non-deterministic energy, the deterministic energy and the total energy need to be calculated. In this algorithm, the deterministic energy is obtained using the same method used in section 4.2.1.1. The same equation for the deterministic energy is obtained,

$$E_{\text{det}} = \int_{-\infty}^{+\infty} |z(t)|^2 dt \quad (4.54)$$

and the same results are obtained for the calculations done with two heart beats and with three heart beats (equations (4.5) and (4.9)). For three heart beats, the deterministic energy obtained is

$$\begin{aligned}
E_{det} = \int_{-\infty}^{+\infty} |z(t)|^2 dt &= \frac{1}{9} \int_0^T y_1^2(t) dt + \frac{1}{9} \int_0^T y_2^2(t) dt + \frac{1}{9} \int_0^T y_3^2(t) dt \\
&+ \underbrace{\frac{2}{9} \int_0^T y_1(t)y_2(t) dt + \frac{2}{9} \int_0^T y_1(t)y_3(t) dt + \frac{2}{9} \int_0^T y_2(t)y_3(t) dt}_{\text{Cross terms}}
\end{aligned} \tag{4.55}$$

The total energy, on the other hand, is found using a different method than the one used in section 4.2.1.2. As suggested in [9] that the total energy of the signal can be calculated from the energy density spectrum of the raw data (original signal). The steps followed to obtain the total energy are shown in the table below.

Table 7: Energy density spectrum and energy calculation steps

		Time	Frequency
Original signal		$x(t)$	$X(j\omega)$
Energy Density Spectrum			$ X(j\omega) ^2$
Energy calculation	Using Parseval's Relation [15]	$E_{total} = \int_{-\infty}^{+\infty} x(t) ^2 dt$	$E_{total} = \frac{1}{2\pi} \int_{-\infty}^{+\infty} X(j\omega) ^2 d\omega$

The total energy of the signal in Figure 19 is calculated in the time domain for n heart beats in the following calculations.

$$E_{total} = \int_{t_1}^{t_2} y_1^2(t) dt + \int_{t_2}^{t_3} y_2^2(t-t_2) dt + \int_{t_3}^{t_4} y_3^2(t-t_3) dt + \dots + \int_{t_n}^{t_{n+1}} y_n^2(t-t_n) dt \tag{4.56}$$

In order to be able to subtract the deterministic energy from the total energy, the equations need to be compatible. Therefore, the bounds of the integral of the total energy need to be modified to match the ones in the deterministic energy. Using a simple u -substitution, $u = t - t_i$, the integrals in the previous equation become

$$E_{total} = \int_0^T y_1^2(t)dt + \int_0^T y_2^2(t)dt + \int_0^T y_3^2(t)dt + \dots + \int_0^T y_n^2(t)dt \quad (4.57)$$

where T is the length of each heart beat.

The final step in the algorithm consists of finding the non-deterministic energy. The latter is calculated for three heart beats in the following calculations. Hence, only the three first terms of the total energy equation are used in the non-deterministic energy calculation. Once again, the following calculations are done in the time domain.

Three heart beats:

For three heart beats, the non-deterministic energy is given by

$$E_{non-det} = E_{total} - E_{det}$$

$$E_{non-det} = \left(1 - \frac{1}{9}\right) \int_0^T y_1^2(t)dt + \left(1 - \frac{1}{9}\right) \int_0^T y_2^2(t)dt + \left(1 - \frac{1}{9}\right) \int_0^T y_3^2(t)dt \quad (4.58)$$

$$- \underbrace{\frac{2}{9} \int_0^T y_1(t)y_2(t)dt - \frac{2}{9} \int_0^T y_1(t)y_3(t)dt - \frac{2}{9} \int_0^T y_2(t)y_3(t)dt}_{\text{Cross terms}}$$

If $y_1(t) = y_2(t) = y_3(t)$, this becomes

$$E_{non-det} = \frac{8}{3} \int_0^T y_1^2(t)dt - \frac{2}{3} \int_0^T y_1^2(t)dt = 2 \int_0^T y_1^2(t)dt \quad (4.59)$$

As observed in equation (4.58), the cross terms are present in the non-deterministic energy and are falsely considered to be cavitation. Unlike in section 4.2.1.3, if $y_1(t) = y_2(t) = y_3(t)$ in equation (4.58), the non-deterministic energy is not zero as shown in (4.59). In theory, if all the heart beats are equal and if there is no cavitation in the signal, the non-deterministic energy should be zero. This is one reason that makes the 2003 algorithm less accurate and robust than the 2004 algorithm.

Now consider the addition of a cavitation or noise component to the heartbeat signal:

$$\begin{aligned}
 y_2(t) &= y_1(t) + \underbrace{\eta_1(t)}_{\text{Cavitation/noise}} \\
 y_3(t) &= y_1(t) + \underbrace{\eta_2(t)}_{\text{Cavitation/noise}}
 \end{aligned} \quad (4.60)$$

It then follows that the non-deterministic energy becomes

$$\begin{aligned}
 E_{non-det} &= \frac{8}{9} \int_0^T y_1^2(t) dt + \frac{8}{9} \int_0^T (y_1^2(t) + 2y_1(t)\eta_1(t) + \eta_1^2(t)) dt + \frac{8}{9} \int_0^T (y_1^2(t) + 2y_1(t)\eta_2(t) + \eta_2^2(t)) dt \\
 &\quad - \frac{2}{9} \int_0^T (y_1^2(t) + y_1(t)\eta_1(t)) dt - \frac{2}{9} \int_0^T (y_1^2(t) + y_1(t)\eta_2(t)) dt \\
 &\quad - \frac{2}{9} \int_0^T (y_1^2(t) + y_1(t)\eta_1(t) + y_1(t)\eta_2(t) + \eta_1(t)\eta_2(t)) dt
 \end{aligned} \quad (4.61)$$

This simplifies to

$$\begin{aligned}
 E_{non-det} &= 2 \int_0^T y_1^2(t) dt + \frac{4}{3} \int_0^T y_1(t)\eta_1(t) dt + \frac{4}{3} \int_0^T y_1(t)\eta_2(t) dt + \underbrace{\frac{8}{9} \int_0^T \eta_1^2(t) dt + \frac{8}{9} \int_0^T \eta_2^2(t) dt}_{\text{Cavitation/noise}} \\
 &\quad - \underbrace{\frac{2}{9} \int_0^T \eta_1(t)\eta_2(t) dt}_{\text{Cavitation/noise}}
 \end{aligned} \quad (4.62)$$

Since the $y_1(t)$ term appears in the calculation for non-deterministic energy as seen in equation (4.62), the above calculations using the 2003 algorithm demonstrate that the non-deterministic energy does not represent the cavitation alone, even if the heart beats ($y_n(t)$) are well aligned at the beat superimposition step, and even if there is no random noise in the signal. The result obtained with the 2003 algorithm is not a good representation of the amount of cavitation in mechanical heart valve patients. Therefore, the 2004 algorithm is superior.

4.2.3.2 Signal with “tails”

In section 4.2.3.1, all the heart beats in the signal had the same length; therefore the signal had no “tails”. In this section, the heart beats in the signal have different lengths, and thus the signal has “tails”. In order to perform the ensemble averaging, all heart beats in the signal need to be the same length. Thus, the heart beats are truncated to have a length equal to that of the shortest heart beat of the signal. All the truncated parts of the signal are referred to as “tails”, and they vary in length from one heart beat to another.

The figure below is an example of a continuous signal with “tails”:

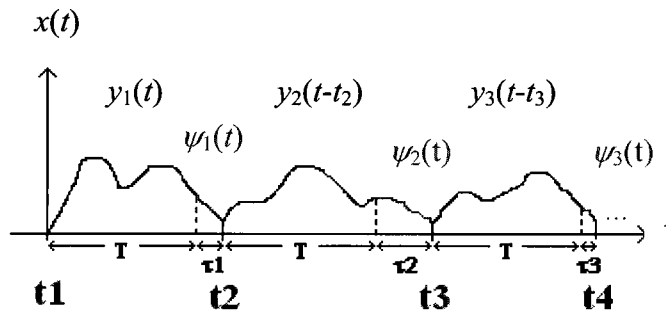


Figure 20: Signal with "tails"

where t_n represents the beginning of each heart beat, T is the length of each heart beat after truncation, τ_n represents the length of the “tail” of each heart beat, $y_n(t)$ represents each truncated heart beat in the signal, and $\psi_n(t)$ represents the “tails” in the signal ($n = 1, 2, 3, \dots$).

In order to obtain the non-deterministic energy, the deterministic energy and the total energy need to be calculated. In this section, the deterministic energy is obtained using the same method used in section 4.2.3.1. As a result, the deterministic energy obtained is the same as equation (4.54), and thus the result obtained with three heart beats

is the same as equation (4.55). Also, the total energy is obtained using the same method used in section 4.2.3.1. The total energy of the signal in Figure 20 is calculated in the time domain for n heart beats as

$$\begin{aligned}
 E_{total} = & \int_0^T y_1^2(t) dt + \underbrace{\int_T^{T+\tau_1} \psi_1^2(t) dt}_{\text{Tail}} + \int_0^T y_2^2(t) dt + \underbrace{\int_T^{T+\tau_2} \psi_2^2(t) dt}_{\text{Tail}} \\
 & + \int_0^T y_3^2(t) dt + \underbrace{\int_T^{T+\tau_3} \psi_3^2(t) dt}_{\text{Tail}} + \dots + \int_0^T y_n^2(t) dt + \underbrace{\int_T^{T+\tau_n} \psi_n^2(t) dt}_{\text{Tail}}
 \end{aligned} \tag{4.63}$$

The final step in the algorithm consists of finding the non-deterministic energy. It is calculated for three heart beats in the following calculations. Hence, only the three first terms of the total energy equation are used in the non-deterministic energy calculation.

The energy is found by integrating in the time domain.

Three heart beats:

For three heart beats and signals with tails, the non-deterministic energy is given by

$$\begin{aligned}
 E_{non-det} = & E_{total} - E_{det} \\
 = & \left(1 - \frac{1}{9}\right) \int_0^T y_1^2(t) dt + \int_T^{T+\tau_1} \psi_1^2(t) dt + \left(1 - \frac{1}{9}\right) \int_0^T y_2^2(t) dt + \int_T^{T+\tau_2} \psi_2^2(t) dt \\
 & + \left(1 - \frac{1}{9}\right) \int_0^T y_3^2(t) dt + \int_T^{T+\tau_3} \psi_3^2(t) dt - \underbrace{\frac{2}{9} \int_0^T y_1(t) y_2(t) dt - \frac{2}{9} \int_0^T y_1(t) y_3(t) dt - \frac{2}{9} \int_0^T y_2(t) y_3(t) dt}_{\text{Cross terms}}
 \end{aligned} \tag{4.64}$$

If $y_1(t) = y_2(t) = y_3(t)$, it then follows that

$$\begin{aligned}
 E_{non-det} = & \frac{8}{3} \int_0^T y_1^2(t) dt - \frac{2}{3} \int_0^T y_1^2(t) dt + \int_T^{T+\tau_1} \psi_1^2(t) dt + \int_T^{T+\tau_2} \psi_2^2(t) dt + \int_T^{T+\tau_3} \psi_3^2(t) dt \\
 = & 2 \int_0^T y_1^2(t) dt + \int_T^{T+\tau_1} \psi_1^2(t) dt + \int_T^{T+\tau_2} \psi_2^2(t) dt + \int_T^{T+\tau_3} \psi_3^2(t) dt
 \end{aligned} \tag{4.65}$$

As observed in equation (4.64) when $y_1(t) \neq y_2(t) \neq y_3(t)$, the cross terms and the tails contribute to the non-deterministic energy and are falsely considered to be cavitation. Unlike in section 4.2.1.3, even if $y_1(t) = y_2(t) = y_3(t)$ in equation (4.64), the non-deterministic energy is not zero as shown in (4.65). In theory, if all the heart beats are equal and if there is no cavitation in the signal, the non-deterministic energy should be zero. There is also an additional contribution from the tails to the non-deterministic energy which was not present in the 2004 algorithm. These reasons also make the 2003 algorithm less accurate and robust than the 2004 algorithm.

The effects of an additional noise or cavitation component to the signal are now considered. The signals are modelled as

$$\begin{aligned} y_2(t) &= y_1(t) + \underbrace{\eta_1(t)}_{\text{Cavitation/noise}} \\ y_3(t) &= y_1(t) + \underbrace{\eta_2(t)}_{\text{Cavitation/noise}} \end{aligned} \quad (4.66)$$

This gives

$$\begin{aligned} E_{non-det} &= \frac{8}{9} \int_0^T y_1^2(t) dt + \int_T^{T+\tau_1} \psi_1^2(t) dt + \frac{8}{9} \int_0^T (y_1^2(t) + 2y_1(t)\eta_1(t) + \eta_1^2(t)) dt + \int_T^{T+\tau_2} \psi_2^2(t) dt \\ &+ \frac{8}{9} \int_0^T (y_1^2(t) + 2y_1(t)\eta_2(t) + \eta_2^2(t)) dt + \int_T^{T+\tau_3} \psi_3^2(t) dt \\ &- \frac{2}{9} \int_0^T (y_1^2(t) + y_1(t)\eta_1(t)) dt - \frac{2}{9} \int_0^T (y_1^2(t) + y_1(t)\eta_2(t)) dt \\ &- \frac{2}{9} \int_0^T (y_1^2(t) + y_1(t)\eta_1(t) + y_1(t)\eta_2(t) + \eta_1(t)\eta_2(t)) dt \end{aligned} \quad (4.67)$$

which becomes

$$\begin{aligned}
E_{non-det} = & 2 \int_0^T y_1^2(t) dt + \frac{4}{3} \int_0^T y_1(t) \eta_1(t) dt + \frac{4}{3} \int_0^T y_1(t) \eta_2(t) dt + \int_T^{T+\tau_1} \psi_1^2(t) dt + \int_T^{T+\tau_2} \psi_2^2(t) dt \\
& + \int_T^{T+\tau_3} \psi_3^2(t) dt + \underbrace{\frac{8}{9} \int_0^T \eta_1^2(t) dt + \frac{8}{9} \int_0^T \eta_2^2(t) dt - \frac{2}{9} \int_0^T \eta_1(t) \eta_2(t) dt}_{\text{Cavitation/noise}}
\end{aligned} \tag{4.68}$$

The above calculations using the 2003 algorithm demonstrate that the non-deterministic energy does not represent the cavitation alone, even if the heart beats $(y_1(t), y_2(t), \dots)$ are well aligned at the beat superimposition step, and even if there is no random noise in the signal. The non-deterministic energy also depends on $y_1(t)$ and the tails as shown in (4.68). The result obtained with the 2003 algorithm is not a good representation of the amount of cavitation in mechanical heart valve patients. Therefore, the 2004 algorithm is superior.

4.3 Discussion of the results in terms of the analysis

As demonstrated in section 4.2, one of the factors affecting the non-deterministic energy result is the signal noise which is random, and thus contributes to the non-deterministic energy. Some other factors making the non-deterministic energy non-zero come into play and are discussed in this section.

The first factor to be discussed that made the non-deterministic energy non-zero in section 4.1 is the misplaced heart beats. This is a factor that applies to both Johansen's 2004 and 2003 algorithms.

The quality of the segmentation of the heart signal has a large impact on how well the heart beats are superimposed. If the segmentation is poorly done, the heart beats will not line up properly. The impact was demonstrated analytically in section 4.2. It was

shown that if the beats are not properly superimposed, the beats that are not lined up will have an impact on the non-deterministic result, which might be falsely interpreted as a greater level of cavitation in the signal. In that case, the non-deterministic energy is *not* a measure of cavitation alone. Figure 21 illustrates a zoomed in view of Figure 8, the superimposed heart beats of the signal.

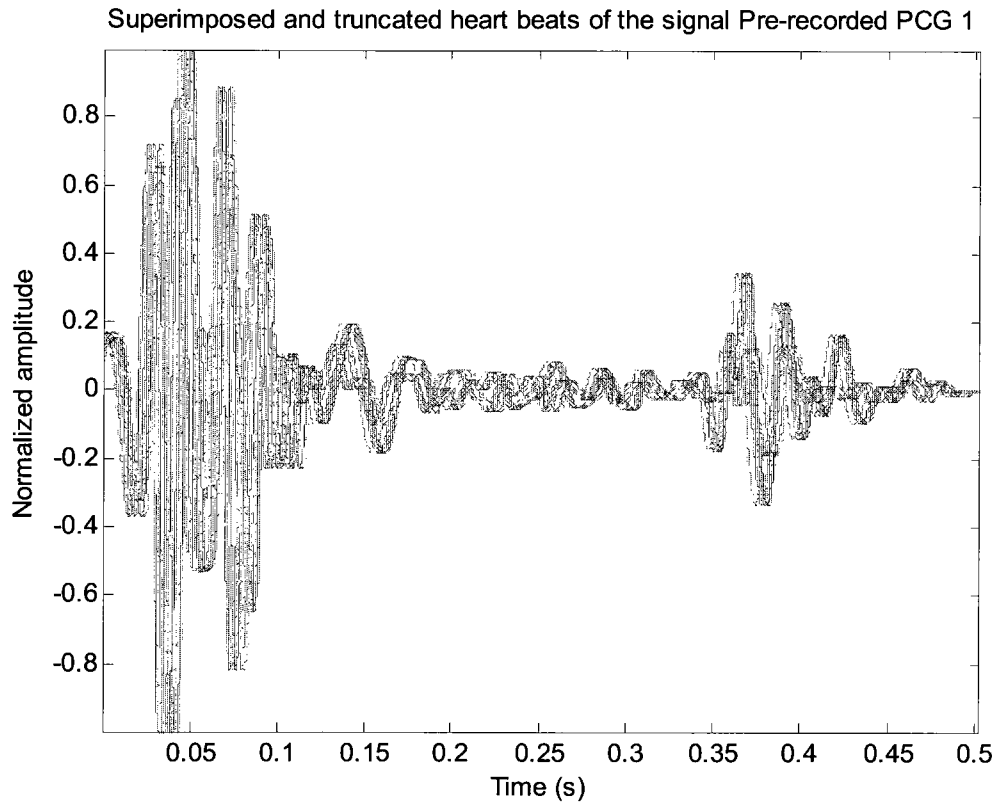


Figure 21: Zoomed in view of the superimposed heart beats in Figure 8

From Figure 21, it is possible to see that some heart beats are not perfectly superimposed. Therefore, it would be of interest to implement an algorithm that aligns the heart beats in the signal to improve the accuracy of the cavitation quantification algorithm. An alignment algorithm has been proposed; explanations and results are presented in chapter 5. As will be seen in chapter 5, this addition greatly improved the non-deterministic

energy results confirming that the misplaced heart beats was a factor that contributed to obtaining a non-deterministic energy value bigger than zero.

An important finding about Johansen's 2003 algorithm without tails and with tails was made in section 4.2. It was that even if the heart beats were perfectly superimposed ($y_1(t) = y_2(t) = y_3(t)$) and that there was no cavitation/noise added to the signal, the non-deterministic energy was not zero. This is the first explanation why the non-deterministic energy values using Johansen's 2003 algorithm were bigger than when using Johansen's 2004 algorithm.

Another factor to be discussed that made the non-deterministic energy non-zero in section 4.1 is the "tails". This is a factor that applies to Johansen's 2003 algorithm only. This also explains why the non-deterministic energy values using Johansen's 2003 algorithm were bigger than when using Johansen's 2004 algorithm.

When calculating the total energy with Johansen's 2004 algorithm, the heart beats are truncated as for the deterministic energy. Therefore, the heart beats are the same length for both the total energy and the deterministic energy. However, when calculating the total energy with Johansen's 2003 algorithm, the original heart signal is used and not the truncated signal. Thus, the truncated portions of the signal ("tails") are retained for the total energy calculation resulting in a larger value of total energy. This implies that the non-truncated portions of the signal contribute to the non-deterministic energy and are falsely considered to be cavitation. As a result, it is observed in Table 1 that the non-deterministic energy calculated with Johansen's 2003 algorithm is larger than that calculated with Johansen's 2004 algorithm. Given all these observations, one can safely conclude that Johansen's 2004 algorithm is superior.

Chapter 5: Improvements and new algorithm

In the previous chapter, it was demonstrated in the closed-form mathematical analysis that Johansen's 2004 algorithm can work as an effective tool to measure cavitation in a signal that essentially repeats. However, it was also shown that poor segmentation of the heart signal and any error in perfectly lining up the heartbeats will lead to a spurious contribution to the non-deterministic energy which could lead to a false indication of additional cavitation in the signal. In order for the non-deterministic energy to be a better representation of the cavitation in a heart signal, this chapter presents improvements to Johansen's algorithm and a new algorithm.

5.1 Improvements to Johansen's algorithm

5.1.1 Segmentation algorithm

The segmentation and alignment method proposed by Johansen in [9] and [10] was a cross-correlation of each heart beat with a chosen template heart beat. The time delay calculated in the cross-correlation was said to enable alignment with reference to the chosen template. However, the characteristics that the template must have were not specified in Johansen's paper. It was not mentioned whether the beats were lined up with the first heart sound (S1) or with the second heart sound (S2) of the template. The time between the occurrence of S1 and S2 in a heart beat generally varies from beat to beat meaning that only one of the two can be aligned with the template. Additionally, it was

not indicated if the template was obtained from the patient itself or from an idealized signal. The results obtained by Johansen could not be reproduced; therefore, another segmentation algorithm was developed which was introduced in Chapter 3, section 3.1.2.

Other heart sound segmentation methods have been introduced using techniques such as the wavelet transform [16, 17], Shannon energy [16-18], mel-frequency cepstral coefficients (MFCC) [16, 19], and the mel-scaled wavelet transform (MSWT) [19]. The segmentation algorithm used in this thesis is the method suggested in [12], which was developed by Karim Courtemanche (Appendix A). In summary, this algorithm used the wavelet transform and Shannon energy techniques in combination with the heart rate approximation to identify the first heart sound component S1 in the stethoscope signal. That information was then used to segment the stethoscope signal at the beginning of each S1 (at the zero-crossing point where the S1 starts) in the heart beats.

A pre-recorded stethoscope test signal was used in the segmentation algorithm suggested in [12]. Firstly, the S1 heart sound components were identified as illustrated in Figure 22. Figure 22 is the Shannon energy plot of the heart signal in Figure 23. Then, the segmentation points were identified as the zero-crossing points at the beginning of each S1, and *not* as the peak of S1. The segmentation points are illustrated in Figure 23 on the pre-recorded stethoscope test signal. These segmentation points were then used to segment the hydrophone signal since the stethoscope and hydrophone data were collected simultaneously. The segmentation of the hydrophone signal is the first step of the cavitation quantification algorithm.

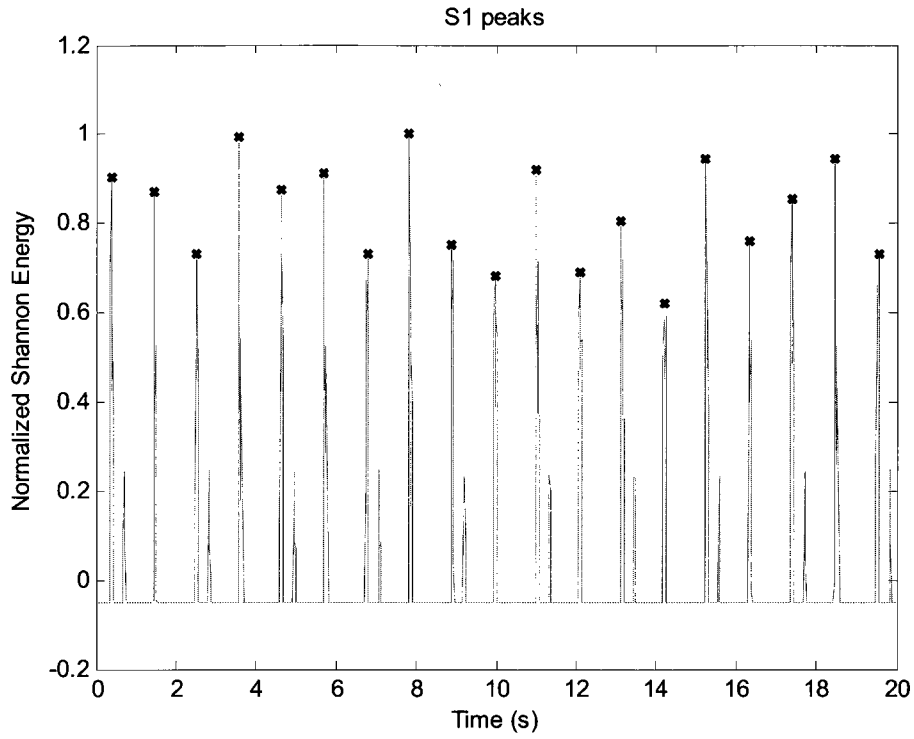


Figure 22: S1 peaks are identified and marked as 'x'

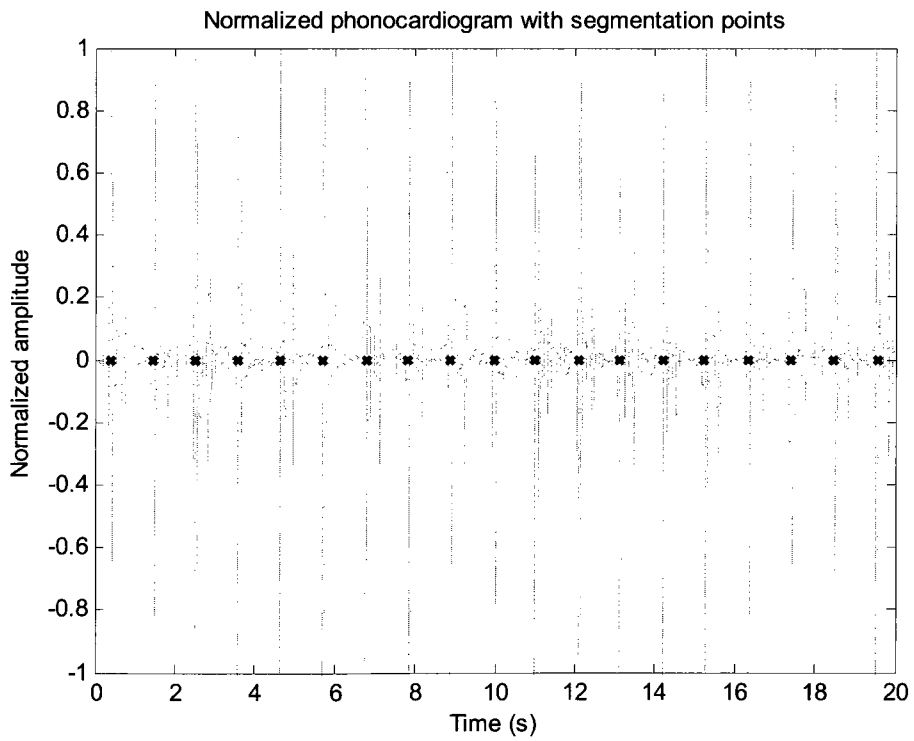


Figure 23: Pre-recorded stethoscope test signal with segmentation points

5.1.2 Energy in the “tails”

Once the hydrophone signal was segmented, each heart beat was truncated for all beats to have the same length. The end part of the beats was truncated since no important information is located there. Those truncated parts are called “tails”, and they vary in length from one heart beat to another since the length of the heart beats themselves is slightly different from beat to beat. Although the “tails” contain no important information, they contain information which has an energy attributed to it. The “tails” do not have an effect on the non-deterministic energy using Johansen’s 2004 algorithm since the heart beats for both the deterministic energy and total energy are truncated, thus making the heart beats the same length for both energy calculations. However, the “tails” have an effect on the non-deterministic energy using Johansen’s 2003 algorithm since the original hydrophone signal is used for the total energy instead of the truncated signal. Thus, the “tails” are retained for the total energy calculation resulting in a larger value of total energy. This implies that the non-truncated portions of the signal contribute to the non-deterministic energy and are falsely considered to be cavitation. From this observation, one can conclude that Johansen’s 2004 algorithm is superior to Johansen’s 2003 algorithm in terms of attempting to capture the true ‘cavitation content’ of a given signal.

The energy in the “tails” was calculated in the improved algorithm written in MATLAB to show its impact on the non-deterministic energy using Johansen’s 2003 algorithm. The results are then compared with the non-deterministic energy obtained using Johansen’s 2004 algorithm. Usually, a hydrophone signal would be used for this section. But for the first set of results, the same pre-recorded stethoscope test signal as

used previously (Pre-recorded PCG 1) was used since it is less noisy than the hydrophone signals and because a stethoscope signal should not contain a cavitation component since it records low frequency sounds. This means that the non-deterministic energy result should theoretically be near zero. A sampling frequency of 44.1 kHz was used.

The energy in the “tails” was calculated in volts squared. For the pre-recorded stethoscope test signal, it was calculated in MATLAB to be 73.8599. The deterministic, total, and non-deterministic energy results obtained using Johansen’s two algorithms are compared in Table 8.

Table 8: Results of the energy obtained with Johansen's two algorithms using the stethoscope signal

Algorithm used	Energy		
	Deterministic energy	Total energy	Non-deterministic energy
Johansen’s 2003 algorithm	266.4151	$1.9026 \cdot 10^4$	$1.8760 \cdot 10^4$
Johansen’s 2004 algorithm	266.4151	994.0005	727.5855

Subtracting the energy in the “tails” from the non-deterministic energy in Johansen’s 2003 algorithm, one would obtain $1.8686 \cdot 10^4$. That value is still far from the non-deterministic energy value obtained with Johansen’s 2004 algorithm. But as explained in section 4.2.3, the cross terms also contribute to the non-deterministic energy in Johansen’s 2003 algorithm and are most likely responsible for the difference in the values. The non-deterministic energy value obtained using Johansen’s 2004 algorithm is more accurate than the value obtained using Johansen’s 2003 algorithm since it is a smaller number which is a better representation of the absence of cavitation.

Then, a hydrophone signal was used in the algorithm to calculate the energy in the “tails”. A hydrophone signal is what is usually used in this algorithm since a hydrophone

can record high frequency sounds including cavitation. That hydrophone signal (MHV Recording 1) was acquired at the University of Ottawa Heart Institute during the first in vitro recording done with a St. Jude Medical bileaflet mechanical heart valve in the aortic position (refer to Chapter 6 for the experimental trials). A sampling frequency of 44.1 kHz was used.

The energy in the “tails” was calculated in volts squared. For the hydrophone signal, it was calculated in MATLAB to be 31.5936. The deterministic, total, and non-deterministic energy results obtained using Johansen’s two algorithms are compared in Table 9.

Table 9: Results of the energy obtained with Johansen’s two algorithms using the hydrophone signal

Algorithm used	Energy		
	Deterministic energy	Total energy	Non-deterministic energy
Johansen’s 2003 algorithm	25.3096	$1.3957 \cdot 10^4$	$1.3931 \cdot 10^4$
Johansen’s 2004 algorithm	25.3096	593.7318	568.4222

By subtracting the energy in the “tails” from the non-deterministic energy in Johansen’s 2003 algorithm, one would obtain a non-deterministic energy of $1.3899 \cdot 10^4$ without the “tails”. That value is still far from the non-deterministic energy value obtained with Johansen’s 2004 algorithm. But as explained in section 4.2.3, the cross terms also contribute to the non-deterministic energy in Johansen’s 2003 algorithm and are most likely responsible for the difference in the values.

The above results demonstrated that there is energy in the “tails” and that they do have an effect on the non-deterministic energy in Johansen’s 2003 algorithm. From these results and the mathematical analysis done in Chapter 4, it is possible to conclude that

Johansen's 2003 algorithm is less accurate and less robust than Johansen's 2004 algorithm; and thus Johansen's 2004 algorithm is superior. For the rest of this thesis, Johansen's 2004 algorithm will be used in the simulations.

5.1.3 Calculation of the energy in the time domain

In Chapter 4, the steps in Johansen's algorithms were written in the time domain and in the frequency domain. It was shown that the deterministic energy and total energy could be calculated in both the time and frequency domain using Parseval's relation. This section will investigate if the energies can be calculated in the time domain with the algorithm coded in MATLAB.

Up until now, the deterministic energy and total energy were calculated in the frequency domain. The Fourier Transform was used to find the energy density spectrum of the signal from which the energy was calculated. To do that, the MATLAB function "fft" was used which is the Discrete Fourier Transform operation. To find the deterministic energy and total energy in the time domain, Parseval's relation was used. Parseval's relation for the Discrete Fourier Transform states that

$$\sum_{n=0}^{N-1} |x[n]|^2 = \frac{1}{N} \sum_{k=0}^{N-1} |X[k]|^2 \quad (5.1)$$

where N is the number of samples [20]. The algorithm that finds the energies in the time domain follows the same steps as the one that finds them in the frequency domain up until the ensemble averaging step. To find the energy in the time domain, the magnitude of the ensemble average (in time) is squared and then summed. This step replaces the frequency domain step of taking the sum of the squared magnitudes of the Discrete Fourier Transform of the ensemble average and dividing the whole equation by N. These

changes were made to the algorithm in MATLAB, and the exact same results were obtained with both versions of the algorithm. The results using Johansen's 2004 algorithm are summarized in Table 10.

Table 10: Comparison of the results obtained with Johansen's 2004 algorithm in both the time and frequency domain

Signal used	Domain	Energy		
		Deterministic energy	Total energy	Non-deterministic energy
Pre-recorded PCG 1	Time	266.42	994.00	727.59
	Frequency	266.42	994.00	727.59
Pre-recorded PCG 2	Time	106.21	898.09	791.88
	Frequency	106.21	898.09	791.88
Pre-recorded PCG 3	Time	432.08	$1.52 \cdot 10^3$	$1.09 \cdot 10^3$
	Frequency	432.08	$1.52 \cdot 10^3$	$1.09 \cdot 10^3$
MHV Recording 1	Time	25.31	593.73	568.42
	Frequency	25.31	593.73	568.42

As observed in Table 10, whether the energies are calculated in the time domain or in the frequency domain, the same result is obtained. For signals with large N, this observation can provide significant computational savings as there is no need to calculate the FFT of the signal to obtain the signal energy.

5.1.4 Aligning the S1 peaks in the signal

As previously mentioned, it was observed that Johansen's algorithm greatly depends on the quality of the heart signal segmentation. The quality of the segmentation has a large impact on how well the heart beats are superimposed. If the segmentation is poorly done, the heart beats will not line up properly. Figure 24 illustrates the superimposed heart beats of the pre-recorded stethoscope test signal used previously (Pre-recorded PCG 1). The first large peak of activity in the heart beats of Figure 24 is the first heart sounds (S1) and the second peak of activity is the second heart sounds (S2).

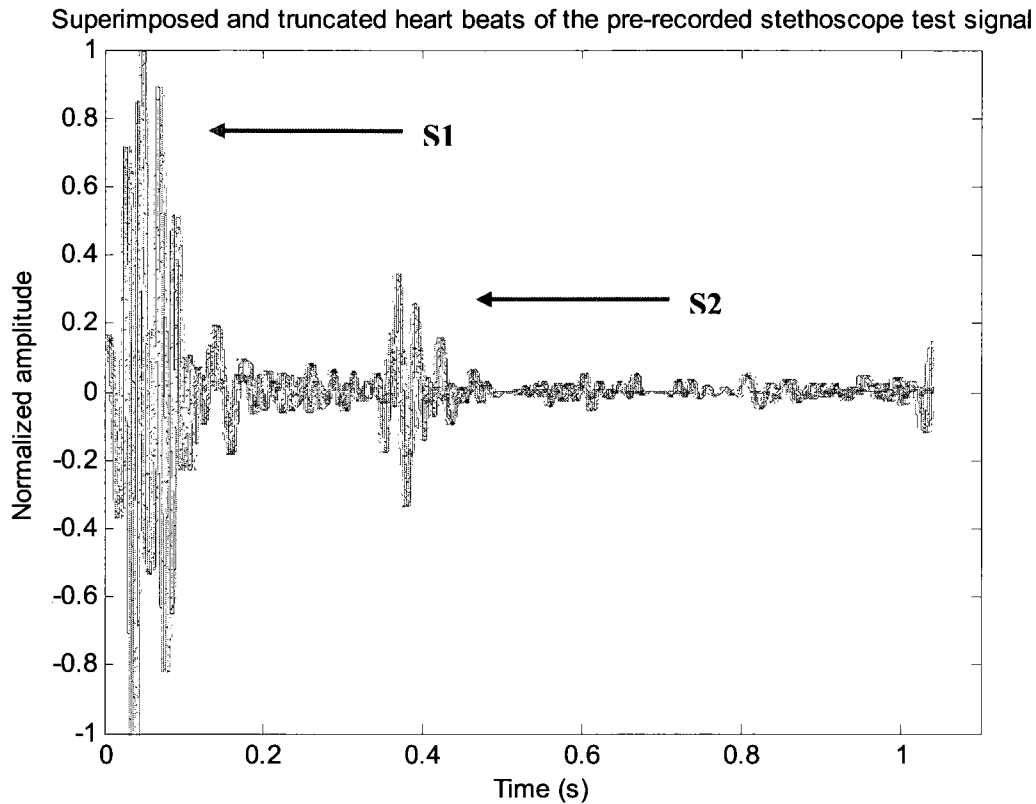


Figure 24: Superimposed heart beats of the pre-recorded stethoscope test signal

The heart beats in Figure 24 are not perfectly lined up, which is not surprising since perfect alignment is practically impossible as the heart does not produce a perfectly periodic heart signal. Therefore, an improvement was proposed so as to align all the S1's in the heart signal after all the heart beats have been superimposed. To do this, the maximum peak of the first quarter of each heart beat, which is the peak of S1, was determined. The S1 is usually contained in the first quarter of the heart beat. The algorithm searches for the maximum peak in the first quarter of the heart beat instead of in the entire heart beat since the S2 peak can sometimes be higher than the S1 peak, in which case MATLAB would detect the S2 peak as the maximum peak instead of S1. After the S1 peaks were found for each individual heart beat, each heart beat was shifted to the left or to the right to line up with the S1 of the first heart beat of the heart signal.

Once all the S1's were lined up, the beginning or the end of the heart beats were truncated so that all the beats have the same length. The larger the shift, the more the heart beat is going to be truncated. As mentioned later in this sub-section, the beats that require a very large shift compared to the other beats are eventually removed from the heart signal since it is considered a 'bad' heart beat. Too much of that heart beat would be truncated after shifting; hence, too much information would be lost. Figure 25 illustrates the superimposed heart beats of the pre-recorded stethoscope test signal before the S1's were aligned, with the S1 peaks marked with red circles.

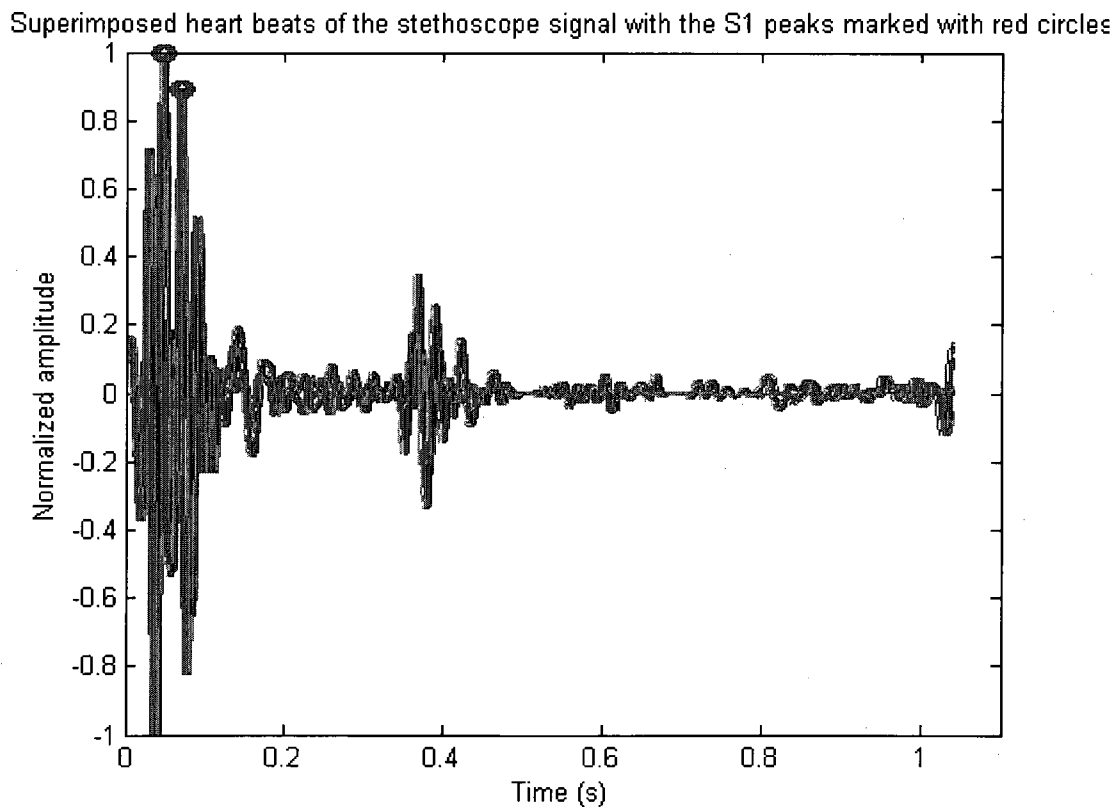


Figure 25: Superimposed heart beats of the pre-recorded stethoscope test signal before the S1's were aligned

Figure 26 illustrates the ensemble average of the heart beats without the S1's aligned; in other words the ensemble average of Figure 25.

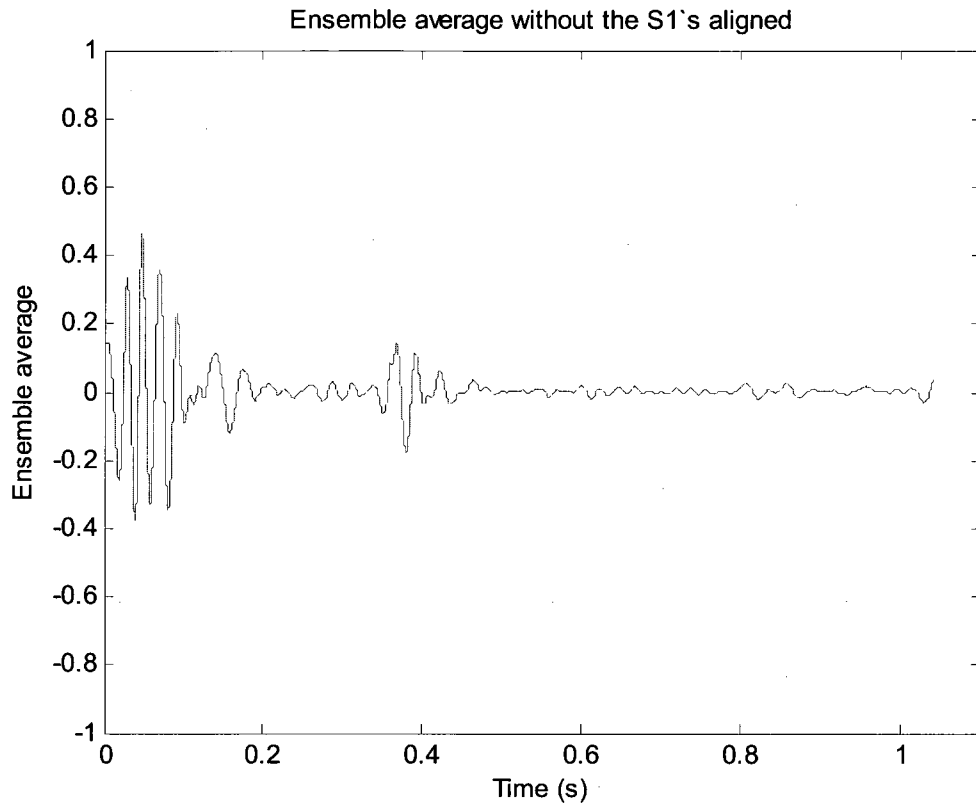


Figure 26: Ensemble average of the heart beats without the S1's aligned

Figure 27 illustrates the superimposed heart beats of the pre-recorded stethoscope test signal after the S1's were aligned, with the S1 peaks marked with red circles. It is observed in Figure 27 that the red circles are aligned; this means that the S1 peaks were properly aligned.

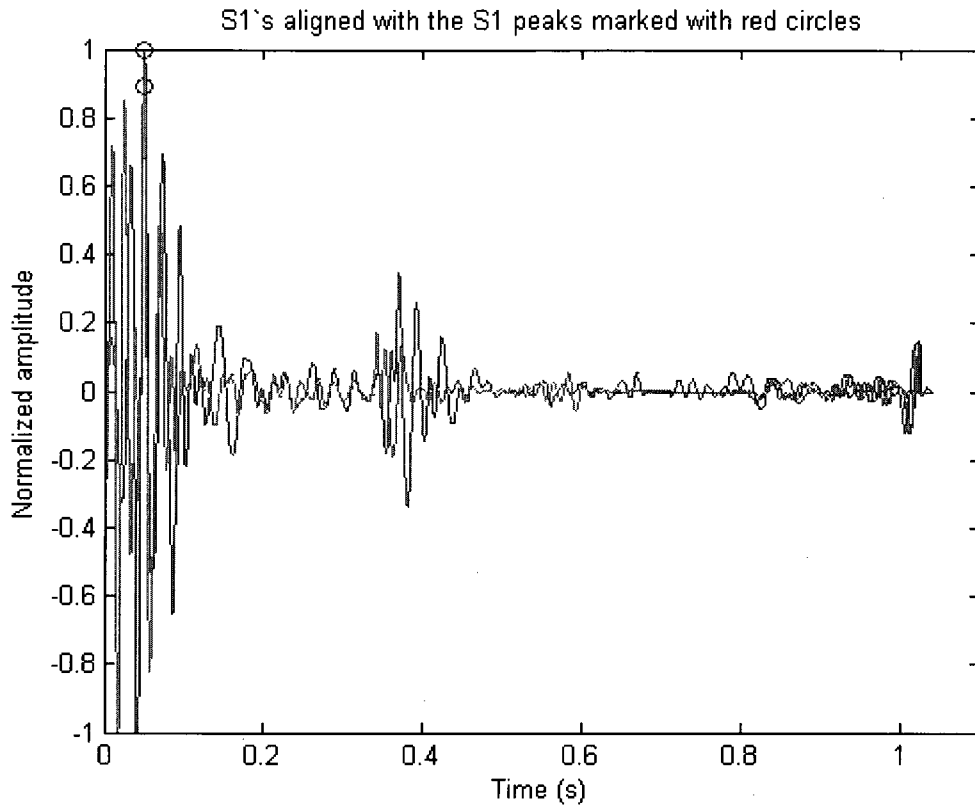


Figure 27: Superimposed heart beats of the pre-recorded stethoscope test signal after the S1's were aligned

Figure 28 illustrates the ensemble average of the heart beats with the S1's aligned; in other words the ensemble average of Figure 27.

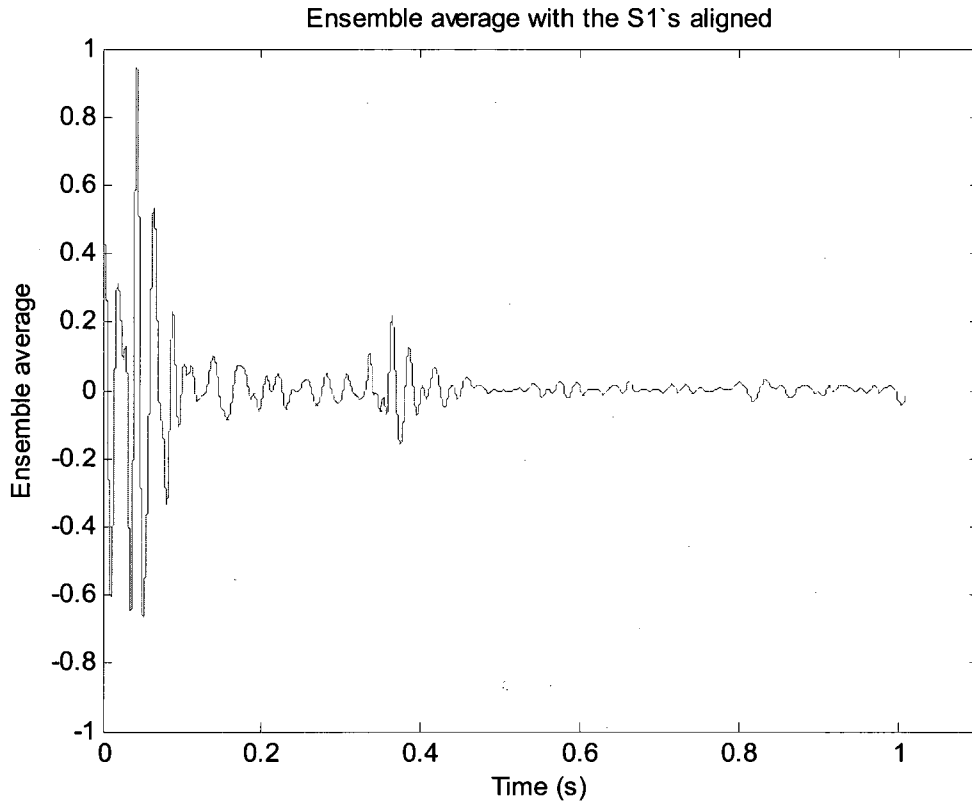


Figure 28: Ensemble average of the heart beats with the S1's aligned

Comparing the ensemble average signals of Figure 26 and Figure 28, one can observe that the peak value of S1 and S2 are larger in Figure 28. That is because the misplaced heart beats in Figure 25 reduce the value of the ensemble average. The more signals are lined up, the higher the ensemble average will be.

The lower ensemble average value impacts the deterministic energy by reducing its value, which in turn impacts the non-deterministic energy value. Therefore, the misplaced heart beats have an impact on the energy results. To demonstrate the impact, the simulations were done with and without the S1's aligned; Table 11 shows the energy results and the percentage of non-deterministic energy in the signal. The percentage of non-deterministic energy in the signal is found from equation (5.2),

$$\% = \frac{E_{\text{non-det}}}{E_{\text{total}}} \times 100 \quad (5.2)$$

where $E_{\text{non-det}}$ is the non-deterministic energy and E_{total} is the total energy. In addition to the four signals used in the previous sub-section, an in vivo stethoscope signal that was recorded by Karim Courtemanche (Karim stethoscope signal 1) was used in the algorithm. The sampling frequency used for the stethoscope signals and for the hydrophone signal was 44.1 kHz.

Table 11: Comparison of the results obtained with and without the S1's aligned

Signal used	S1	% of non-det energy	Energy		
			Deterministic energy	Total energy	Non-deterministic energy
Pre-recorded PCG 1	Not aligned	73.20	266.42	994.00	727.59
	Aligned	35.18	624.23	962.98	338.76
Pre-recorded PCG 2	Not aligned	88.17	106.21	898.09	791.88
	Aligned	6.82	836.76	897.99	61.23
Pre-recorded PCG 3	Not aligned	71.59	432.08	1.52×10^3	1.09×10^3
	Aligned	47.81	781.33	1.50×10^3	715.65
Karim stethoscope signal 1	Not aligned	51.29	229.67	471.52	241.85
	Aligned	48.40	225.76	437.49	211.73
MHV Recording 1	Not aligned	95.74	25.31	593.73	568.42
	Aligned	77.81	130.89	589.89	458.99

Comparing the results obtained with and without the S1's aligned, one can observe in Table 11 that for the first four signals, the results improved with the S1's aligned. The percentage was lower with the S1's aligned which is a better representation

of the absence of cavitation. The misplaced heart beats were causing the large difference in percentages between the signal with the S1's aligned and the one without the S1's aligned which confirms that the poorly lined up beats have an impact on the results. Johansen's algorithm is thus very sensitive to the lining up issues and greatly depends on the quality of the segmentation algorithm. The results were also improved with the S1's aligned in the fifth signal. However, hydrophone signals are very noisy; therefore the percentage remains high. Additionally, since that signal was a hydrophone recording of the mechanical heart valve, it could possibly have a cavitation component in it which could possibly be another explanation for the higher percentage. More details about this signal are provided in chapter 6.

Test for the quality of the segmentation

This improvement to the algorithm can also be used as a test of the quality of the segmentation by looking at the S1 shift values. Whether the quality of the input heart signal was bad or the segmentation was poorly done, the algorithm helps the user to choose whether to discard the signal if the majority of the S1 shifts are too large, or to simply remove the beats that require a large S1 shift.

To demonstrate the functionality of this test, it will be tested on the five signals used previously and the results will be gathered in Table 14. The steps will first be described in detail below for the first signal (Pre-recorded PCG 1).

The shifts required to align all the S1 peaks with the S1 peak of the first heart beat of the heart signal are shown in Table 12. The shift number represents the number of samples by which the beat needed to be shifted. A negative number represents a left shift

and a positive number represents a right shift. There are 18 beats in the stethoscope signal (Pre-recorded PCG 1).

Table 12: Shifts for the signal Pre-recorded PCG 1

Heart beat number	Shift in samples
1	0
2	-679
3	102
4	-1018
5	33
6	-1087
7	135
8	-985
9	271
10	-849
11	-68
12	-747
13	304
14	-816
15	-35
16	-714
17	61
18	-1059

In this signal, there are a total of 44,474 samples (1.0085 sec) in each heart beat after truncation. The average shift in samples is 497.94 (11.29 msec) and the standard deviation in the shifts in samples is 417.78 (9.47 msec). The cutoff for the Pre-recorded PCG 1 signal was chosen to be a shift of 1000 (22.67 msec) as the majority of heart beats had shifts of less than 1000. The sign of the shift represents the direction, therefore the absolute value of the shift number is considered. Any beat with a shift larger than 1000 will be removed prior to calculation of any energies. Thus, beats number 4, 6 and 18 were removed in the above stethoscope signal. Table 13 shows the energy results and the percentage of non-deterministic energy in the stethoscope signal with all the beats, and with the three beats removed.

Table 13: Energy results for the Pre-recorded PCG 1 signal with all beats and with three beats removed

Signal used	Beats	% of non-det energy	Energy		
			Deterministic energy	Total energy	Non-deterministic energy
Pre-recorded PCG 1	All beats	35.18	624.23	962.98	338.76
	Beats 4, 6 and 18 removed	33.11	656.68	981.71	325.03

Now, the average shift in samples is 386.60 and the standard deviation in the shifts in samples is 363.41. Comparing the results obtained with all beats and with three beats removed, one can observe that the results were slightly improved with removed beats. The beats were removed prior to the ensemble averaging; therefore, the heart beats were better aligned when the averaging was done which resulted in a greater deterministic energy value. This in turn reduced the non-deterministic energy value, which reduced the percentage of non-deterministic energy. The lower percentage is a better representation of the absence of cavitation.

The same steps are now accomplished with the four remaining signals and the results are summarized in Table 14. It includes the energy results and the percentage of non-deterministic energy for four different signals with all the beats included, and with some beats removed. The cutoff for the signal Pre-recorded PCG 2 was chosen to be a shift of 250 as the majority of heart beats had shifts of less than 250. The shift values for this signal were much smaller than the one for the signal Pre-recorded PCG 1. The cutoff for the signal Pre-recorded PCG 3 was chosen to be a shift of 770, and for the signal Karim stethoscope signal 1, it was chosen to be 500. Finally, the cutoff for the signal MHV Recording 1 was chosen to be a shift of 850. The cutoff values for each signal were

chosen by evaluating the shift values; the ones that were large compared to the others were removed, which explains why every signal has a different number of beats removed.

Table 14: Results obtained with all beats and with some beats removed

Signal used (samples in HB)	Beats	Ave shift (sam- ples)	STD shift (sam- ples)	% of non-det energy	Energy		
					Det energy	Total energy	Non-det energy
Pre- recorded PCG 2 (HB: 46671)	All beats	127.06	86.98	6.82	836.76	897.99	61.23
	Beats 2 and 6 removed	107.38	68.96	6.87	816.82	877.10	60.27
Pre- recorded PCG 3 (HB: 36672)	All beats	470.27	304.46	47.81	781.33	1.50*10 ³	715.65
	Beats 17, 20 and 21 removed	419.32	296.65	44.60	843.53	1.52*10 ³	678.99
Karim stethoscope signal 1 (HB: 34861)	All beats	117.52	280.32	48.40	225.76	437.49	211.73
	Beats 5 and 18 removed	36.89	70.89	41.86	273.14	469.80	196.66
MHV Recording 1 (HB: 36510)	All beats	499	296.24	77.81	130.89	589.89	458.99
	Beats 8, 11, 21, 22 removed	406.28	240.36	73.56	156.91	593.44	436.53

In Table 14, HB is heart beat, Ave is average, STD is standard deviation, det is deterministic and non-det is non-deterministic. Comparing the results obtained in Table 14, one can observe that the results were slightly improved with removed beats for all signals with the exception of the Pre-recorded PCG 2 signal. However, the Pre-recorded PCG 2 signal already has a very low percentage of non-deterministic energy and its shift values are very small, which is why removing some beats barely made a difference in the results. For that signal, no heart beats would need to be removed since the results were already very good. It was already a good representation of the absence of cavitation.

In conclusion, it was shown in section 5.1.4 that aligning the S1 peaks greatly improved the results. It was observed that this step is crucial when using Johansen's algorithm since it is very sensitive to the lining up issues and it greatly depends on the quality of the segmentation algorithm. Additionally, it was demonstrated that this improvement to the algorithm can also be used to test if the segmentation was successfully accomplished by looking at the S1 shift values.

5.1.5 Aligning the S2 peaks in the signal

It was shown in section 5.1.4 that the results improved by aligning the S1 peaks in the signal. This section will investigate the impact of aligning the S2 peaks instead of the S1 peaks on the results. Then, one of the two will be used in the algorithm for the remainder of the thesis.

The improvement proposed in this section is to align all the S2 peaks in the heart signal after all the heart beats have been superimposed. To do this, the maximum peak of the last three-quarters of each heart beat was determined. The S2 peak is generally contained in the last three-quarters of the heart beat. After the S2 peaks were found, they were all shifted to the left or to the right to line them up with the S2 peak of the first heart beat of the heart signal. Then, the beginning or the end of the heart beats was truncated for all beats to have the same length. The larger the shift, the more the heart beat is going to be truncated. As mentioned in the previous sub-section, the beats that require a very large shift compared to the other beats are removed from the heart signal since it is considered a 'bad' heart beat. Too much of that heart beat would be truncated after shifting; hence, too much information would be lost.

Figure 29 illustrates the superimposed heart beats of the pre-recorded stethoscope test signal before the S2's were aligned, with the S2 peaks marked with red circles.

Superimposed heart beats of the stethoscope signal with the S2 peaks marked with red circles

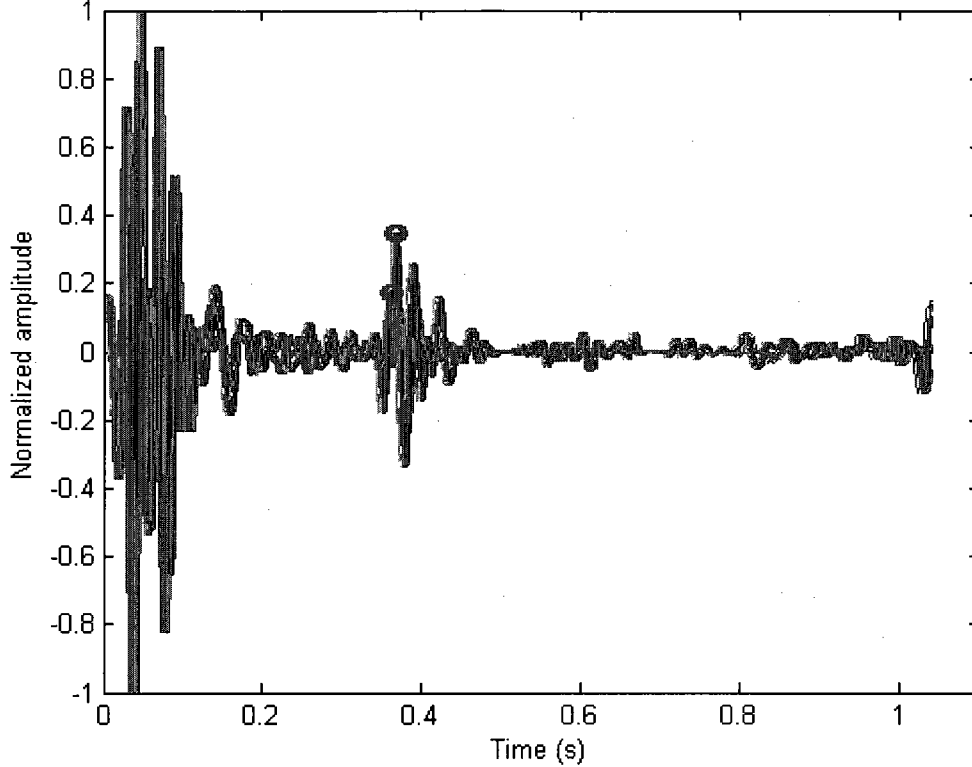


Figure 29: Superimposed heart beats of the pre-recorded stethoscope test signal before the S2's were aligned

Figure 30 illustrates the ensemble average of the heart beats without the S1's aligned; in other words the ensemble average of Figure 29.

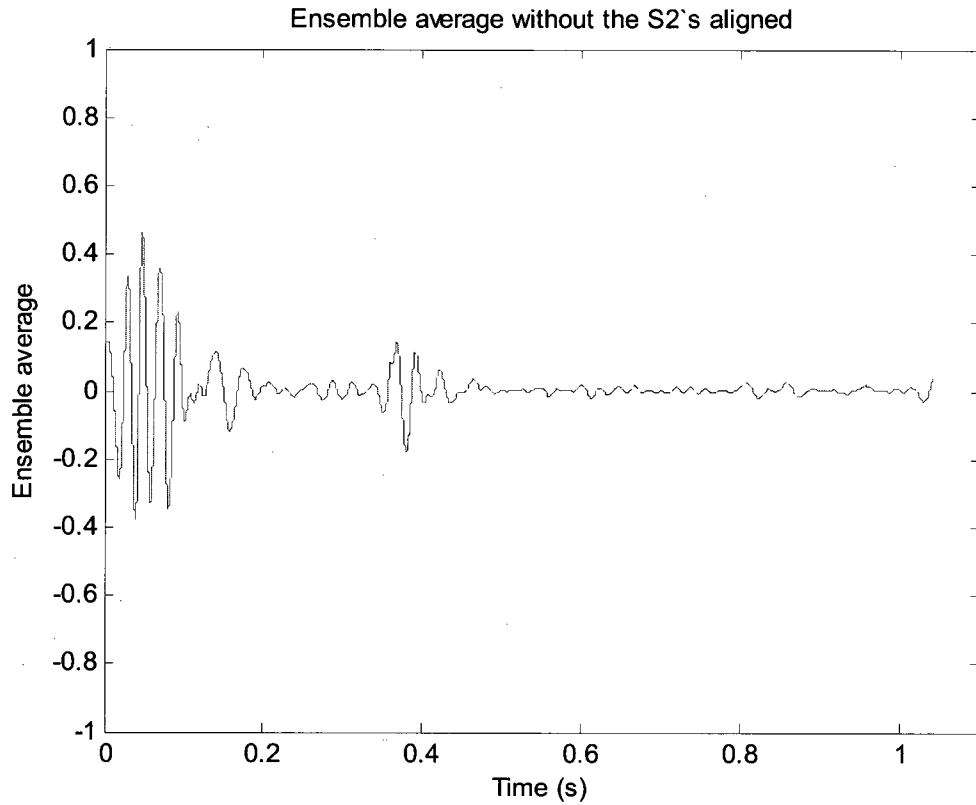


Figure 30: Ensemble average of the heart beats without the S2's aligned

Figure 31 illustrates the superimposed heart beats of the pre-recorded stethoscope test signal after the S2's were aligned, with the S2 peaks marked with red circles. It is observed in Figure 31 that the red circles are aligned; this means that the S2 peaks were properly aligned.

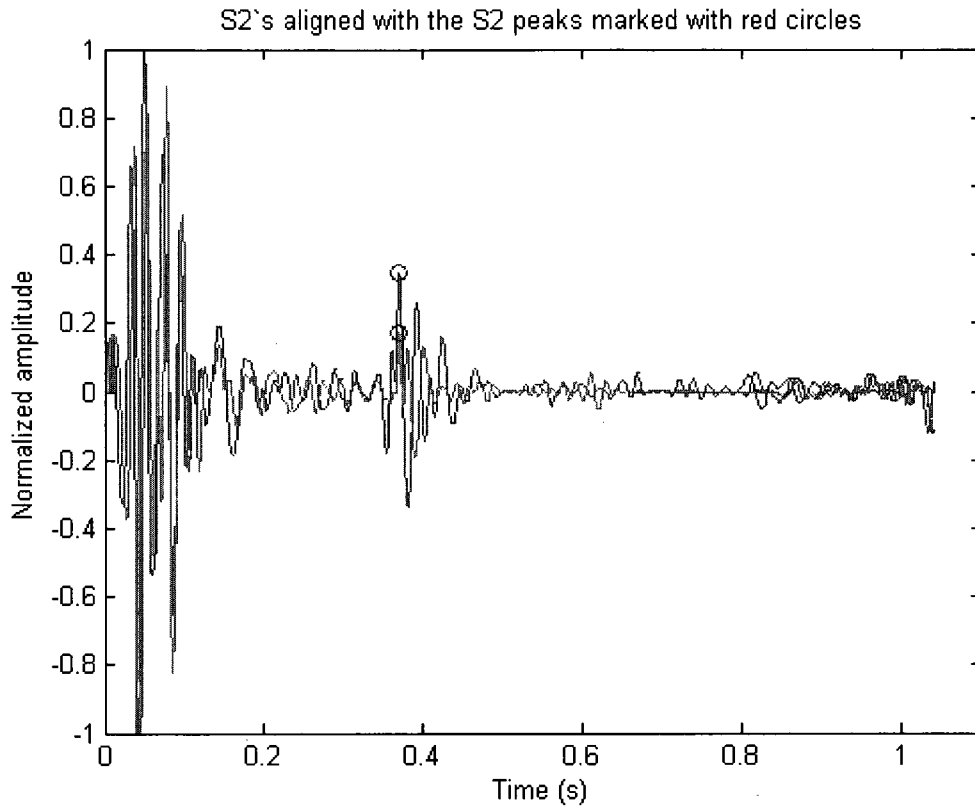


Figure 31: Superimposed heart beats of the pre-recorded stethoscope test signal after the S2's were aligned

Figure 32 illustrates the ensemble average of the heart beats with the S2's aligned; in other words the ensemble average of Figure 31.

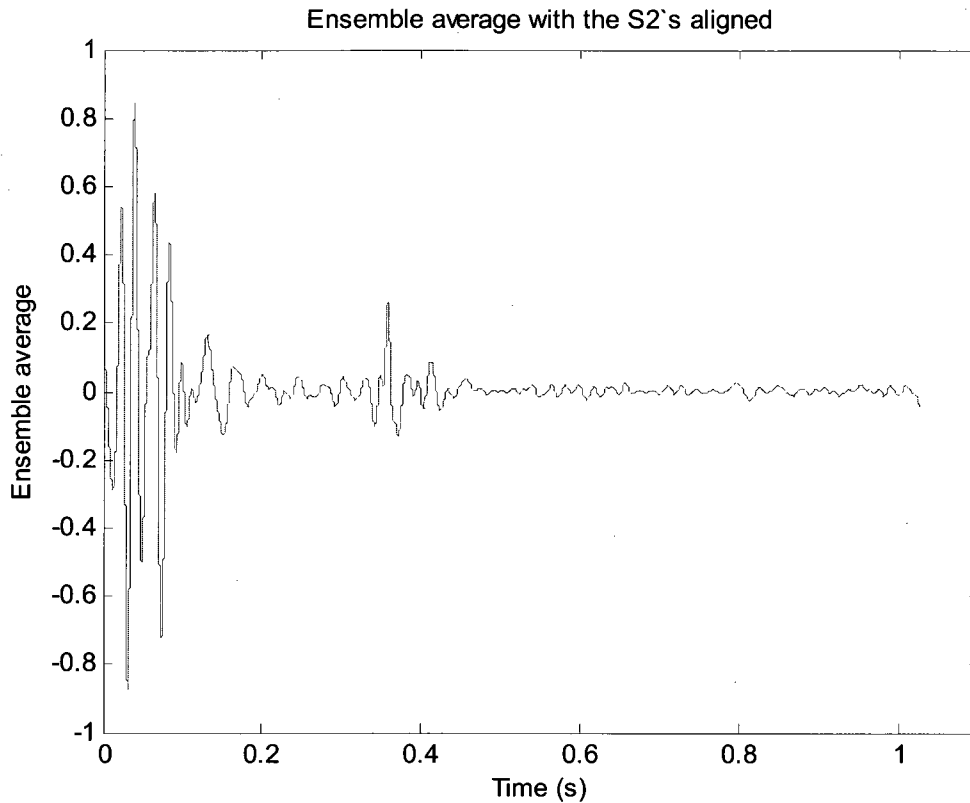


Figure 32: Ensemble average of the heart beats with the S2's aligned

Comparing the ensemble average signals of Figure 30 and Figure 32, one can observe that the peak values of S1 and S2 are larger in Figure 32. That is because the misplaced heart beats in Figure 29 reduce the value of the ensemble average. The more signals are lined up, the higher the ensemble average will be.

The lower ensemble average value impacts the deterministic energy by reducing its value, which impacts the non-deterministic energy value. Therefore, the misplaced heart beats have an impact on the energy results. To demonstrate the impact, the simulations were done with and without the S2's aligned; Table 15 showing the energy results and the percentage of non-deterministic energy in the signal. The sampling frequency used was again 44.1 kHz.

Table 15: Comparison of the energy results obtained with and without the S2's aligned

Signal used	S2	% of non-det energy	Energy		
			Deterministic energy	Total energy	Non-deterministic energy
Pre-recorded PCG 1	Not aligned	73.20	266.42	994.00	727.59
	Aligned	29.87	691.23	985.57	294.35
Pre-recorded PCG 2	Not aligned	88.17	106.21	898.09	791.88
	Aligned	6.16	842.66	897.96	55.29
Pre-recorded PCG 3	Not aligned	71.59	432.08	1.52*10 ³	1.09*10 ³
	Aligned	63.47	544.78	1.49*10 ³	946.43
Karim stethoscope signal 1	Not aligned	51.29	229.67	471.52	241.85
	Aligned	77.49	96.72	429.71	332.98
MHV Recording 1	Not aligned	95.74	25.31	593.73	568.42
	Aligned	93.21	32.05	472.10	440.05

Comparing the results obtained with and without the S2's aligned, one can observe in Table 15 that for the majority of the signals, the results were improved with the S2's aligned meaning that the percentage of non-deterministic energy was reduced. The only exception is the signal called Karim stethoscope signal 1, where the results were worse than before the alignment. The misplaced heart beats were causing the difference in percentages between the signal with the S2's aligned and the one without the S2's aligned which again confirms that the poorly lined up beats have an impact on the results. The percentage results obtained with the S1 peaks aligned and with the S2 peaks aligned are summarized in Table 16.

Table 16: Comparison of the percentage results obtained with the S1 peaks and with the S2 peaks aligned

Signal used	% of non-deterministic energy	
	S1 peaks aligned	S2 peaks aligned
Pre-recorded PCG 1	35.18 %	29.87 %
Pre-recorded PCG 2	6.82 %	6.16 %
Pre-recorded PCG 3	47.81 %	63.47 %
Karim stethoscope signal 1	48.40 %	77.49 %
MHV Recording 1	77.81 %	93.21 %

The percentage of non-deterministic energy for the two first signals was slightly better with the S2 peaks aligned rather than with the S1 peaks aligned. However, the percentage was much better for the last three signals with the S1 peaks aligned.

Additionally, for the signal called Karim stethoscope signal 1, the percentage result was slightly better with the S1 peaks aligned compared to the results with no peaks aligned, but was worst with the S2 peaks aligned.

When using the improved algorithm, the non-deterministic energy should be calculated with the S1 peaks aligned and with the S2 peaks aligned. Then, the alignment method giving the best result between the two is the one that should be used in that simulation. However, for the purpose of the thesis, the S1 peak alignment method will be used in the algorithm from now on.

5.2 New algorithm using the Short-Time Fourier Transform

5.2.1 The Short-Time Fourier Transform (STFT)

The time and frequency domains are two different ways of looking at the same signal. When using the Fourier Transform, the temporal occurrence of a specific event is lost (it resides in the phase information). Consequently, the frequency information can not be localized to a certain time. For the purpose of this research, it would be useful to have a time-frequency method that enables us to analyze and interpret the time-varying spectral contents [21]. It would be interesting to know when the high frequencies occur in the heart signal, since cavitation bubble implosion creates high-frequency pressure fluctuations when it is present. The time-frequency method proposed herein for use in the analysis of these signals is the Short-Time Fourier Transform (STFT).

Firstly, a nonstationary signal $x(t)$ is segmented into quasi-stationary parts $x_k(n)$ by applying a moving window to the signal. Then, the Fourier Transform is computed for the k^{th} segment as

$$X_k(\omega) = \sum_{n=0}^{M-1} x_k(n) \cdot e^{-j\omega n} \quad (5.3)$$

The array of spectra $X_k(\omega)$ for $k = 1, 2, \dots, K$ will describe the time-varying spectral characteristics of the signal [22]. The k^{th} segment $x_k(n)$ may be expressed as the multiplication of the signal $x(n)$ with a window function $w(n)$ which may be positioned at any time instant m . The resulting segment may be expressed as $x(n)w(n-m)$. In

practice, the Fourier Transform should not have to be computed for every possible window position, that is, for every m . To reduce the computation time, it is common practice for the adjacent windows to overlap for half of the segment samples. Overlapping is desirable in order to maintain continuity in the STFT [22]. The Fourier Transform of every segment becomes

$$X(m, \omega) = \sum_{n=0}^{M-1} x(n)w(n-m) \cdot e^{-j\omega n} \quad (5.4)$$

The expression given in (5.4) is called the Short-Time Fourier Transform. The STFT modulus square $|X(m, \omega)|^2$ is called a spectrogram [21]. In MATLAB, the spectrogram can be displayed in a 2D or 3D representation.

The limitation imposed by the use of a window is related to the uncertainty principle, which is written as

$$\Delta t \times \Delta \omega \geq \frac{1}{2} \quad (5.5)$$

where Δt is the time extent (duration) of the signal $x(t)$ and $\Delta \omega$ is the frequency extent (bandwidth) of its Fourier Transform $X(\omega)$. The limitation implies that a signal and its Fourier Transform cannot be made arbitrarily narrow. It is not possible to simultaneously obtain a high time and frequency resolution. Reducing the analysis window duration will increase the time resolution of the STFT, but will compromise the frequency resolution. On the other hand, increasing the window duration will lead to a loss in time resolution, but will increase the frequency resolution [22].

5.2.2 Using the STFT in the algorithm

There are a few advantages to using the STFT instead of the Fourier Transform in the algorithm. First, with the STFT, it is possible to know when the high frequencies occur in the heart beats by looking at the 2D and 3D spectrogram representations of the total heart signal. This is interesting for the purpose of this research since it gives an idea of when the cavitation occurs in the heart beats. Additionally, it is possible to plot the non-deterministic energy values against time with the STFT allowing visualization of the location of the non-deterministic energy in the heart beat. Finally, similar steps as used previously were followed to find the non-deterministic energy with the STFT, and it provided more information about the location of energy in the signal without complicating the algorithm.

The STFT of the signals was computed in MATLAB using the function *spectrogram* included in the *Signal Processing Toolbox*. The spectrogram is the magnitude of the STFT. The function that was used to obtain the spectrogram for the deterministic energy is as given below

$$[spec_det, f, t] = spectrogram(ens_ave, window, noverlap, nfft, Fs); \quad (5.6)$$

and the one used to obtain the spectrogram for the total energy is given by

$$[spec_total, f, t] = spectrogram(X_shifted2(:, m), window, noverlap, nfft, Fs); \quad (5.7)$$

The function *spectrogram* in (5.6) returns the spectrogram of the input signal vector *ens_ave*, the ensemble average of the superimposed heart beats of the heart signal. The function *spectrogram* in (5.7) returns the spectrogram of the input signal vector *X_shifted2* for every *m* heart beats of the heart signal. For both, the S1 peaks of the heart

beats were aligned, and no heart beats were removed from the signal as the values obtained for the percentage of non-deterministic energy were similar.

In the algorithm, the *window* was chosen to be a Hamming window of length *nfft*, where *nfft* is the FFT length. The Hamming window is the default window in MATLAB. The *noverlap* is the number of samples by which the consecutive segments overlap. The *noverlap* value was chosen to be *nfft*/2, which produces 50% overlap between segments. It was chosen by trial and error to be *nfft* = 1024 since it gave a good time resolution and an acceptable frequency resolution. In order to provide a reasonably good estimate of when the cavitation occurs in the heart beats, a better time resolution is preferred. The sampling frequency used was $F_s = 44.1$ kHz.

Each column of *spec_det* and *spec_total* contains an estimate of the short-term, time-localized frequency content of *ens_ave* and *X_shifted2*, respectively. The time increases across the columns of *spec_det* and *spec_total*, and the frequency increases down the rows [23]. In both (5.6) and (5.7), the frequency vector *f* and the time vector *t* are returned, and are used to plot the 3D spectrogram representations.

5.2.3 Results

Up until now, the deterministic energy and total energy were calculated in the frequency domain using the Fourier Transform. The Fourier Transform was used to find the energy density spectrum of the signal from which the energy was calculated. Now, the deterministic energy and the total energy will be calculated in the frequency domain using the Short-Time Fourier Transform.

The first step to obtaining the deterministic energy was to calculate the spectrogram of the ensemble average of the heart beats. Figure 33 illustrates the 3D

representation of the spectrogram of the ensemble averaged heart beat for the first pre-recorded stethoscope test signal (Pre-recorded PCG 1) which is representative of the other stethoscope signals.

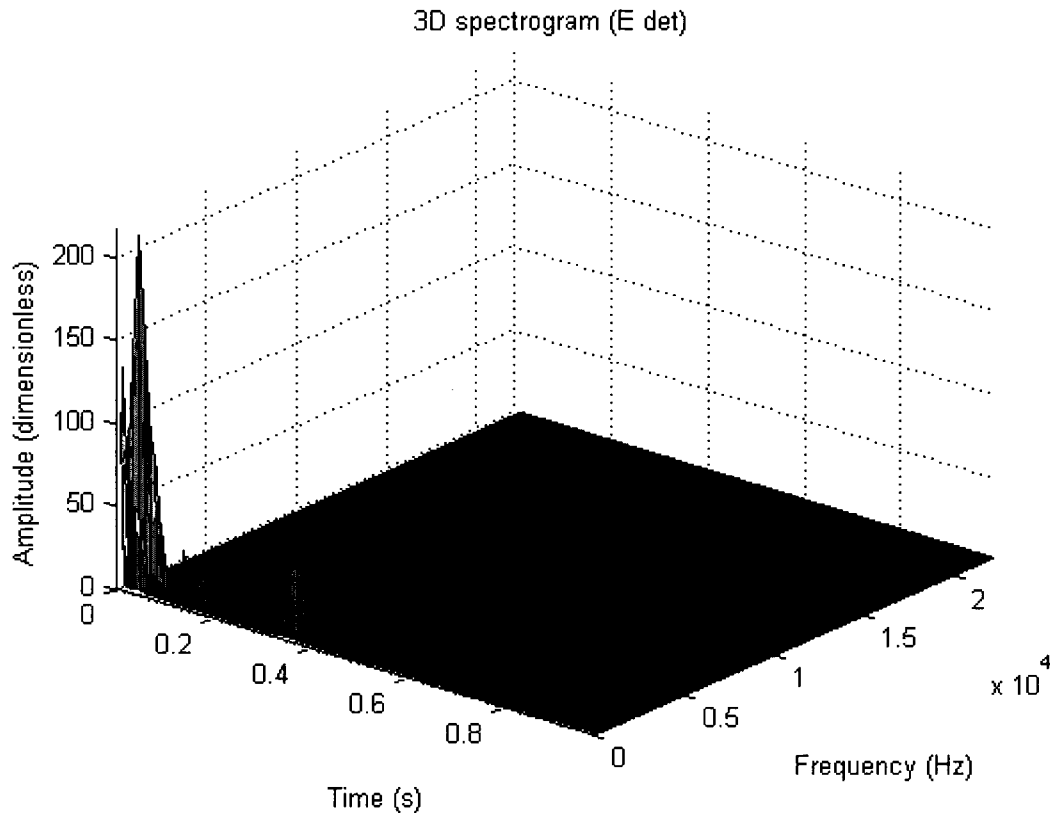


Figure 33: 3D representation of the spectrogram of the ensemble averaged heart beat for the first pre-recorded stethoscope test signal

As observed in Figure 33, no high frequencies are present since a stethoscope records low frequency sounds only. In addition to the frequency information, it is also possible to see where the S1 and S2 peaks are located in time.

The next step was to calculate the energy density spectrum of the STFT of the ensemble average, from which the deterministic energy was calculated. When the deterministic energy was calculated using the Fourier Transform, the result obtained was a single number representing the energy in the signal. However, with the STFT, the result

obtained is a time evolution of the deterministic energy in the signal. Therefore, it is possible to plot the time evolution of the deterministic energy as shown in Figure 34.

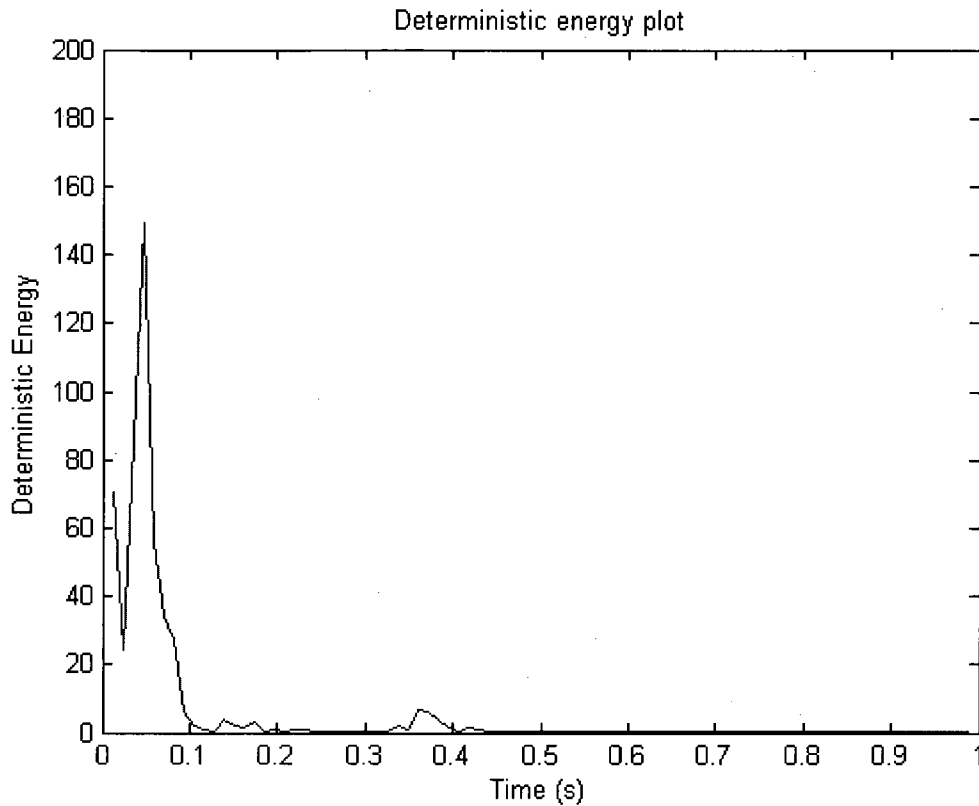


Figure 34: The time evolution of the deterministic energy

In Figure 34, the S1 and S2 peaks can be observed clearly since they are the deterministic component of the heart signal. To obtain the deterministic energy of the whole signal (as represented by a single number), the deterministic energy at each time was summed.

Once the deterministic energy is found, the total energy calculation has to be accomplished. The first step to obtaining the total energy was to calculate the spectrogram of each heart beat in the signal. Thus, for a signal with 18 heart beats, 18 spectrograms were obtained. Figure 35 illustrates the 3D representation of the first of 18 spectrograms for the first pre-recorded stethoscope test signal (Pre-recorded PCG 1) which is representative of the other stethoscope signals.

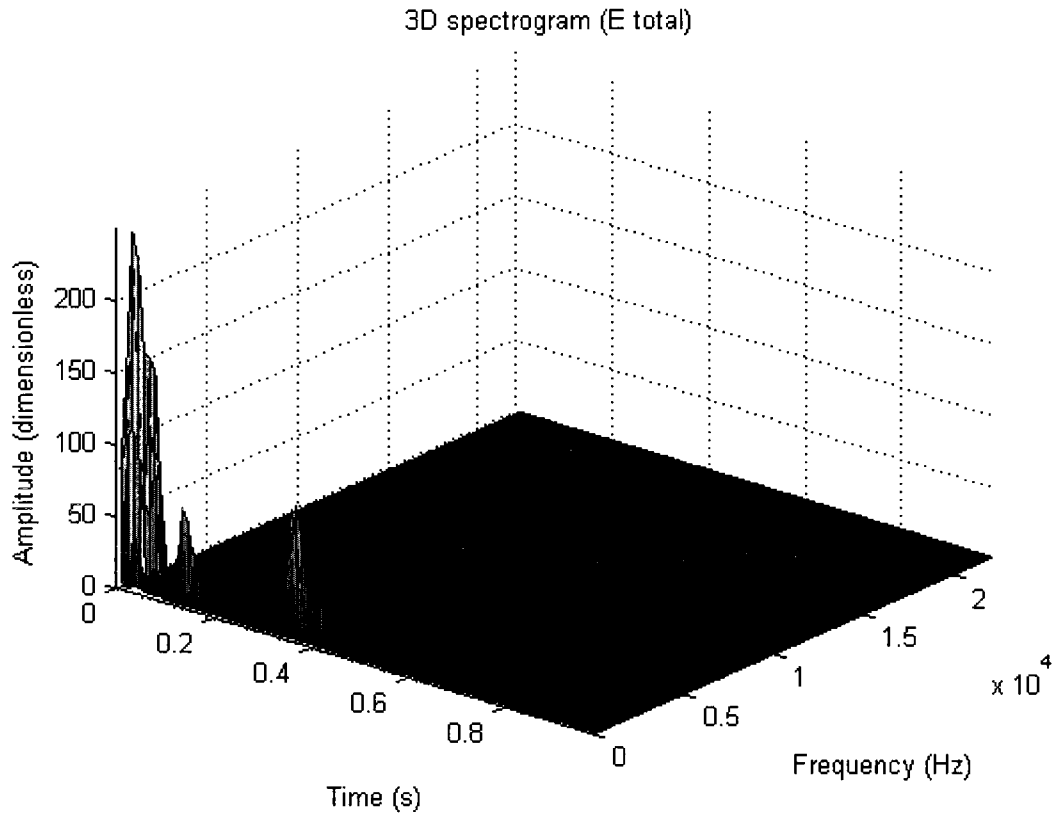


Figure 35: 3D representation of the spectrogram for the first heart beat of the first pre-recorded stethoscope test signal

The next step was to calculate the energy density spectrum of the STFT of each heart beat in the signal. In other words, the energy density spectrum is determined for each heart beat. Then, the energy is calculated from each energy density spectrum result, followed by a calculation of the mean energy representing the total energy. When the total energy was calculated using the Fourier Transform, the result obtained was a single number representing the energy in the signal. However, with the STFT, the result obtained is a time evolution of the total energy in the signal. Therefore, it is possible to plot the time evolution of the total energy as shown in Figure 36.

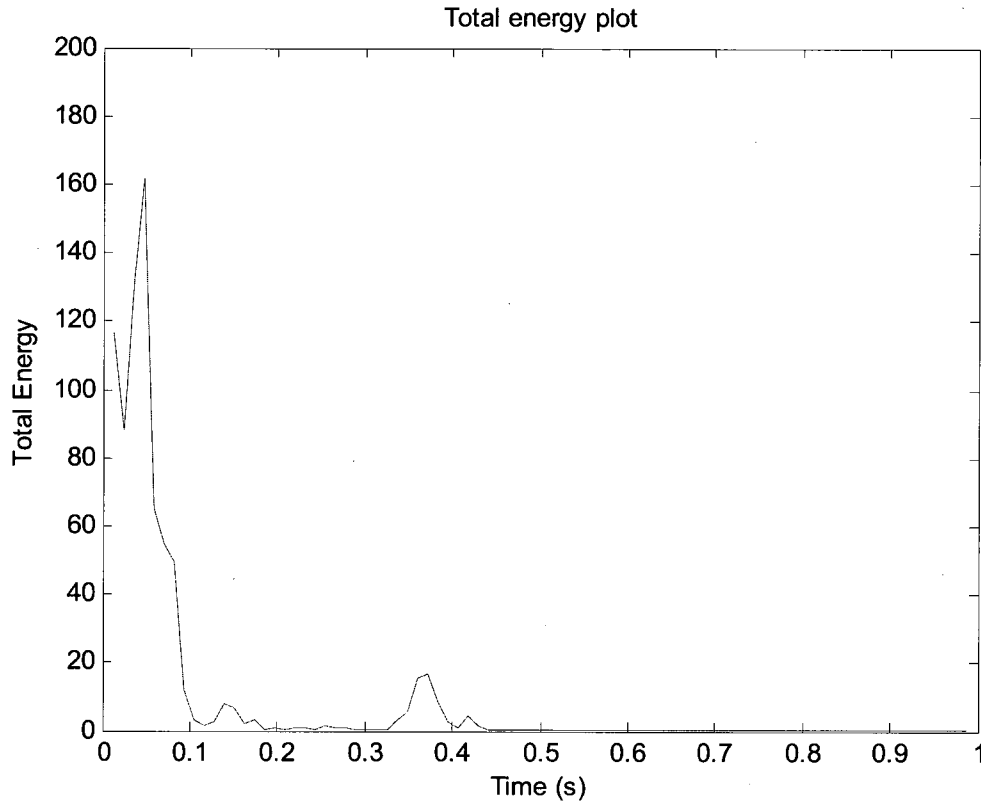


Figure 36: The time evolution of the total energy

The S1 and S2 peaks can also be observed in Figure 36 along with some noise which is not deterministic. To obtain the total energy of the whole signal (as represented by a single number), the total energy at each time was summed.

The final step was to calculate the non-deterministic energy by subtracting the deterministic energy from the total energy. When the non-deterministic energy was calculated using the Fourier Transform, the result obtained was a single number representing the non-deterministic energy in the signal since two single numbers were subtracted. However, with the STFT, the result obtained is a time evolution of the non-deterministic energy in the signal. Therefore, it is possible to plot the time evolution of the non-deterministic energy as shown in Figure 37.

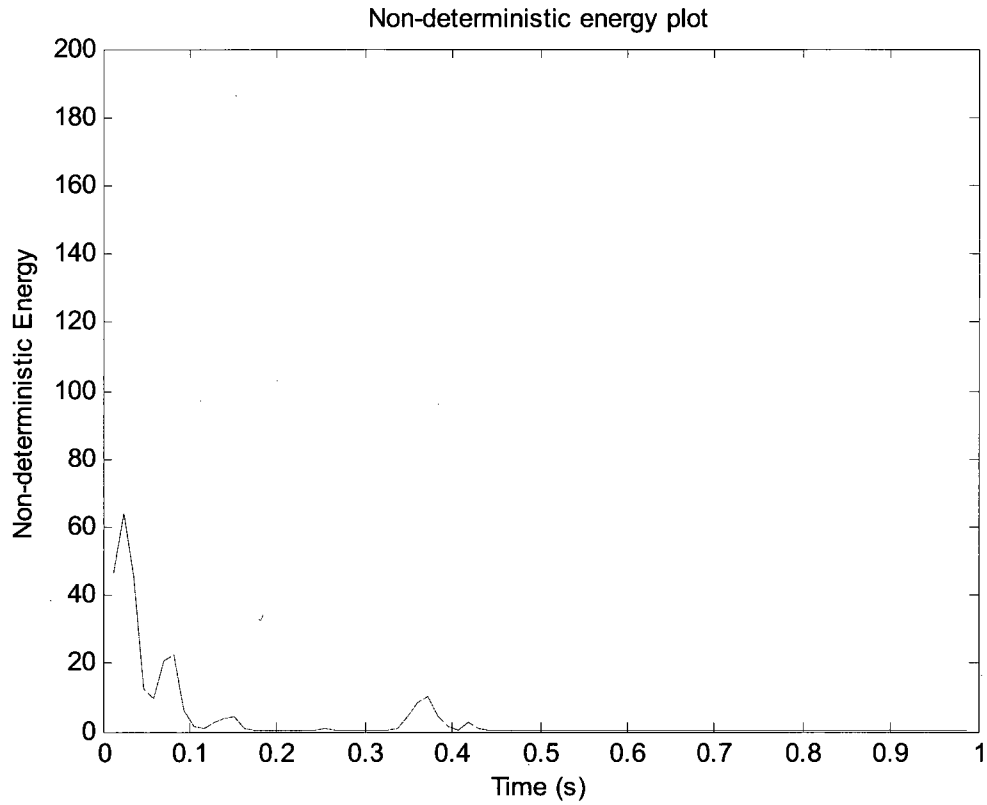


Figure 37: The time evolution of the non-deterministic energy

To obtain the non-deterministic energy of the whole signal (as represented by a single number), the non-deterministic energy at each time was summed. The deterministic energy, the total energy and the non-deterministic energy are all combined in Figure 38.

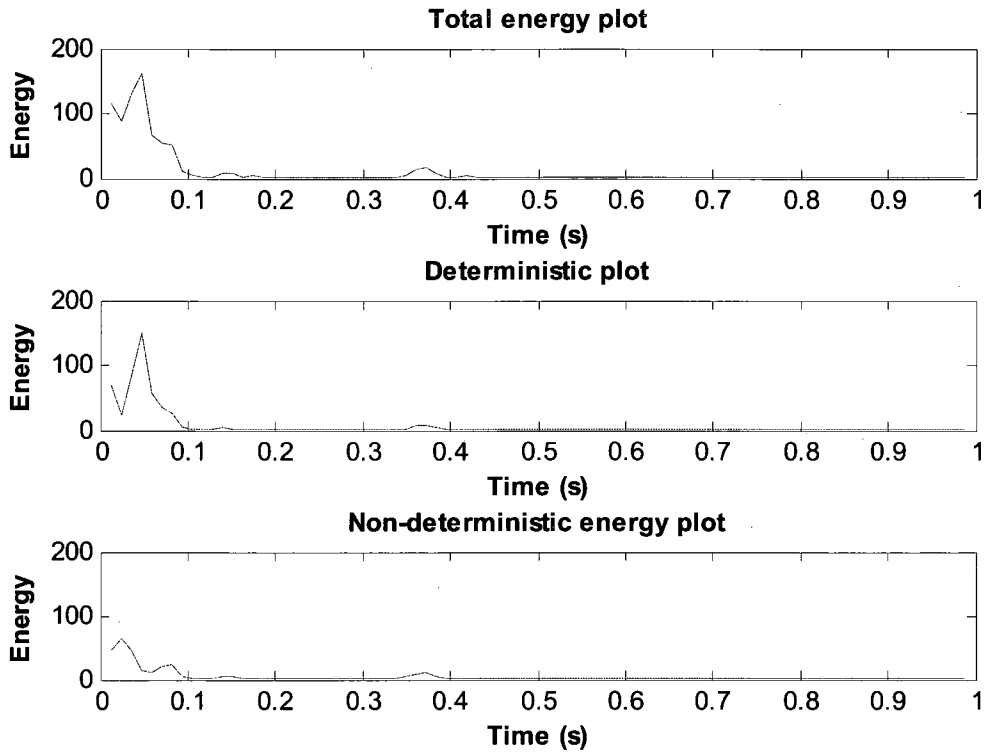


Figure 38: The time evolution of the total, deterministic, and non-deterministic energy

Instead of obtaining a single value for the non-deterministic energy, the new algorithm allows us to see the non-deterministic values as it evolves across a heart beat. It is possible to see where the non-deterministic energy comes from in the signal. The first and second lumps in the non-deterministic energy plot most likely represent the parts of the S1 and S2 peaks that were not perfectly lined up. The rest of the non-deterministic energy most likely comes from the noise in the signal.

In order to know if the results using the STFT agree with the results using the Fourier Transform, the percentage of non-deterministic energy obtained with both methods are compared in Table 17 for a few signals. The percentage of non-deterministic energy in the signal obtained with the STFT is found using equation (5.2) but with the total energy and non-deterministic energy obtained using the STFT. To use that equation,

a single number for the total energy and non-deterministic energy is required. As mentioned previously, to obtain the total energy of the whole signal as represented by a single number, the total energy at each time is summed. The same is done for the non-deterministic energy.

Note that for the all signals in both methods, the S1 peaks were aligned and no heart beats were removed from the signal.

Table 17: Comparison of the percentage results obtained with the STFT and with the FT

Signal used	% of non-deterministic energy	
	Fourier Transform	Short-Time Fourier Transform
Pre-recorded PCG 1	35.18 %	36.11 %
Pre-recorded PCG 2	6.82 %	6.87 %
Pre-recorded PCG 3	47.81 %	46.81 %
Karim stethoscope signal 1	48.40 %	45.17 %

As observed in Table 17, the percentage results obtained with both methods are very similar. Therefore, the Short-Time Fourier Transform can be used instead of the Fourier Transform to obtain the energy in the signal.

5.3 Summary of the new algorithm

To conclude this chapter, the new algorithm is summarized in this section. The new algorithm calculates the non-deterministic energy by subtracting the deterministic energy from the total energy, as Johansen had suggested in his papers.

The first step consists of finding the deterministic energy. To obtain this, the heart signal was segmented at the beginning of each heart beat using the segmentation algorithm described in section 5.1.1. Then, each heart beat was truncated for all beats to have the same length. The truncated heart beats were then superimposed one over the other, and the S1 peaks were aligned as described in section 5.1.4. Then, the heart beats were truncated again since the alignment moved the heart beats. The user can then decide by looking at the shift values whether it is preferable to discard the signal, to remove some heart beats from the signal, or to keep the signal as it is. Once the heart beats were aligned, they were averaged to obtain an average heart beat signal. This eliminates unwanted noise as well as reduces the signal parts that do not repeat from beat to beat. The Short-Time Fourier Transform of the average heart beat was then implemented and the energy density spectrum was calculated. Finally, the energy was calculated from the energy density spectrum to obtain the deterministic energy. This results in the time evolution of the deterministic energy. To obtain the deterministic energy of the whole signal (as represented by a single number), the deterministic energy at each time was summed.

The second step consists of determining the total energy. As for the deterministic energy, the heart signal was segmented at the beginning of each heart beat followed by the truncation of each beat to make them the same length. The truncated heart beats were then superimposed one over the other, and the S1 peaks were aligned as described in section 5.1.4. Then, the heart beats were truncated again since the alignment moved the heart beats. These last few commands were executed in order for the heart beats to have the same length as the heart beats in the deterministic energy step. If some beats were

removed from the signal in the deterministic energy step, they were automatically removed for this step. The Short-Time Fourier Transform *of each heart beat* in the signal was then implemented and the energy density spectrum was calculated for each beat. Finally, the energy was calculated from each energy density spectrum result, followed by a calculation of the mean of these energies, and this last value is the total energy. This results in the time evolution of the total energy. To obtain the total energy of the whole signal represented by a single number, the total energy at each time was summed.

The final step in the new algorithm consists of subtracting the deterministic energy from the total energy to obtain the non-deterministic energy, as stated previously. This can be obtained as an evolution of the non-deterministic energy in time by subtracting the corresponding total and deterministic energies. Alternatively, to return to Johansen's algorithm, the total single-value energies can be used by summing the time-evolution of energies as mentioned above.

Chapter 6: Experimental testing

Experimental testing was accomplished by performing in vitro measurements using a left-heart simulator in a laboratory at the University of Ottawa Heart Institute, and by passing the signals obtained through the new algorithm. The left-heart simulator used in this experiment is a mechanical system that simulates the activity in the left portion of the heart and is designed for in vitro testing of bioprosthetic and mechanical heart valves [24].

6.1 Description of the experimental setup

6.1.1 Left-heart simulator

The left heart simulator used in this experiment was purchased from ViVitro Labs Inc. (Victoria, Canada). Designed to be physiologically realistic, it can assess the function of heart valves and other devices under simulated cardiac conditions [25]. The left heart simulator can be set to different cardiac outputs, systolic/diastolic pressures, heart rates and dP/dt (the temporal rate of change of the left ventricular pressure). The simulator consists of a Superpump system, a viscoelastic impedance adapter, a left heart model, flow and pressure measuring systems, a waveform generator, and a PC data acquisition system [24].

The Superpump system generates physiological simulation of velocity, pressure and waveforms of the cardiovascular system [25]. It consists of a piston-in-cylinder pump head that is driven by a low inertia DC electric motor. The latter is driven by a power

amplifier [24]. The viscoelastic impedance adapter is located between a fluid flow generator (the Superpump) and the left heart model. It simulates viscoelastic behaviour producing realistic ventricle pressure waveforms. It acts as a damper; damping the pressure and flow waveforms. The left heart model in this simulator is a compact, compliant model of the left heart and load system [25]. The left heart model consists of transparent chambers to allow monitoring of the valve during testing. In the model, sites are available for pressure transducers to measure wall pressures, and for flow transducers. The left heart model contains a hydraulic chamber, which itself contains the model ventricle. The left heart model is attached to the Superpump via the viscoelastic impedance adapter [24].

The left heart simulator also consists of flow and pressure measuring systems. The flow measuring system consists of a single wave flow meter and compatible electromagnetic flow transducer [25]. The pressure measuring system consists of three elements; a Tri-Pack TP 2001 chassis, amplifiers, and pressure transducers. The amplifiers are designed to measure physiological pressures in non-clinical and in vitro environments. Finally, the left heart simulator consists of a waveform generator and a PC data acquisition system. The waveform generator generates analog voltage waveforms. For one, it is used as input to the power amplifier of the Superpump system. Additionally, it is connected to the Tri-Pack chassis which powers the amplifier in board for pressure measurement [24]. The PC data acquisition system is designed for monitoring, acquisition and analysis of data for assessment of heart valves.

Photographs of the left-heart simulator with all its components are shown in Figure 39 and Figure 40.

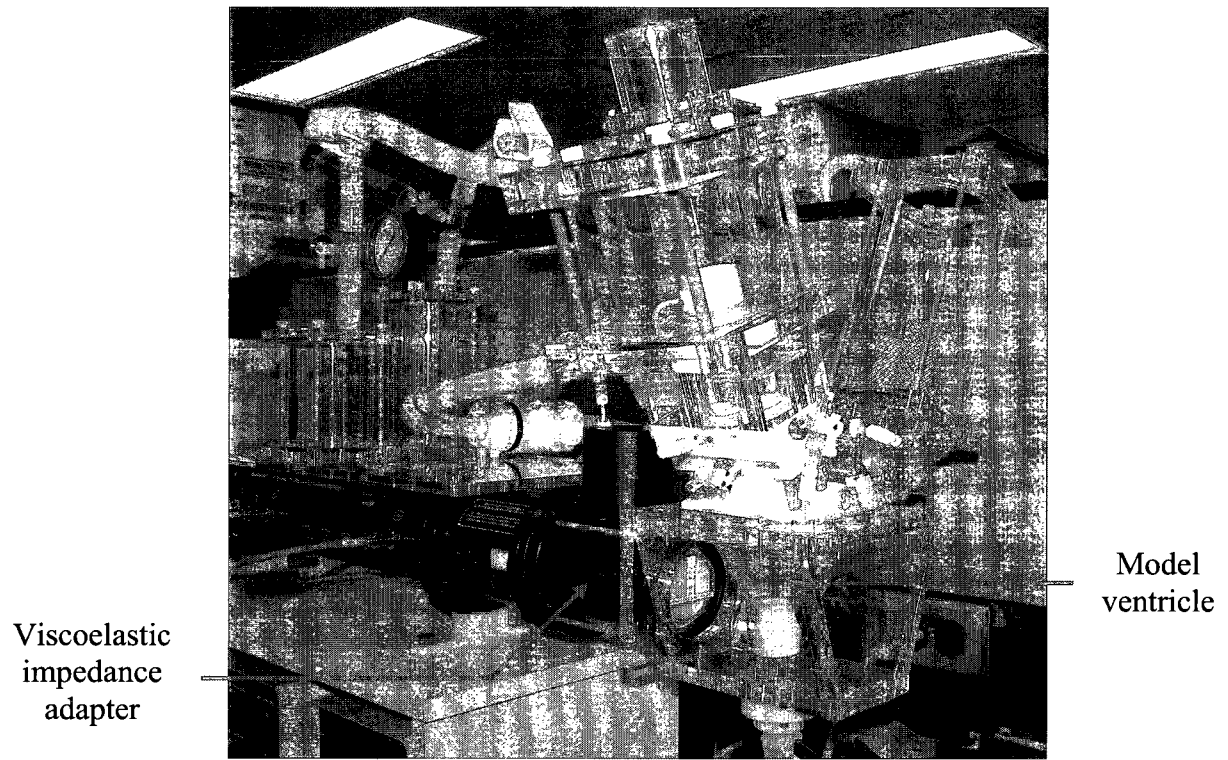


Figure 39: Top part of the left-heart simulator [24]

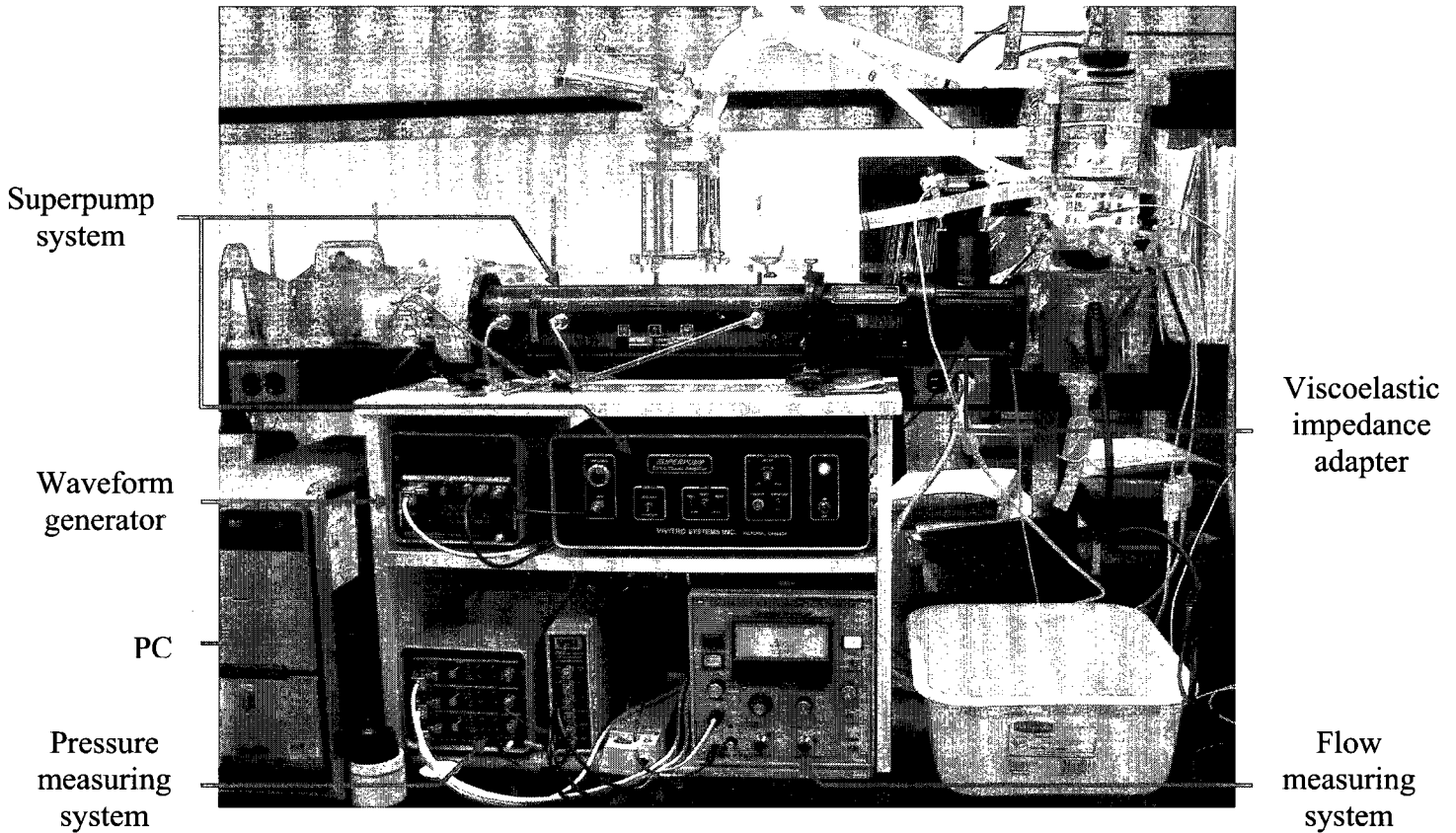


Figure 40: Front view of the left-heart simulator

6.1.2 Materials and signal acquisition

The valves used in this experiment were a bioprosthetic valve of type Magna from Edwards Lifescience (Irvine, California, USA) [24], and a St. Jude Medical bileaflet mechanical heart valve (Figure 42). The bioprosthetic valve was an aortic trileaflet bovine pericardial valve and it had a commercial denomination of 27 mm (Figure 41). The mechanical heart valve had pyrolytic carbon occluders. Its interior diameter was 18 mm and its exterior diameter including the cuff was 28 mm. Its commercial denomination was 23 mm.

The same bioprosthetic mitral valve was used during the whole experiment. It was a bileaflet bovine pericardial valve provided by the manufacturer of the simulator, and it

had a diameter of 21 mm. The heart valves were mounted to the left-heart simulator with the use of silicone rubber rings. They provide a fluid seal between the valve and the heart simulator flanges.

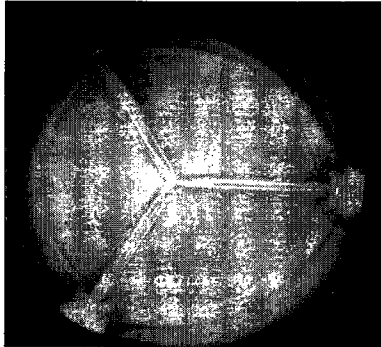


Figure 41: Bioprosthetic valve, Magna 27mm

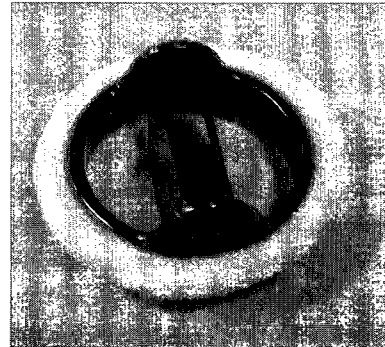


Figure 42: St. Jude Medical bileaflet mechanical heart valve

The test fluid used in this experiment was saline. Saline is a popular choice for these types of experiments since it can mimic blood to a certain extent, and its transparency makes it possible to examine valve performance [24]. The quiescent volume of the left ventricle in this experiment was 140 mL. It was determined by pouring fluid inside the ventricle until the level reached the valve mounting orifice. Then, the fluid was removed with a syringe and measured.

The high-speed digital camera used in this experiment was the Phantom 4.0. It was used to record videos and to acquire images of the valves and cavitation at over 3,000 frames per second. Previous studies acquired high-speed digital images of MHV cavitation at 3,000 frames per second [9, 11]. Figure 43 and Figure 44 demonstrate the high-speed camera setup to record the aortic valve and the mitral valve, respectively.

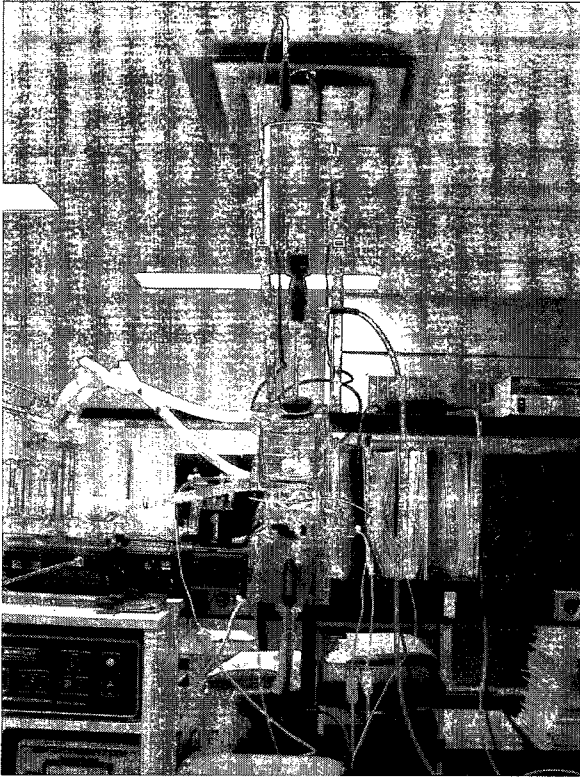


Figure 43: High-speed camera setup to observe the aortic valve



Figure 44: High-speed camera setup to observe the mitral valve

An endoscope was attached to the camera at one end and was inserted through a black rubber plug at the other end, as shown in Figure 43 and Figure 44. It allowed a close up view of the valve and cavitation, if present. Additionally, a light source and a fiber optic cable were used to illuminate the recording site.

The stethoscope and the hydrophone used in this experiment were the Welch Allyn Elite Electronic Stethoscope (Figure 45) and the Brüel & Kjaer Type 8103 Miniature Hydrophone (Figure 46), respectively. The stethoscope was used to record the sounds coming from the valve, and the hydrophone was used to record the sounds coming from the cavitation.

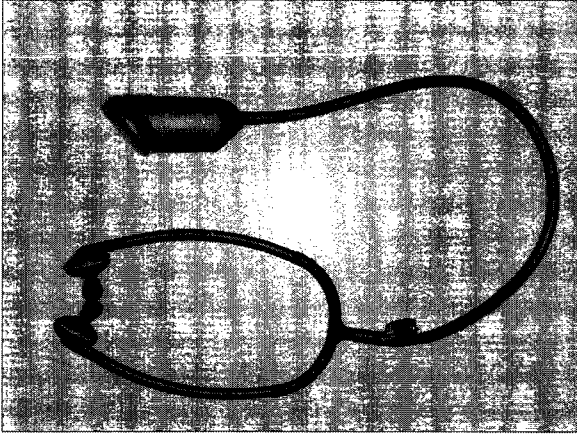


Figure 45: Electronic stethoscope

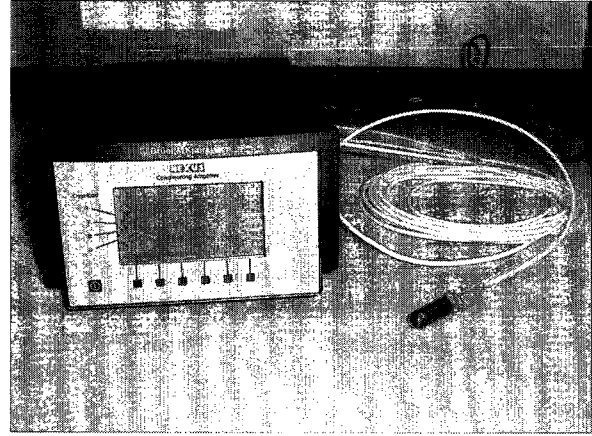


Figure 46: Hydrophone and amplifier

The stethoscope and the hydrophone are both very sensitive; a slight movement creates large amounts of noise. Therefore, for this experiment, the instruments were immobilized during recording to minimize noise. The setup is illustrated in Figure 47.

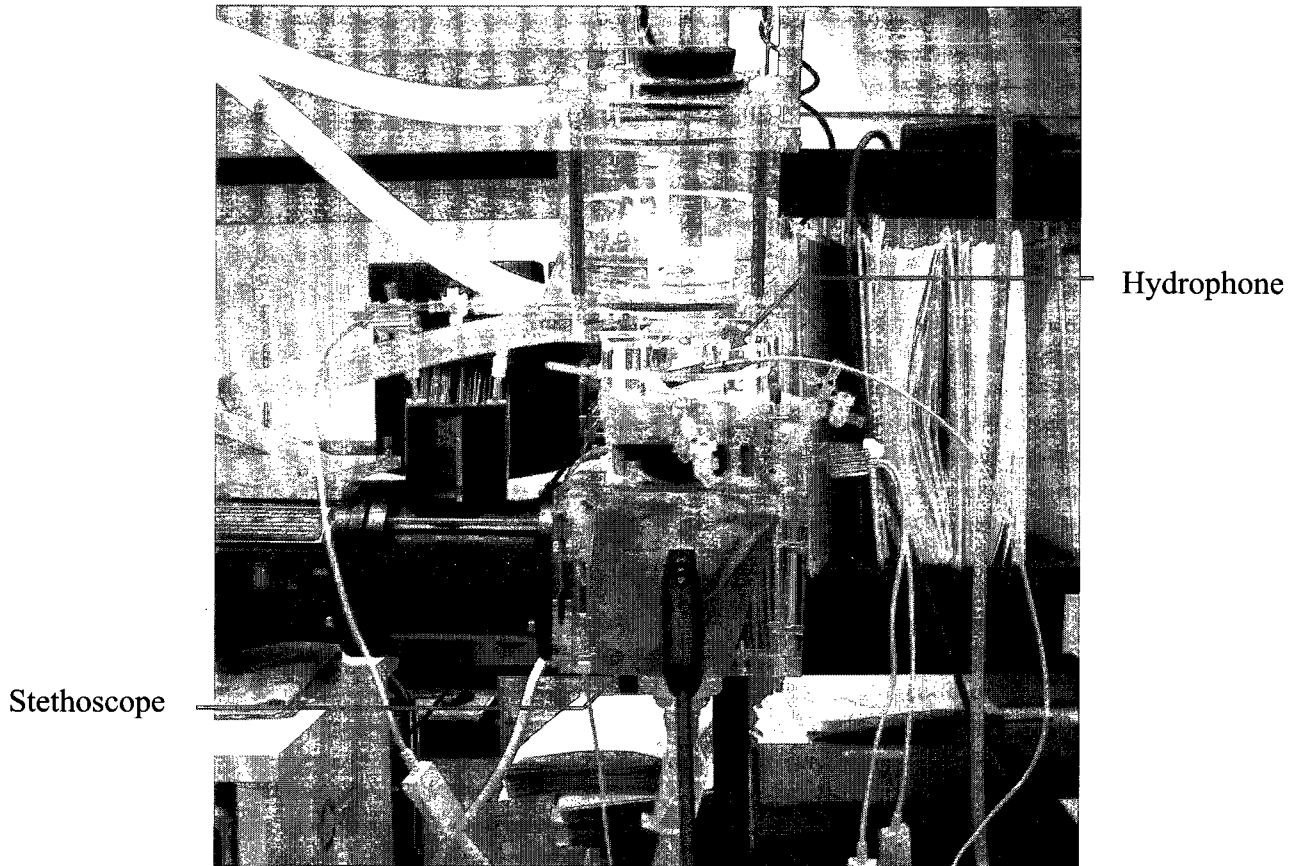


Figure 47: Stethoscope and hydrophone setup

As shown in Figure 47, the stethoscope and hydrophone are immobilized on the aortic side to record the sounds coming from the aortic valve. They can be moved to the mitral side if needed to record the sounds coming from the mitral valve. Both instruments were connected to a laptop where the data was collected simultaneously and was later analysed in MATLAB.

6.2 Experiment

The experiment was conducted at room temperature. Many trials were conducted with different cardiac parameters to try to obtain cavitation near the mechanical heart valve. The most important cardiac parameters in this experiment were the cardiac output,

the systolic/diastolic pressure and the heart rate. The cardiac output is the volume of blood that is pumped by the heart in a minute. It is measured in litres/minute. The cardiac output equals the amount of blood expelled from one ventricle during a single heart beat times the number of beats per minute: $Cardiac\ output = stroke\ volume \times heart\ rate$ [26]. In this experiment, cardiac outputs of 3.1L/min and 4.5L/min were used. The normal blood pressure is a systolic/diastolic pressure of 120/80 mmHg. The diastolic pressure is the minimum pressure that occurs just at the end of diastole. The systolic pressure is the maximum pressure that occurs midway into systole [26]. The diastole is the resting or filling phase of the heart cycle, and the systole is the contractile or pumping phase of the heart cycle [27]. In this experiment, systolic/diastolic pressures of 120/80 mmHg and 120/85 mmHg were used. The heart rate is determined by the number of heart beats per minute. The resting rate is about 70 beats per minute [28]. In this experiment, heart rates of 70 beats per minute and 100 beats per minute were used.

6.2.1 Experimental trials

In the first trial, the 27 mm bioprosthetic valve was used for the aortic valve. The left-heart simulator was set to have a cardiac output of 3.1 L/min, a systolic/diastolic pressure of 120/80 mmHg, and a heart rate of 70 beats per minute. Five signal recordings were accomplished for this trial and no visible cavitation was observed with the camera.

Cavitation bubble implosion creates very high-frequency pressure fluctuations (HFPPFs) due to the transient bubble collapse [1]. It was observed in previous studies that the cavitation signature in the pressure signal appeared in the frequency range of 35 kHz to 350 kHz, and that there were no components in this range when no cavitation was present [6]. Previous studies have also found HFPPFs above 35 kHz in patients with

mechanical heart valves, and no HFPPs above 35 kHz in patients with normal or bioprosthetic valves [1]. The results obtained in this experiment were in agreement with the previous observations; no cavitation was obtained with the bioprosthetic heart valve over the range of experimental parameters used.

In the second trial, the bileaflet mechanical heart valve was used for the aortic valve. The left-heart simulator was set to have a cardiac output of 3.1 L/min, a systolic/diastolic pressure of 120/80 mmHg, and a heart rate of 70 beats per minute. During this trial, no cavitation was observed either. This result was surprising since cavitation was expected.

To try to obtain cavitation near the valve, the cardiac parameters were modified for the third trial. Once again, the bileaflet mechanical heart valve was used for the aortic valve. This time, the left-heart simulator was set to have a cardiac output of 4.5 L/min, a systolic/diastolic pressure of 120/85 mmHg, and a heart rate of 100 beats per minute. Adjusting the pump settings allows a range of different dP/dt values (loading rates) [9] to be obtained. It has been shown previously that the level of cavitation is a function of dP/dt [9]; thus changing the pump settings values should increase the chances of cavitation. Additionally, to maximize the chances of observing cavitation, the viscoelastic impedance adapter was filled with water. This action has the same effect as removing it completely as it no longer dampens the pressure and flow waveforms. As a result, there is a bigger impact on the valve when the saline water is being pumped towards the valve and should increase the chances of cavitation. Even with all these changes, no cavitation was observed.

For the last trial, the bileaflet mechanical heart valve was set in mitral position. Recordings with the camera were done with the same cardiac parameters used in the second trial and in the third trial. No cavitation was observed in either case.

6.2.2 Discussion

There are a few possible explanations for the fact that no cavitation was observed during the experiments. The first possibility is that there was insufficient lighting in the experiment. Previous studies used a strobe light to illuminate the valve [1, 6]. Strobe lighting provides intermittent illumination of a rotating or vibrating object [29]. It makes a moving object appear to be slowed down or stationary by producing illumination in very short, brilliant bursts that always occur when the moving part is in the same phase of its motion. Modern electronic stroboscopes achieve a flash duration of about one microsecond and flashing rates ranging from 110 to 150,000 per minute [29]. That type of light is a lot brighter than the one that was used in this experiment which could have affected the detection of cavitation in the recording.

Another possibility is the type of valve that was used in this experiment. In a previous study, it was found that the bileaflet valves such as the St. Jude Medical valve and the CarboMedics valve required a higher dP/dt to obtain cavitation than tilting disc valves such as the Medtronic Hall and the Omnicarbon valve [1]. In another study, the data obtained suggested that the CarboMedics bileaflet valve was less likely to cause cavitation than the investigated tilting disc valves [9]. Since the valve used in this experiment was the St. Jude Medical bileaflet valve, it could have diminished the chances of producing cavitation near the mechanical heart valve.

Comparison with other heart simulator setups

Another possible explanation as to why cavitation was not observed in our experiment is the physiologically realistic nature of the heart simulator. The heart simulator setups used for this type of study have been quite varied. There is no standard setup (e.g. gold standard) for cavitation detection. Previous studies have shown that cavitation has been detected in vitro with different setups than the one used in this experiment [4, 6, 9, 11, 30]. The following will discuss the different setups and will compare them with the setup used in this experiment.

The heart simulator setup used in this experiment was a physiologically realistic setup as explained at the beginning of the chapter. At the time the heart simulator was purchased, the idea was to find the most physiologically realistic simulator possible.

The first setup that is compared with the setup used in this experiment was used by Chandran and Aluri, and Lee *et al.* [30, 31]. The setup is illustrated in Figure 48.

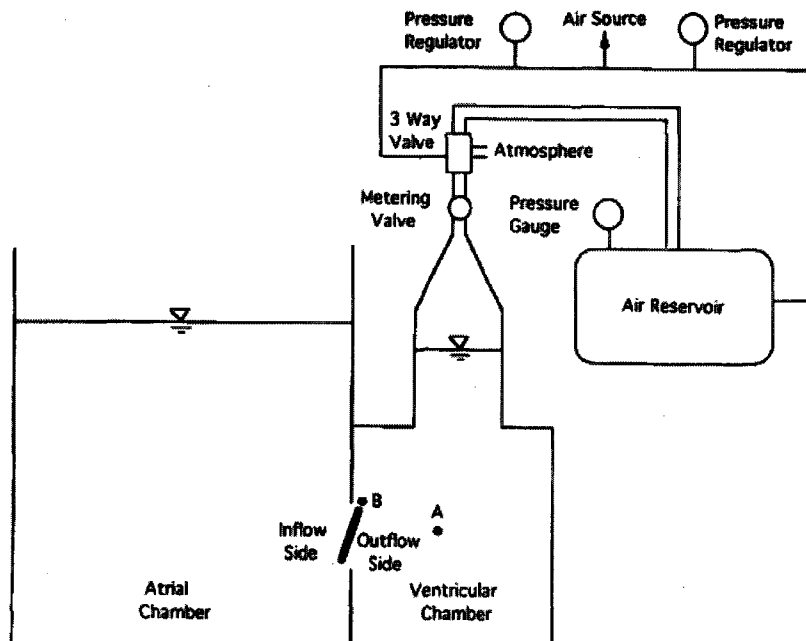


Figure 48: Setup used by Chandran and Aluri, and Lee *et al.* [30, 31]

Instead of a pulsatile flow system, the setup illustrated in Figure 48 simulates a single closing event of mechanical heart valves in the mitral position [30, 31]. As shown in the figure, the valve is positioned between two rectangular valve holders and incorporated between the ventricular and atrial flow chambers. The atrial chamber was opened to the atmosphere and was kept at a constant atrial pressure of between 5 and 7 mmHg during valve closure [30]. Initially, the valve was fully opened. As the three-way electro-pneumatic valve was turned on, the valve started closing since the air incoming into the ventricular chamber applied pressure to the fluid [31]. The loading rate was controlled by changing the air reservoir pressure or by changing the orifice area of the metering valve [31]. Very similar setups were also used by Johansen *et al.* and Sohn *et al.* [9, 11].

Comparing this setup with the one used in our experiment, one can suspect that the setup illustrated in Figure 48 is less physiologically realistic than the setup used in our experiment (Figure 40). Unlike the setup used in this thesis as shown in Figure 40, the setup in Figure 48 does not have a pump system that generates physiological simulation of velocity, pressure and waveforms of the cardiovascular system. It does not have a viscoelastic impedance adapter that simulates viscoelastic behaviour producing realistic ventricle pressure waveforms. Additionally, there is no model ventricle in the setup of Figure 48. Overall, it is a less complex and realistic setup than the one used in our experiment shown in Figure 40. Since it is not physiologically realistic, it should not be concluded from that study that the same results would occur *in vivo*.

The other setup that is compared with the setup used in this experiment was used by Garrison *et al.* and Zapanta *et al.* at the Pennsylvania State University [4, 6]. The mock circulatory loop that was employed in that study is illustrated in Figure 49.

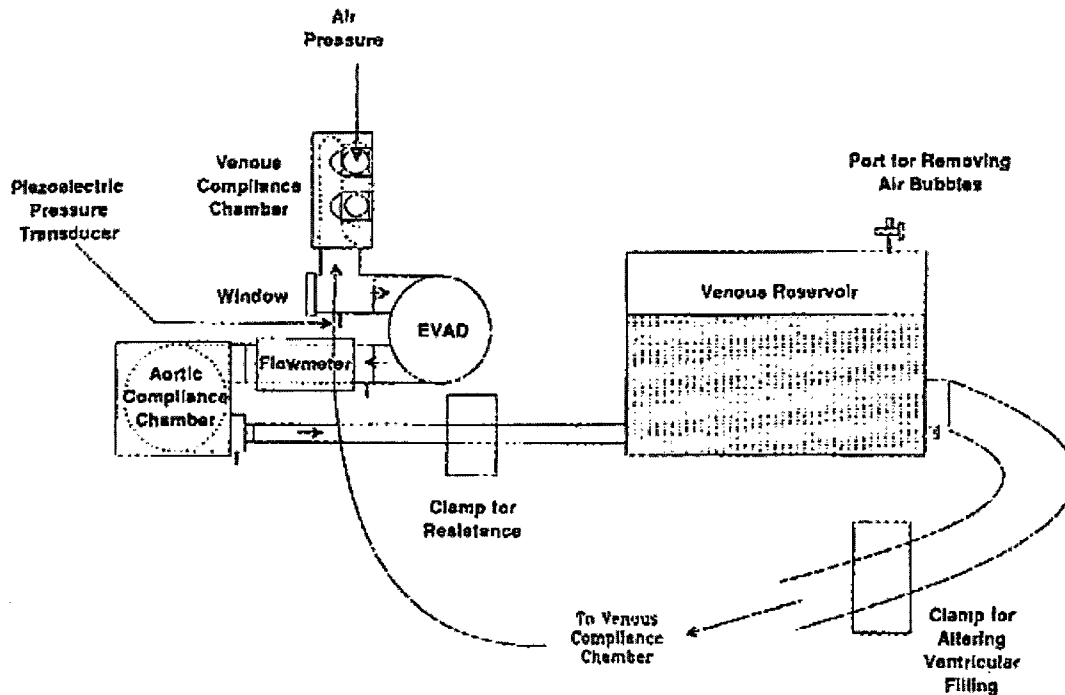


Figure 49: Setup used by Garrison *et al.* [6]

The Penn State mock circulatory loop was used to model physiologic flow conditions and to reproduce the resistance and compliance of the systemic circulation [4]. The pumping assembly consists of the 70cc Penn State Electric Ventricular Assist Device (EVAD). The pump contains mechanical heart valves and a Biomer blood sac located inside a plastic case [6]. The fluid in the system is pumped by the Penn State EVAD into the Biomer blood sac in the aortic compliance chamber. Then, the fluid travels from the aortic compliance chamber to the venous reservoir. The fluid then empties into the venous compliance chamber through a Plexiglas elbow connector equipped with a glass window, and finally returns to the EVAD [6]. The clamp that is found between the aortic compliance chamber and venous reservoir provides peripheral resistance. The clamp that is found between the venous reservoir and venous compliance chamber is used to induce

cavitation by reducing pump filling. To alter the venous filling pressure, the venous reservoir can be raised or lowered [6].

Each compliance chambers consist of two 70cc Biomer blood sacs and a Plexiglas box with just enough room to contain one full sac and an empty one [6]. In one sac, there is loop fluid that flows through it; and in the other sac, air pressure is supplied from pressurized air tanks that provide a relatively constant pressure with changing volume. The blood sacs fill and the air sacs empty during systole, and the opposite occurs during diastole [6].

The setup used by Zapanta *et al.* is very similar to the one used by Garrison *et al.* since the setup comes from the same laboratory at Pennsylvania State University. Their function is the same, but the figures look slightly different. The setup used by Zapanta *et al.* is illustrated in Figure 50. A laser sweeping system was added to the setup used by Zapanta. That group used a laser sweeping technique to measure mitral valve closing velocities and decelerations [4]. Further details are provided in the paper by Zapanta *et al.* [4].

The setup used by Garrison and Zapanta appears to be more physiologically realistic than the one used by Chandran and Aluri. However, it is hard to compare it with the setup used in our experiments as described in Section 6.1 since the characteristics of the pump used by Garrison and Zapanta are not known.

In the setup used by Garrison and Zapanta, a clamp was used to induce cavitation by reducing pump filling. In the setup described in section 6.1, nothing was added to induce cavitation. The intent was to try to create cavitation from a physiological setup without adding components to induce cavitation. However, it seems that the other setups

were designed in such a way so as to obtain cavitation. Therefore, it is difficult to judge whether they are physiological setups or not, and if their cavitation results could be reproduced in vivo.

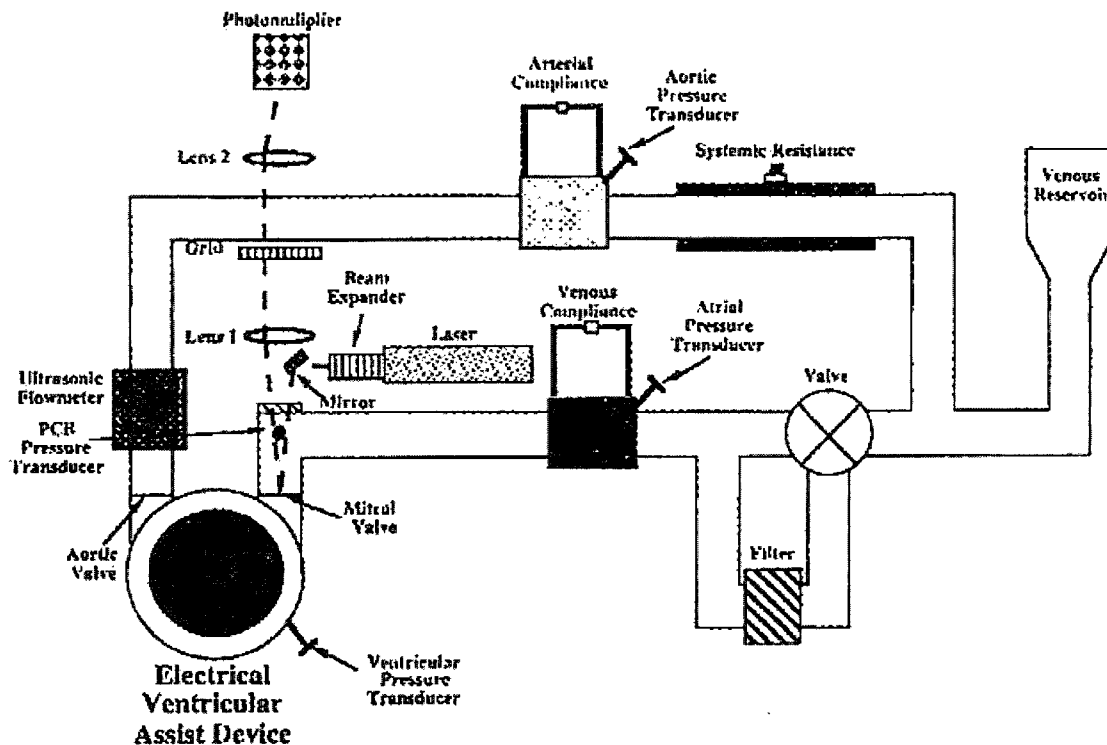


Figure 50: Setup used by Zapanta *et al.* [4]

6.3 Results and discussion

The signals obtained in the experiments discussed in the previous section were subsequently analyzed using the new cavitation quantification algorithm. The data captured by the stethoscope and the hydrophone were collected simultaneously in a laptop, and then analyzed in MATLAB.

The first step of the new cavitation quantification algorithm consisted of segmenting the hydrophone signal. However, the hydrophone signal is difficult to

segment properly since it is a very noisy signal. It is much easier to segment the stethoscope signal since it is a cleaner signal. Once the stethoscope signal was segmented in MATLAB, these segmentation points were used to segment the hydrophone signal. This could be done since the stethoscope and hydrophone data were collected simultaneously. The next step was to truncate each heart beat for all beats to have the same length. The truncated heart beats were then superimposed one over the other, and the S1 peaks were aligned. These first few steps are common to both the deterministic and total energy calculations.

The first step in the deterministic energy calculation was to take the average of the heart beats to obtain an average heart beat signal. The next step was to calculate the spectrogram of the ensemble average of the heart beats. Figure 51 illustrates the 3D representation of the spectrogram of the ensemble average of the heart beats for the first signal obtained during the second trial using the bileaflet mechanical heart valve (MHV Recording 1), with a heart rate of 70 beats per minute.

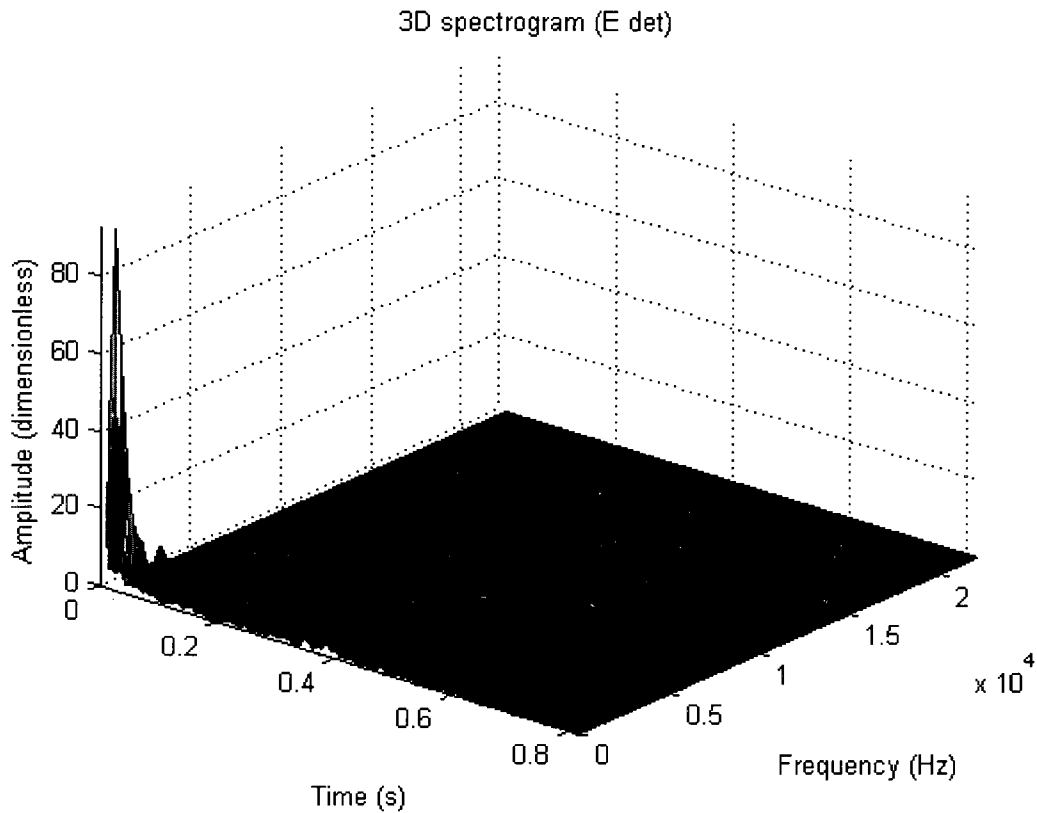


Figure 51: 3D representation of the spectrogram of the ensemble average of the signal MHV recording 1 (70 beats/min)

The 3D spectrogram display in MATLAB (Figure 51) can be rotated to show the projection on the frequency plane. This was done as shown in Figure 52 to determine the frequencies in the spectrogram.

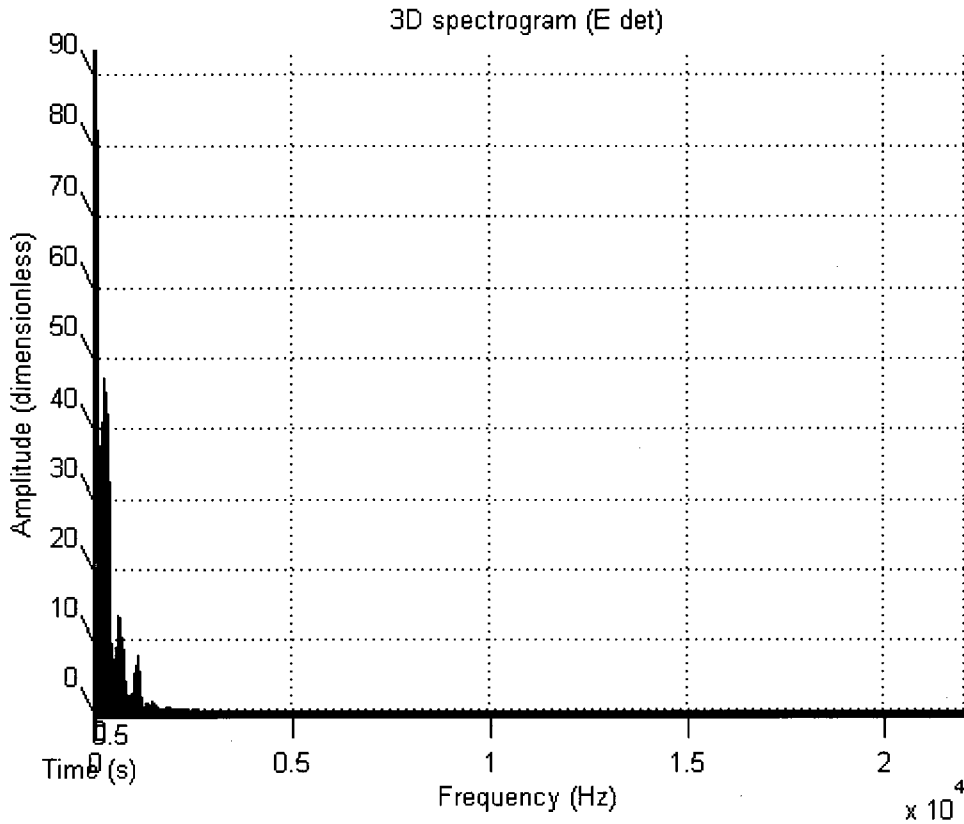


Figure 52: Rotated 3D representation of the spectrogram of the ensemble average of the signal MHV recording 1 (70 beats/min)

As observed in Figure 51 and Figure 52, there is no signal above approximately 2500 Hz. No high-frequency pressure fluctuations can be observed under 22 kHz in Figure 52; therefore, no cavitation is present under 22 kHz. In addition to the frequency information, it is also possible to see, from Figure 51, the noise in the signal as well as where the S1 and S2 peaks are located in time.

The next step was to calculate the energy density spectrum of the STFT of the ensemble average, from which the deterministic energy was calculated. When the deterministic energy was calculated using the Fourier Transform, the result obtained was a single number representing the energy in the signal. However, with the STFT, the result

obtained is a time evolution of the deterministic energy in the signal. Therefore, it is possible to plot the time evolution of the deterministic energy as shown in Figure 53.

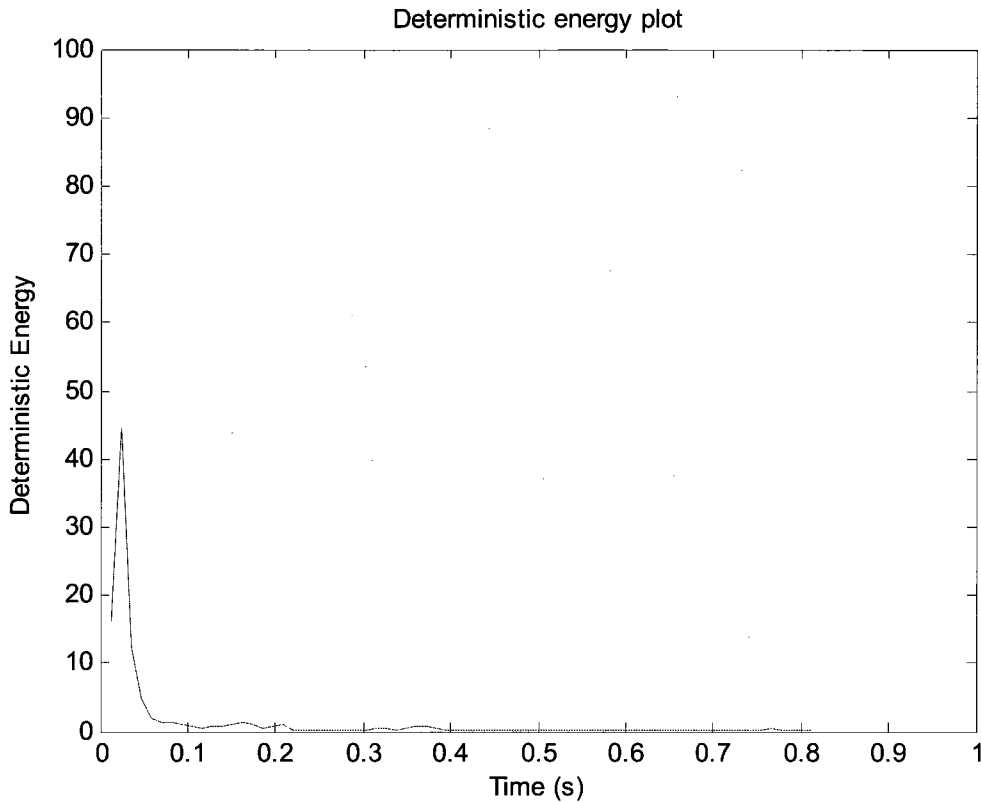


Figure 53: Time evolution of the deterministic energy

Figure 53 illustrates the deterministic energy which includes the S1 peak and a very small S2 peak. The S2 peak is small since the S2 peaks of the heart beats in the signal were not properly lined up. To obtain the deterministic energy of the whole signal represented by a single number, the deterministic energy at each time was summed. As a result, the deterministic energy obtained was 98.52.

Once the deterministic energy was obtained, the total energy calculation was accomplished. The first step to obtaining the total energy was to calculate the spectrogram of each heart beat in the signal. Thus, for a signal with 22 heart beats, 22 spectrograms were obtained. Figure 54 illustrates the 3D representation of the first of 22

spectrograms for the first signal obtained during the second trial using the bileaflet mechanical heart valve (MHV Recording 1), with a heart rate of 70 beats per minute.

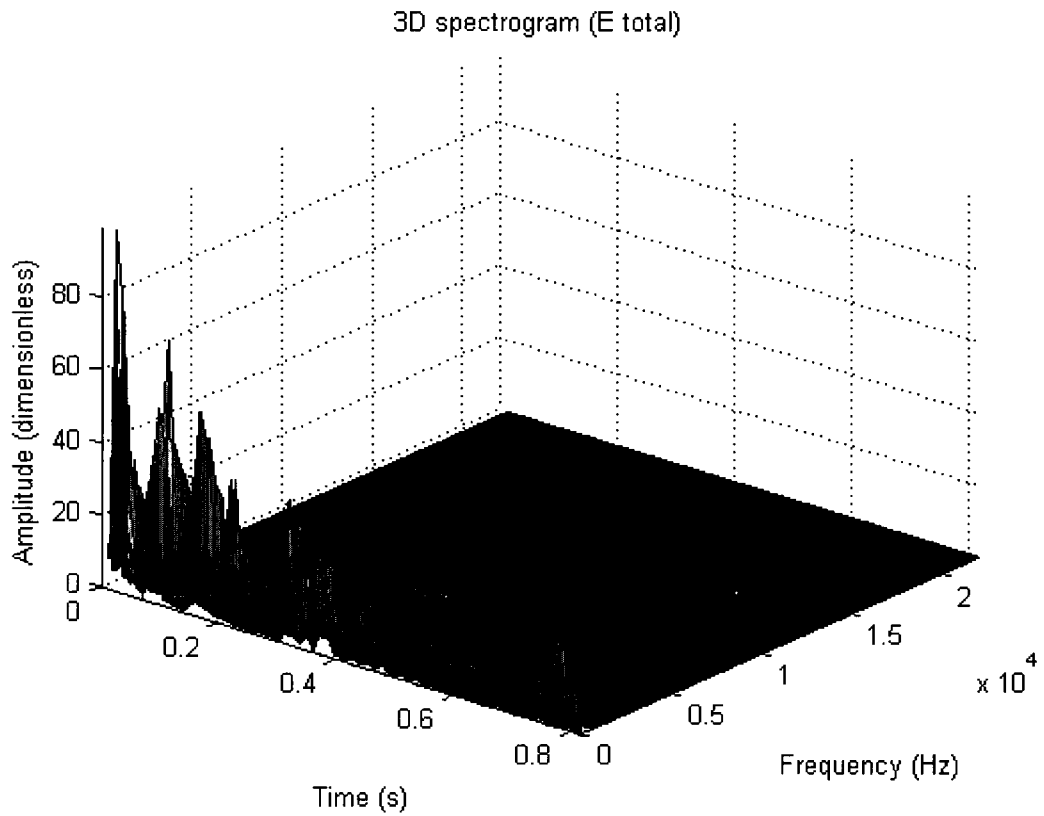


Figure 54: 3D representation of the spectrogram for the first heart beat of the signal MHV recording 1 (70 beats/min)

The 3D spectrogram display in MATLAB (Figure 54) can be rotated to show the projection on the frequency plane. This was done as shown in Figure 55 to determine the frequencies in the spectrogram.

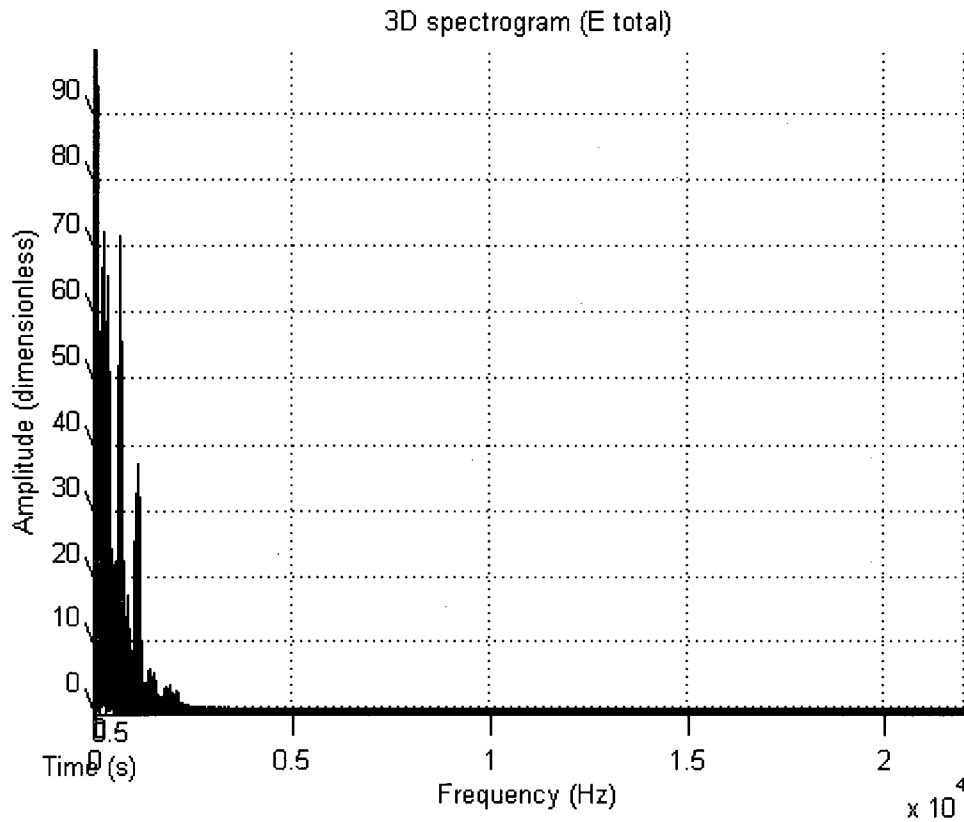


Figure 55: Rotated 3D representation of the spectrogram for the signal MHV recording 1 (70beats/min)

As observed in Figure 55, there is no signal above approximately 3000 Hz. Additionally, one can see from Figure 54 and Figure 55 that no high-frequency pressure fluctuations can be observed under 22 kHz; therefore, no cavitation is present under 22 kHz. In addition to the frequency information, it is also possible to see from Figure 54 the noise in the signal as well as where the S1 and S2 peaks are located in time.

The next step was to calculate the energy density spectrum of the STFT of each heart beat in the signal. In other words, the energy density spectrum is determined for each heart beat. Then, the energy is calculated from each energy density spectrum result, followed by a calculation of an average of this energy which represents the total energy. When the total energy was calculated using the Fourier Transform, the result obtained

was a single number representing the energy in the signal. However, with the STFT, the result obtained is a time evolution of the total energy in the signal. Therefore, it is possible to plot the time evolution of the total energy as shown in Figure 56.

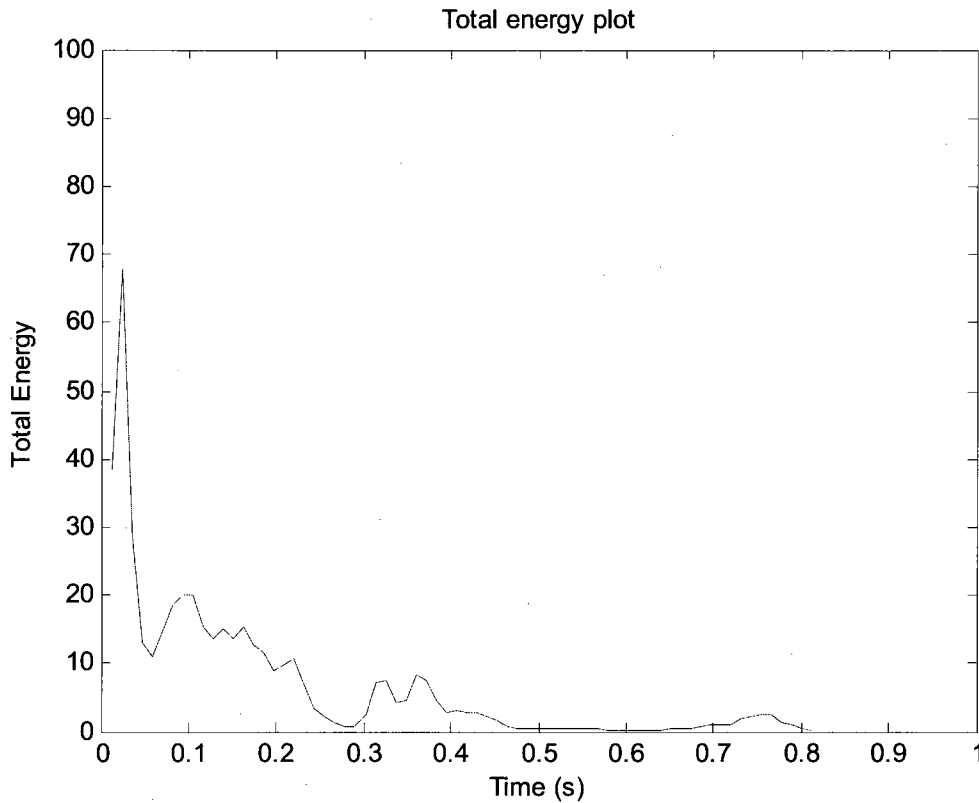


Figure 56: The time evolution of the total energy

From Figure 56, one can observe that there is a lot of noise in the hydrophone signal compared to the stethoscope signal (figures in Chapter 5). As a result, it is hard to tell which peak represents S2 in Figure 56. For the stethoscope signals, the S1 and S2 peaks could easily be distinguished in the total energy plot. To obtain the total energy of the whole signal represented by a single number, the total energy at each time was summed. As a result, the total energy obtained was 458.40.

The final step was to calculate the non-deterministic energy by subtracting the deterministic energy from the total energy. When the non-deterministic energy was

calculated using the Fourier Transform, the result obtained was a single number representing the non-deterministic energy in the signal since two single numbers were subtracted. However, with the STFT, the result obtained is a time evolution of the non-deterministic energy in the signal. Therefore, it is possible to plot the time evolution of the non-deterministic energy as shown in Figure 57.

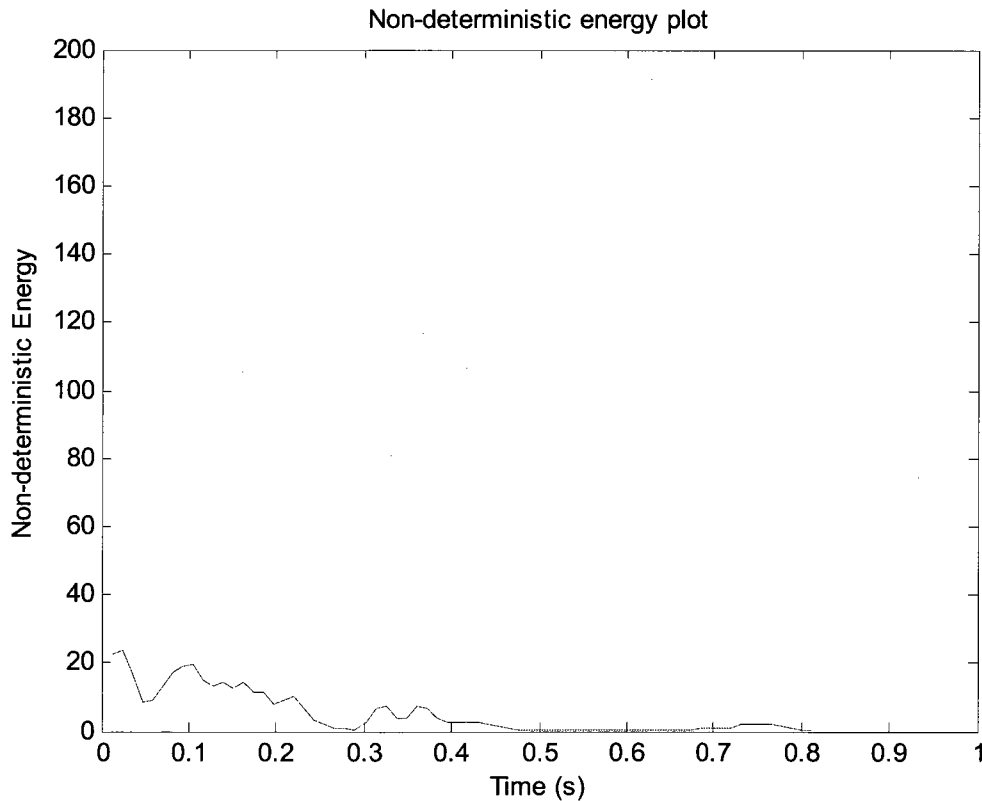


Figure 57: The time evolution of the non-deterministic energy

To obtain the non-deterministic energy of the whole signal represented by a single number, the non-deterministic energy at each time was summed. As a result, the non-deterministic energy obtained was 359.88. Hence, the percentage of non-deterministic energy in the signal was 78.51 %. This number is higher than the numbers obtained with the stethoscope signal in Chapter 5 section 5.2.3 due to the noise in the hydrophone signal which is a non-deterministic (random) component of the signal. It was previously

observed that the hydrophone signal is noisier than the stethoscope signal by looking at the recorded signals. Therefore, the new algorithm successfully detected the much greater non-deterministic energy in the hydrophone signal, compared to the stethoscope signal, and quantified the amount of non-deterministic energy in the signal.

The deterministic energy, the total energy, and the non-deterministic energy are all combined in Figure 58.

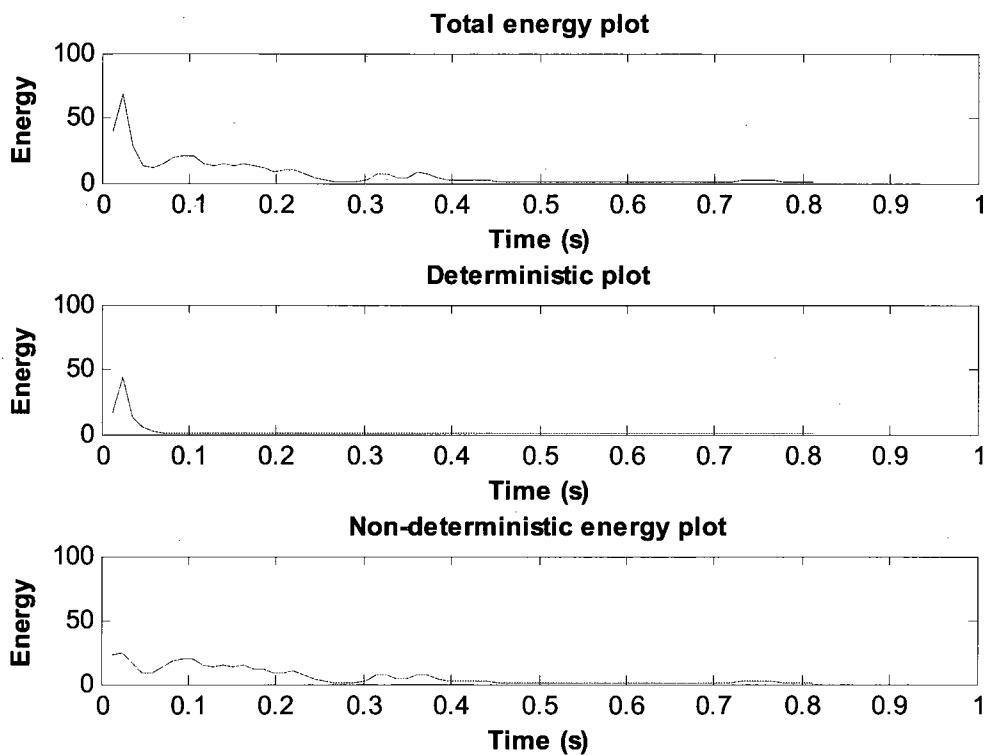


Figure 58: The time evolution of the deterministic, total, and non-deterministic energy

Instead of obtaining a single value for the non-deterministic energy, the new algorithm allows to see the non-deterministic values at each time instant. It is possible to see where the non-deterministic energy comes from in the signal. The non-deterministic energy, as shown in the plot, most likely represents the parts of the S1 and S2 peaks that were not lined up properly, and also the noise in the signal.

The previous steps are also applied on a signal that has a heart rate of 100 beats per minute, MHV recording 3. The first step is to obtain the deterministic energy. Figure 59 illustrates the 3D representation of the spectrogram for the ensemble averaged heart beat of a signal obtained during the third trial using the bileaflet mechanical heart valve (MHV Recording 3), with a heart rate of 100 beats per minute.

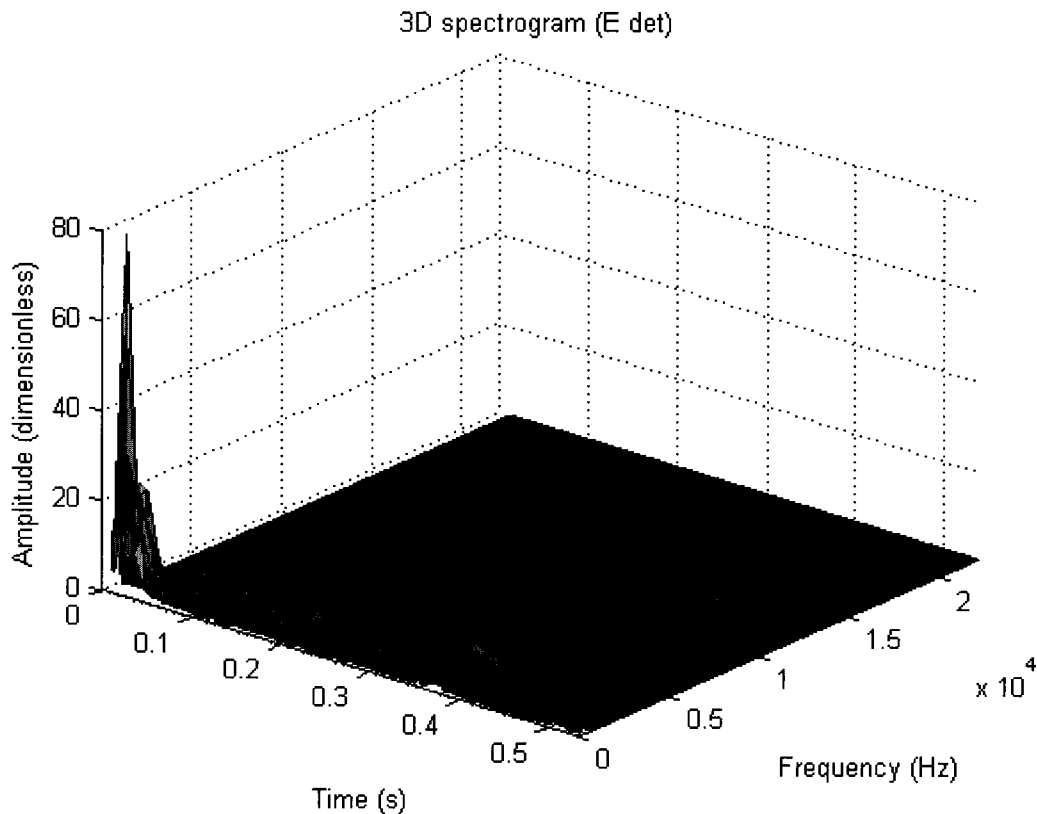


Figure 59: 3D representation of the spectrogram of the ensemble averaged heart beat for the signal MHV recording 3 (100 beats/min)

Comparing Figure 51 with Figure 59, it is harder to distinguish the S2 peak in Figure 59. Since the heart rate was faster for the second calculation (100 beats/min), the segmentation was more difficult to execute and was not as well performed as for the calculation with a heart rate of 70 beats/min. Therefore, the results of the second calculation are not as accurate as for other calculations, which is why only one signal was

calculated with 100 beats/min in Table 18. The 3D spectrogram display in MATLAB (Figure 59) can be rotated to show the projection on the frequency plane. This was done as shown in Figure 60 to determine the frequencies in the spectrogram.

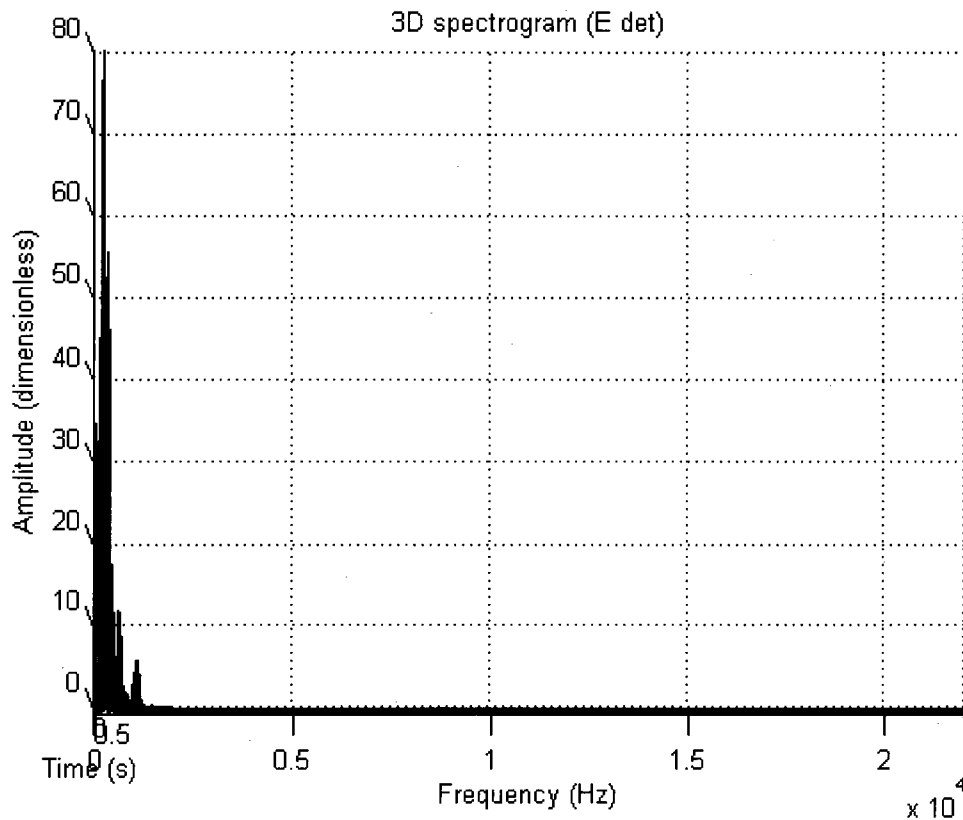


Figure 60: Rotated 3D representation of the spectrogram of the ensemble averaged heart beat for the signal MHV recording 3 (100 beats/min)

As observed in Figure 59 and Figure 60, no high-frequency pressure fluctuations are present under 22 kHz; therefore, no cavitation is present under 22 kHz.

The second step is to obtain the total energy. Figure 61 illustrates the 3D representation of the first of many spectrograms for a signal obtained during the third trial using the bileaflet mechanical heart valve (MHV Recording 3), with a heart rate of 100 beats per minute.

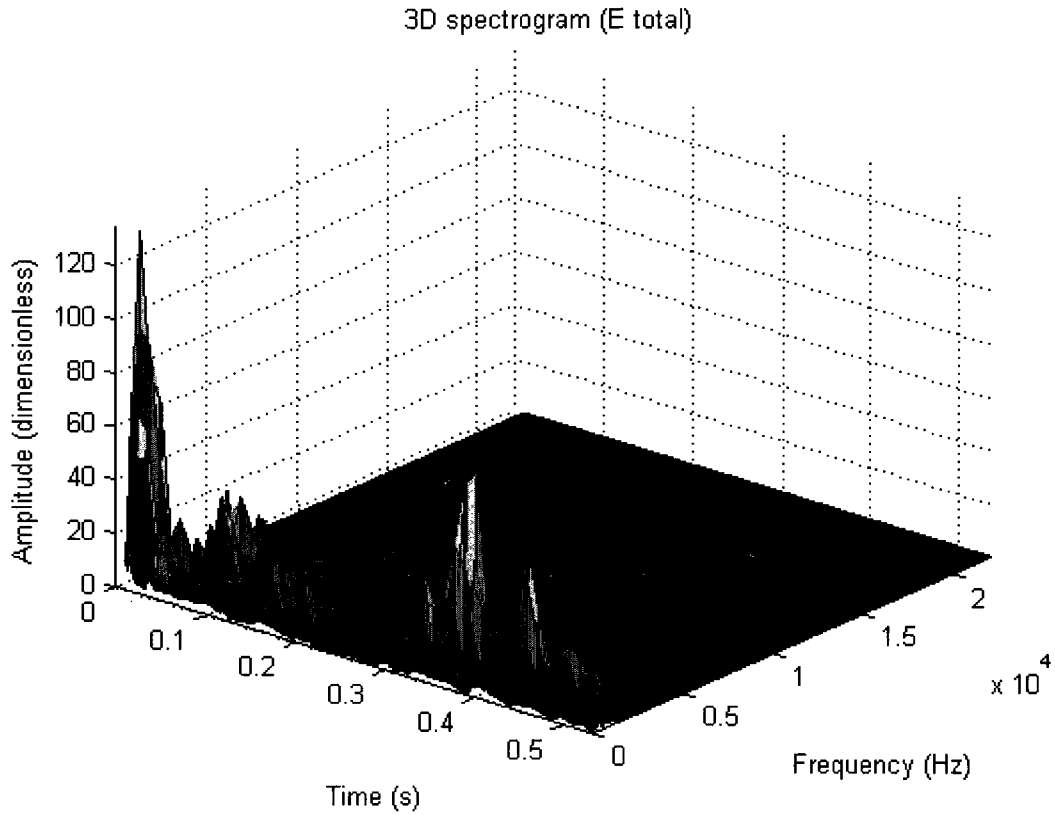


Figure 61: 3D representation of the spectrogram of the first heart beat for the signal MHV recording 3 (100 beats/min)

The 3D spectrogram display in MATLAB (Figure 61) can be rotated to show the projection on the frequency plane. This was done as shown in Figure 62 to determine the frequencies in the spectrogram.

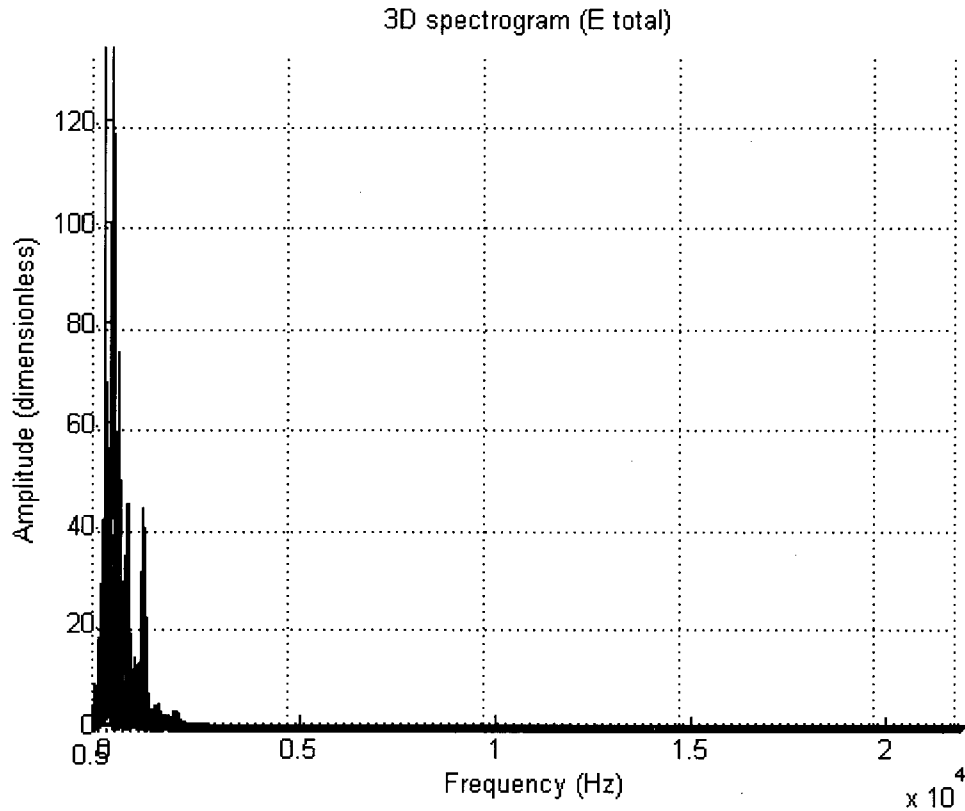


Figure 62: Rotated 3D representation of the spectrogram of the first heart beat for the signal MHV recording 3 (100 beats/min)

As observed in Figure 61 and Figure 62, no high-frequency pressure fluctuations are present under 22 kHz; therefore, no cavitation is present under 22 kHz.

The final step is to obtain the non-deterministic energy. The deterministic energy, the total energy, and the non-deterministic energy are all combined in Figure 63 for comparison purposes.

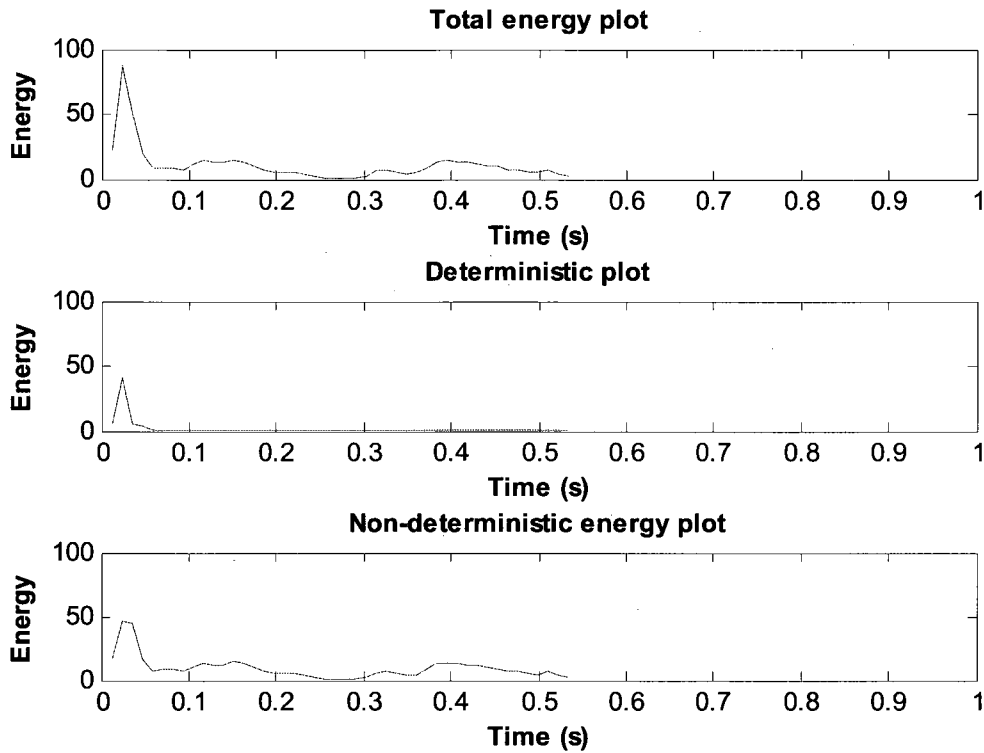


Figure 63: The time evolution of the deterministic, total, and non-deterministic energy

In the deterministic energy and total energy plots in Figure 63, the S1 peak can be clearly distinguished. The S2 peak however is not visible or barely distinguishable since the segmentation was not as successful as for the signals with 70 beats/min, and thus the S2 peaks of the heart beats in the signal were not properly lined up. This then affected the non-deterministic energy result.

The percentage of non-deterministic energy in the signal was 85.78 %. This number is higher than the number obtained with the signal MHV recording 1. This was most likely caused by the poor segmentation since the deterministic energy was lower for a higher total energy compared to the signal MHV recording 1. This resulted in a higher non-deterministic energy value. The non-deterministic energy plot in Figure 63 illustrates an S1 peak. If the heart beats were properly lined up, the S1 peak would not have

appeared in the non-deterministic energy plot. This demonstrates the importance of the segmentation algorithm and the alignment of the heart beats.

Next, the previous steps were applied on a signal recorded from a bioprosthetic heart valve for comparison purposes. Figure 64 illustrates the 3D representation of the spectrogram of the ensemble averaged heartbeat for a signal obtained during the first trial using a bioprosthetic valve of type Magna (27 mm), which was an aortic trileaflet bovine pericardial valve (Bioprosthetic valve recording 1). The recording was executed with a heart rate of 70 beats per minute. The sampling frequency used for the hydrophone signal was 44.1 kHz.

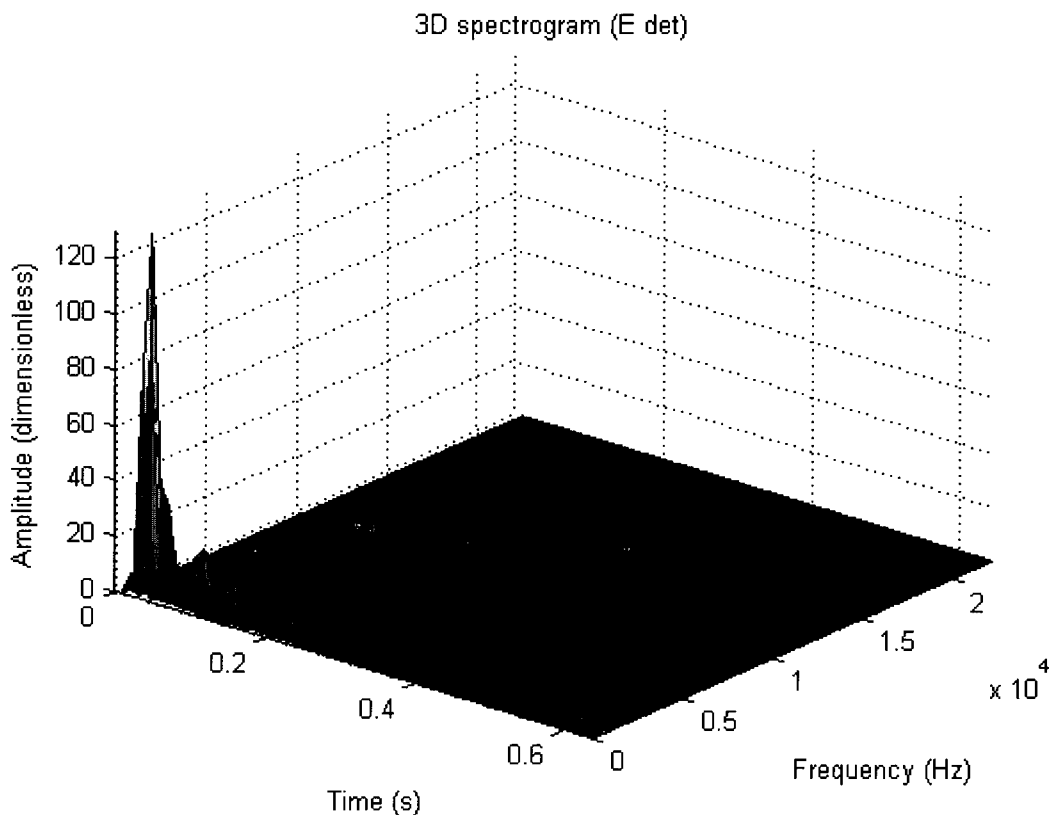


Figure 64: 3D representation of the spectrogram of the ensemble averaged heart beat for the signal Bioprosthetic valve recording 1

The 3D spectrogram display in MATLAB (Figure 64) can be rotated to show the projection on the frequency plane. This was done as shown in Figure 65 to determine the frequencies in the spectrogram.

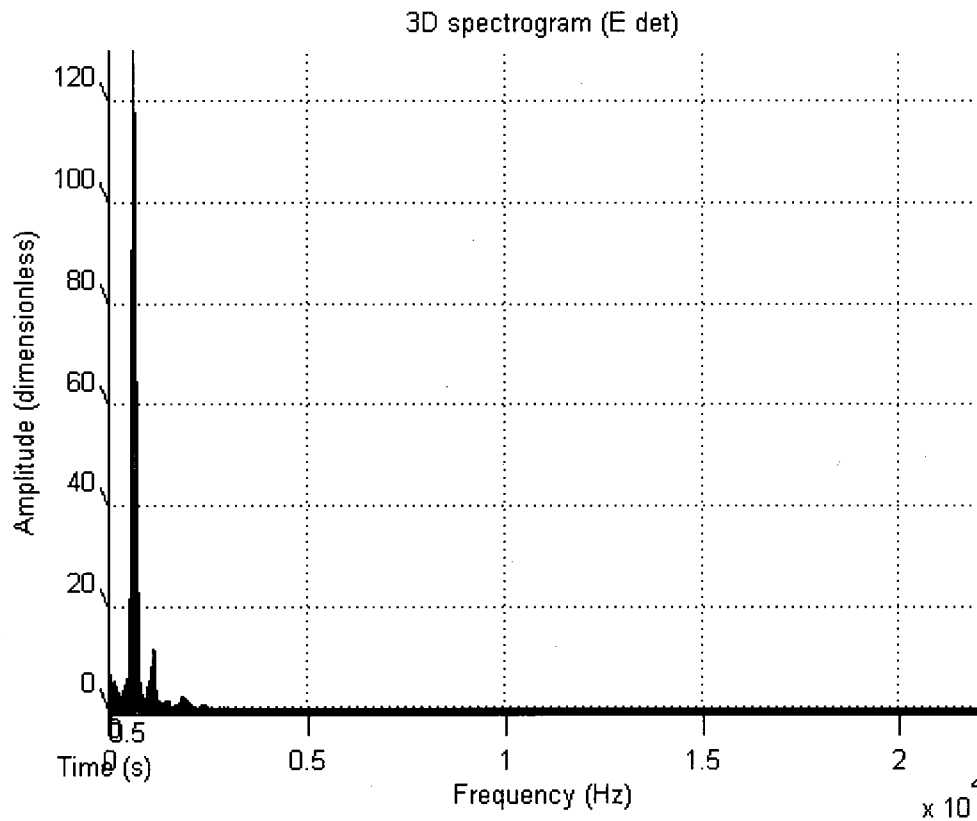


Figure 65: Rotated 3D representation of the spectrogram of the ensemble averaged heart beat for the signal Bioprosthetic valve recording

As observed in Figure 64 and Figure 65, no high-frequency pressure fluctuations are present under 22 kHz; therefore, no cavitation is present under 22 kHz.

The second step consists of obtaining the total energy. Figure 66 illustrates the 3D representation of the first of many spectrograms for a signal obtained during the first trial using a bioprosthetic valve of type Magna (27 mm), which was an aortic trileaflet bovine pericardial valve (Bioprosthetic valve recording 1).

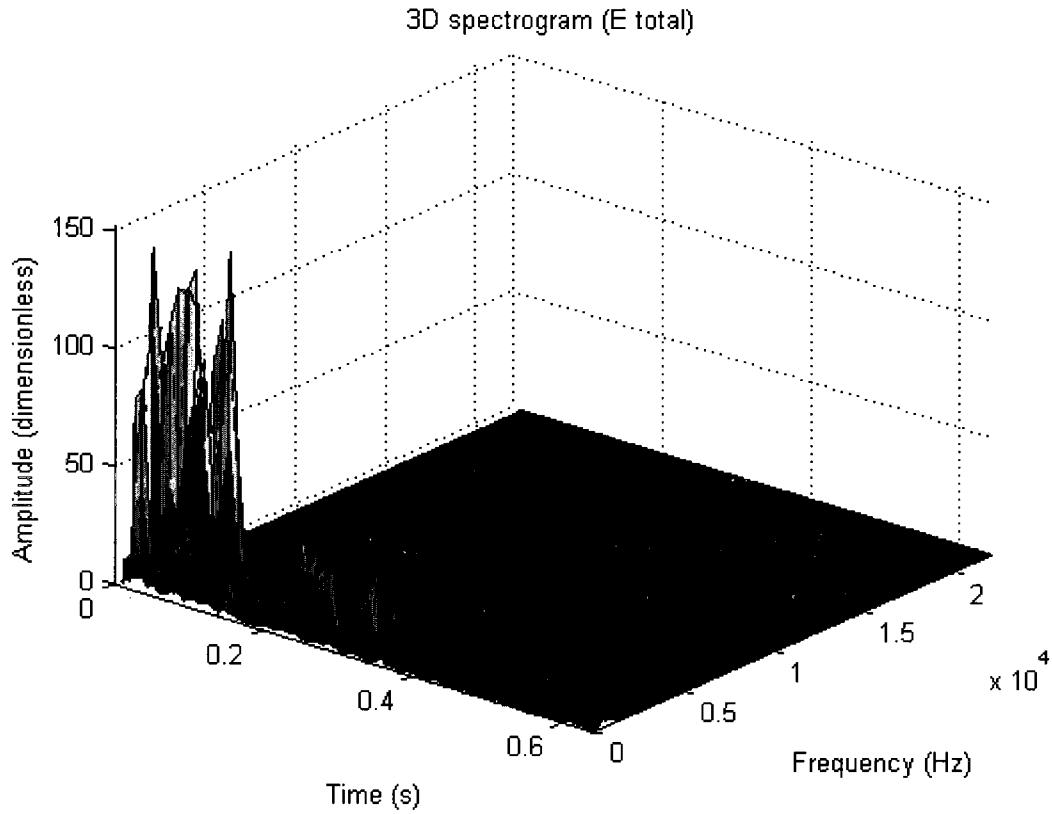


Figure 66: 3D representation of the spectrogram of the first heart beat for the signal Bioprosthetic valve recording 1

The 3D spectrogram display in MATLAB (Figure 66) can be rotated to show the projection on the frequency plane. This was done as shown in Figure 67 to determine the frequencies in the spectrogram.

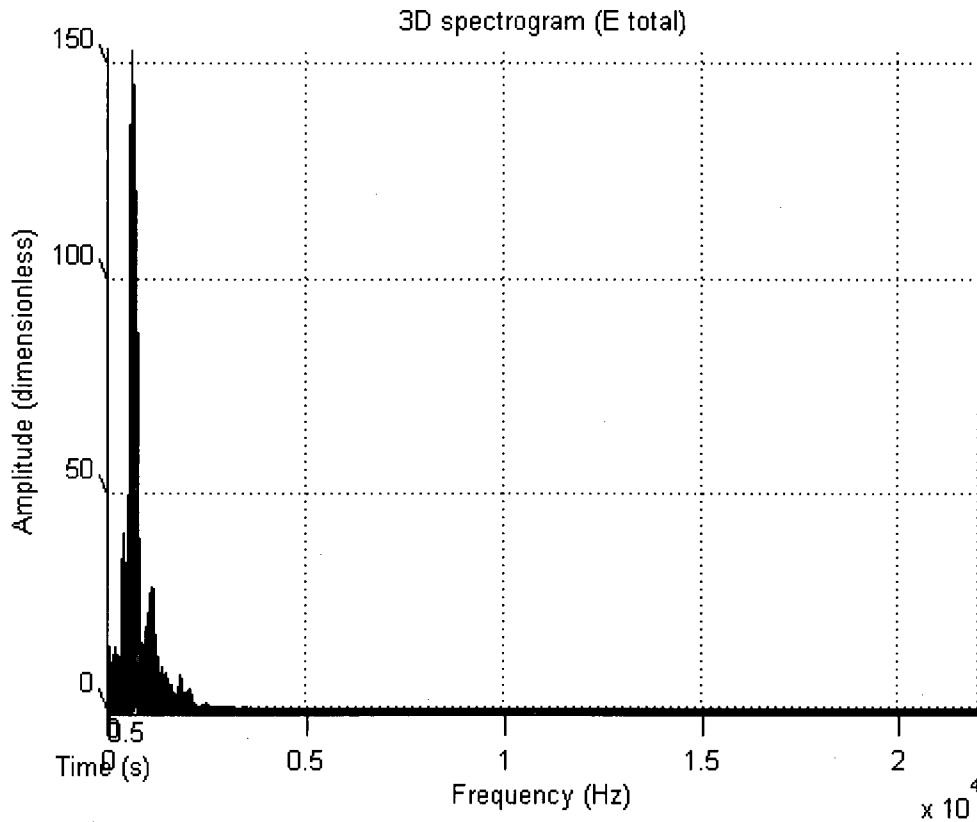


Figure 67: Rotated 3D representation of the spectrogram of the first heart beat for the signal Bioprosthetic valve recording

As observed in Figure 66 and Figure 67, no high-frequency pressure fluctuations are present under 22 kHz; therefore, no cavitation is present under 22 kHz. That result was expected since as explained in section 6.2.1, no cavitation is expected with bioprosthetic heart valves.

The final step is to obtain the non-deterministic energy. The deterministic energy, the total energy, and the non-deterministic energy are all combined in Figure 68 for comparison purposes.

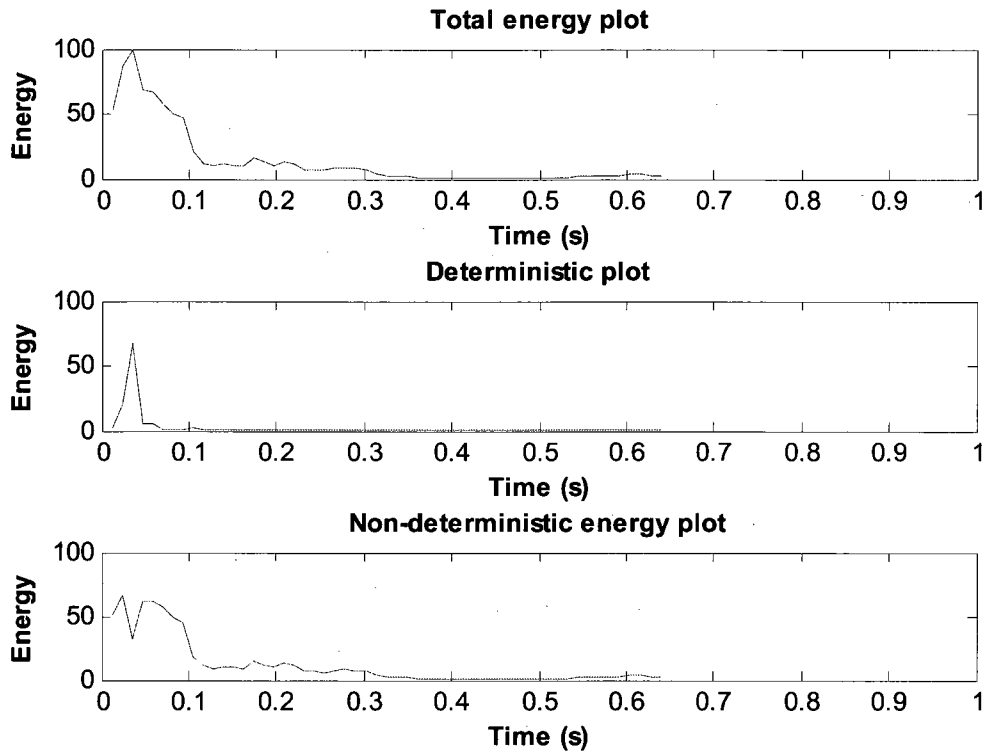


Figure 68: The time evolution of the deterministic, total, and non-deterministic energy

In the deterministic energy and total energy plots in Figure 68, the S1 peak can be clearly distinguished. The S2 peak however is not visible or barely distinguishable since the hydrophone signal was very noisy, thus making it difficult to properly align the S1 peaks. Because of the noise, there are many peaks in the S1, in the S2, and everywhere else in the signal. Therefore, the S1 maximum peak that the algorithm detected might not have been the right one, which would have affected the alignment. This affected the deterministic energy result, which in turn affected the non-deterministic energy result.

The percentage of non-deterministic energy in the signal was 85.04 %. This number is higher than the number obtained with the signal MHV recording 1. In theory, the non-deterministic energy percentage should have been smaller since as mentioned earlier in this chapter, mechanical heart valves produce cavitation but not bioprosthetic

heart valves. This was most likely due to the noise in the hydrophone signal since during recording, it was noticed that the signal was very noisy. The noise increases the non-deterministic energy since it is a random component in the signal. The noise also makes it difficult to properly segment and line up the heart beats, affecting the energy results.

The deterministic, total, and non-deterministic energy results as well as the percentage of non-deterministic energy obtained using the Short-Time Fourier Transform are summarized in Table 18 for different hydrophone signals. The details of three of these signals were presented previously in this section.

Table 18: Comparison of the energy results obtained using the STFT

Signal used	% of non-deterministic energy	Energy		
		Deterministic energy	Total energy	Non-deterministic energy
MHV recording 1 (70 beats/min)	78.51	98.52	458.40	359.88
MHV recording 2 (70 beats/min)	67.91	147.04	458.16	311.12
MHV recording 3 (100 beats/min)	85.78	70.12	493.16	423.04
Bioprosthetic valve recording 1	85.04	114.62	766.31	651.69
Bioprosthetic valve recording 2	89.50	72.30	688.85	616.55

Looking at the plots of the recorded signals as well as the results presented in this section, it was observed that the hydrophone signal was much noisier than the stethoscope signal. The new algorithm successfully detected the much greater non-

deterministic energy in the hydrophone signal, compared to the stethoscope signal, and quantified the amount of non-deterministic energy in the signal.

In order to know if the results using the STFT agree with the results using the Fourier Transform, the percentage of non-deterministic energy obtained with both methods are compared below for a few signals. Note that for the all signals in both methods, the S1 peaks were aligned and no heart beats were removed from the signal.

Table 19: Comparison of the percentage results obtained with the FT and with the STFT

Signal used	% of non-deterministic energy	
	Fourier Transform	Short-Time Fourier Transform
MHV recording 1 (70 beats/min)	77.81 %	78.51 %
MHV recording 2 (70 beats/min)	69.09 %	67.91 %
MHV recording 3 (100 beats/min)	86.64 %	85.78 %
Bioprosthetic valve recording 1	85.45 %	85.04 %
Bioprosthetic valve recording 2	89.31 %	89.50 %

As observed in Table 19, the percentage results obtained with both methods are very similar. Therefore, the Short-Time Fourier Transform can be used instead of the Fourier Transform to obtain the energy in the signal, with the additional benefit of giving insight into the temporal location in the heart beat where the energies occur.

The frequency range of the hydrophone used to make the recordings was 0.1 Hz to 180 kHz [32]. Therefore, to use the hydrophone to its full potential, a sampling frequency of at least 360 kHz would have been needed.

$$\begin{aligned}
 2 \times F_{Max} &< F_s \\
 2 \times 180 \text{kHz} &< 360 \text{kHz}
 \end{aligned}
 \tag{6.1}$$

However, the experimental data acquisition setup used was a prototype limited to 96 kHz, due to the maximum data rate of the sound card. A sampling frequency of 44.1 kHz was used to record the experimental data since no cavitation was observed experimentally. Even though the cavitation in frequencies over 22 kHz could not be observed with the 3D representation of the spectrogram, no cavitation was visually observed with the high-speed digital camera in vitro. It is highly probable that there was no cavitation present near the mechanical heart valve during the in vitro experiment. A more sophisticated and expensive data acquisition system would be required to confirm this with the spectrogram analysis. However, this research has established the validity of the segmentation algorithm and alignment method used to analyse the experimental data.

Chapter 7: Conclusions and Future Work

7.1 Conclusions

In this research, signal processing algorithms for the detection and quantification of cavitation in a heart beat signal were considered. Specifically, two algorithms presented by Johansen were chosen for further analysis as they presented the most potentially effective algorithms presented in the literature to date that had actually been implemented on biological signals acquired in vivo. In this thesis, Johansen's two algorithms were implemented and compared. A closed-form mathematical analysis of the algorithms was accomplished and a discussion of the results was done in light of the analysis. Moreover, improvements to Johansen's algorithms were proposed, such as a new segmentation algorithm, calculation of the energy in the "tails", alignment of the S1 and S2 peaks in the signal, and the implementation of the Short-Time Fourier Transform to study the time evolution of the energy in the signal. Then, to test the new improved algorithm, stethoscope and hydrophone signals were recorded in the laboratory at the University of Ottawa Heart Institute. A description of the experimental setup and experiments has been provided as well as the results obtained with the recorded signals. Many conclusions were reached in this research and are presented here.

Firstly, it can be concluded that the theory behind Johansen's algorithm is sound, and that the non-deterministic energy does indeed represent the cavitation in the signal if the heart beats are perfectly aligned and if there is no random noise in the signal. However, it is not as accurate in practice as it is in theory since many additional factors

are involved such as noise, equipment, and segmentation issues. These factors contribute to the non-deterministic energy and could impact the detection of the cavitation signal.

Additionally, it can be concluded that Johansen's algorithm is very sensitive to the alignment issues and greatly depends on the quality of the segmentation algorithm. It was demonstrated in the closed-form mathematical analysis in chapter 4 that if a heart beat is misplaced (not lined up), then the factor by which it is misplaced appears in the non-deterministic energy result meaning that the non-deterministic energy is *not* a measure of cavitation alone. Therefore, if the beats are not properly superimposed, the beats that are not lined up will have an impact on the non-deterministic energy result, which might be falsely interpreted as a greater level of cavitation in the signal.

Another conclusion reached in this research is that Johansen's 2004 algorithm is superior to Johansen's 2003 algorithm. It was demonstrated in the closed-form mathematical analysis for Johansen's 2003 algorithm that the non-deterministic energy does not represent the cavitation alone, even if the heart beats are well aligned at the beat superimposition step, and even if there is no random noise in the signal. Therefore, the result obtained with Johansen's 2003 algorithm is not a good representation of the amount of cavitation in mechanical heart valve patients. Additionally, it was found that when a signal with "tails" is used in Johansen's 2003 algorithm, the tails contribute to the non-deterministic energy and are falsely considered to be cavitation. That additional contribution from the tails to the non-deterministic energy was not present in the 2004 algorithm. Therefore, it is possible to conclude that Johansen's 2003 algorithm is less accurate and less robust than Johansen's 2004 algorithm.

From chapter 5, it can be concluded that the energy can also be calculated in the time domain, and not only in the frequency domain. This is an advantage for large signals since it can provide significant computational savings as there is no need to calculate the FFT of the entire signal to obtain the signal energy. Additionally, it can be concluded that aligning the S1 peaks and the S2 peaks after superimposition of the heart beats is an improvement to Johansen's algorithm since it reduces the amount of misplaced heart beats and, the non-deterministic energy becomes a better representation of cavitation.

Another conclusion that can be drawn is that using the Short-Time Fourier Transform improves Johansen's algorithm. The energy result obtained with the STFT is a time evolution of the energy in the signal. The STFT permits the observation of the non-deterministic energy values as they evolve across a heart beat. It is possible to see where the non-deterministic energy is located in the signal. This additional information is provided while preserving the same energy result accuracy of the algorithm that uses the Fourier Transform alone.

Additionally, it can be concluded that the new algorithm with STFT properly detects the non-deterministic energy in a signal since it detected, as seen in chapters 5 and 6, that the hydrophone signals had a higher non-deterministic energy than the stethoscope signals. This is correct since the hydrophone signals were much noisier than the stethoscope signals, and since noise is random in a signal, it is a non-deterministic component of a signal.

Another conclusion is that the heart simulator at the University of Ottawa may be more physiologically realistic than other experimental setups used in cavitation research. Of particular significance, no cavitation was observed under normal physiological

conditions with our heart simulator. Therefore, it is likely that cavitation occurs under critical conditions. This supports the in vitro observation by Graf *et al.* that almost all the investigated MHVs generated cavitation when dP/dt was well above the physiological range, and that only a few valves generated cavitation at dP/dt within the physiological range [1].

The improved algorithm that was developed in chapter 5 can be applied for more applications than just cavitation. It can be used to detect and measure any random event in a heart signal. It could be used to detect heart conditions that are characterized by a random event in the heart signal such as some cardiac arrhythmia events.

7.2 Future Work

The conclusions reached as a result of the research work performed for this thesis point to future avenues of investigation.

Future research needs to be done to investigate under which conditions the MHVs generate cavitation. In order to successfully investigate this problem, a more sophisticated data acquisition system would be required.

Additionally, it would be of interest for this research to find a better way to acquire the heart signal in vivo with the hydrophone to record a less noisy signal. This could possibly be accomplished with the addition of a medium between the hydrophone and the patient that would provide good acoustic coupling [5], or with a new low noise hydrophone design.

References

- [1] P. Johansen, "Mechanical heart valve cavitation," *Expert Review of Medical Devices*, vol. 1, pp. 95-104, 2004.
- [2] L. H. Herbertson, V. Reddy, K. B. Manning, J. P. Welz, A. A. Fontaine, and S. Deutsch, "Wavelet transforms in the analysis of mechanical heart valve cavitation," *Journal of Biomechanical Engineering*, vol. 128, pp. 217-222, 2006.
- [3] R. A. Rodriguez, M. Ruel, M. Labrosse, and T. Mesana, "Transcranial Doppler and acoustic pressure fluctuations for the assessment of cavitation and thromboembolism in patients with mechanical heart valves," *Interactive Cardiovascular and Thoracic Surgery*, vol. 7, pp. 179-183, 2008.
- [4] C. M. Zapanta, D. R. Stinebring, S. Deutsch, D. B. Geselowitz, and J. M. Tarbell, "A comparison of the cavitation potential of prosthetic heart valves based on valve closing dynamics," *Journal of Heart Valve Disease*, vol. 7, pp. 655-667, 1998.
- [5] T. S. Andersen, P. Johansen, B. O. Christensen, P. K. Paulsen, H. Nygaard, and J. M. Hasenkam, "Intraoperative and postoperative evaluation of cavitation in mechanical heart valve patients," *Annals of Thoracic Surgery*, vol. 81, pp. 34-41, 2006.
- [6] L. A. Garrison, T. C. Lamson, S. Deutsch, D. B. Geselowitz, R. P. Gaumond, and J. M. Tarbell, "An in-vitro investigation of prosthetic heart valve cavitation in blood," *Journal of Heart Valve Disease*, vol. 3, 1994.
- [7] E. U. Dexter, S. Aluri, R. R. Radcliffe, H. Zhu, D. D. Carlson, T. E. Heilman, K. B. Chandran, and W. E. Richenbacher, "In vivo demonstration of cavitation potential of a mechanical heart valve," *ASAIO Journal*, vol. 45, pp. 436-441, 1999.
- [8] C. M. Zapanta, D. R. Stinebring, D. S. Sneckenberger, S. Deutsch, D. B. Geselowitz, J. M. Tarbell, A. J. Snyder, G. Rosenberg, W. J. Weiss, W. E. Pae, and W. S. Pierce, "In vivo observation of cavitation on prosthetic heart valves," *ASAIO Journal*, vol. 42, 1996.
- [9] P. Johansen, K. B. Manning, J. M. Tarbell, A. A. Fontaine, S. Deutsch, and H. Nygaard, "A New Method for Evaluation of Cavitation Near Mechanical Heart Valves," *Journal of Biomechanical Engineering*, vol. 125, pp. 663-670, 2003.
- [10] P. Johansen, T. S. Andersen, J. M. Hasenkam, and H. Nygaard, "In-vivo prediction of cavitation near a Medtronic Hall valve," *The Journal of heart valve disease*, vol. 13, pp. 651-658, 2004.
- [11] K. Sohn, K. B. Manning, A. A. Fontaine, J. M. Tarbell, and S. Deutsch, "Acoustic and visual characteristics of cavitation induced by mechanical heart valves," *Journal of Heart Valve Disease*, vol. 14, pp. 551-558, 2005.
- [12] K. Courtemanche, V. Millette, and N. Baddour, "Heart sound segmentation based on mel-scaled wavelet transform," in *31st Conference of the Canadian Medical and Biological Engineering Society* Montreal, Quebec, Canada, 2008.

- [13] S. Chao, "Automatic Phonocardiogram Segmentation Using the Sliding Window Autocorrelation Algorithm," Ottawa, Ontario, Canada: Carleton University, 2009.
- [14] V. Millette, N. Baddour, and M. Labrosse, "Quantification of cavitation in mechanical heart valve patients," in *32nd Conference of the Canadian Medical and Biological Engineering Society* Calgary, Alberta, Canada, 2009.
- [15] A. V. Oppenheim, A. S. Willsky, and S. H. Nawab, *Signals & Systems*, 2nd ed. New Jersey: Prentice Hall, 1997.
- [16] D. Kumar, P. Carvalho, M. Antunes, P. Gil, J. Henriques, and L. Eugénio, "A new algorithm for detection of S1 and S2 heart sounds," in *ICASSP, IEEE International Conference on Acoustics, Speech and Signal Processing - Proceedings*, Toulouse, 2006.
- [17] P. Wang, Y. Kim, L. H. Ling, and C. B. Soh, "First heart sound detection for phonocardiogram segmentation," in *Annual International Conference of the IEEE Engineering in Medicine and Biology - Proceedings*, Shanghai, 2005, pp. 5519-5522.
- [18] H. Liang, H. Liang, S. Lukkarinen, and I. Hartimo, "Heart sound segmentation algorithm based on heart sound envelopogram," in *Computers in Cardiology 1997*, 1997, pp. 105-108.
- [19] P. Wang, Y. Kim, and C. B. Soh, "Feature extraction based on mel-scaled wavelet transform for heart sound analysis," in *Annual International Conference of the IEEE Engineering in Medicine and Biology - Proceedings*, Shanghai, 2005, pp. 7572-7575.
- [20] Wikipedia, "Discrete Fourier Transform," http://en.wikipedia.org/wiki/Discrete_Fourier_transform, 2009.
- [21] S. Braun, *Discover Signal Processing: An interactive guide for engineers*. Chichester: John Wiley & Sons, 2008.
- [22] R. M. Rangayyan, *Biomedical Signal Analysis: A Case-Study Approach*. New York: IEEE Press, Wiley-Interscience, 2002.
- [23] MathWorks, "MATLAB Help," 2006.
- [24] M. A. Lzeik, "Left-Heart Simulator and Patient-Prosthesis Mismatch," University of Ottawa, Ottawa, Ontario December 2007.
- [25] "ViVitro Model Left Heart," Victoria, British Columbia: ViVitro Labs Inc., http://www.vivitrolabs.com/ViVitro_ProductsMLH.html, 2009.
- [26] W. Kapit, R. I. Macey, and E. Meisami, *The physiology coloring book*, 2nd ed. San Francisco: Addison Wesley Longman, 2000.
- [27] J. G. Webster, *Medical Instrumentation: Application and Design*, 3rd ed. New Jersey: John Wiley & Sons, 1998.
- [28] S. Parker, *The Human Body Book*. New York: Dorling Kindersley, 2007.
- [29] "Stroboscope," in *The New Encyclopædia Britannica*, 15th ed. vol. 11 Chicago, 1990.
- [30] K. B. Chandran and S. Aluri, "Mechanical valve closing dynamics: Relationship between velocity of closing, pressure transients, and cavitation initiation," *Annals of Biomedical Engineering*, vol. 25, pp. 926-938, 1997.

- [31] C. S. Lee, K. B. Chandran, and L. D. Chen, "Cavitation dynamics of Medtronic Hall mechanical heart valve prosthesis: Fluid squeezing effect," *Journal of Biomechanical Engineering*, vol. 118, pp. 97-105, 1996.
- [32] "Brüel & Kjaer 8103 Miniature Hydrophone with integral 6m cable terminated 10-32UNF microdot plug," Nærum, <http://www.bksv.com/Products/TransducersConditioning/AcousticTransducers/Hydrophones/8103.aspx>, 2009.

Appendix A: Conference paper

K. Courtemanche, V. Millette, and N. Baddour, “Heart sound segmentation based on mel-scaled wavelet transform,” in *31st Conference of the Canadian Medical and Biological Engineering Society*, Montreal, Québec, Canada, 2008.

HEART SOUND SEGMENTATION BASED ON MEL-SCALED WAVELET TRANSFORM

Karim Courtemanche¹, Véronique Millette², Natalie Baddour²

¹*Faculty of Science, McGill University*

²*Department of Mechanical Engineering, University of Ottawa*

ABSTRACT

The identification and segmentation of heart beats in a phonocardiogram signal is of great interest, with applications ranging from diagnosis to use as a timing source. This paper proposes a new algorithm for the identification of the first and second (S1 and S2) heart sounds and for segmentation of the signal. The proposed algorithm is a novel combination of documented techniques, leading to improved segmentation accuracy. The Shannon Energy is first used to find sounds of interest. The algorithm subsequently uses the Mel-Scaled Wavelet Transform (MSWT) which is a modified Mel-Frequency Cepstral Coefficient (MFCC) algorithm with the Discrete Wavelet Transform (DWT) in order to reduce the impact of noise on the coefficients. The coefficients and sounds of interest are used to distinguish S1 from S2 and segment the signal accordingly. The algorithm is tested on real signals and is compared to a simpler Shannon Energy algorithm and to a traditional MFCC based algorithm. The new algorithm presents an improvement in accuracy especially when signals contain noise. It is therefore less susceptible to outside interference and could be used more accurately in a hospital setting.

INTRODUCTION

Auscultation is a valuable method for the detection of many heart disorders and dysfunctions. There are other diagnostic methods available such as the electrocardiogram (ECG), the echocardiogram and the ultrasound, but heart sound auscultation is the most common one due to its low cost and non-invasive ability to provide information concerning the heart valves and hemodynamics of the heart. The phonocardiogram (PCG) is a recording of the heart sounds and murmurs. It contains the first and second (S1 and S2) sound components associated with the closure of the valves during systole and diastole, as well as any abnormal components. The segmentation of the heart beats in a phonocardiogram is done prior to the analysis of the heart sounds for diagnostic purposes [1-3]. Many different methods of heart sound segmentation and identification have been introduced

in the past using techniques such as the wavelet transform [2-4], Shannon energy [1-9], mel-frequency cepstral coefficients (MFCC) [1, 3, 9, 10], and the mel-scaled wavelet transform (MSWT) [10].

The time-domain and frequency-domain features alone were found to be insufficient since the heart sound signals contain non-stationary characteristics. Therefore, the wavelet transform, a time-frequency representation technique, has been proposed to characterize recorded heart sounds, providing information on the time-frequency content of the phonocardiogram during the whole cardiac cycle [10, 11]. The wavelet transform eliminates high frequency noise, but can make false detection for noises overlapping in frequency. Consequently, as an attempt to reduce the false detections, a method combining the wavelet transform and Shannon energy has been proposed to locate the fundamental heart sound lobes which are computed from the low frequency components of the signal [2, 3].

To identify these heart sound components, many authors have proposed a different method based on mel-frequency cepstral coefficient (MFCC). To extract the features from the phonocardiogram signal, MFCC is used, giving good results for clean heart sounds. However, since it is sensitive to the recording frequency response, its performance is not as good in a noisy environment. Therefore, P. Wang *et al.* have proposed to replace the MFCC by the mel-scaled wavelet transform (MSWT) which applies the wavelet transform to the mel spectrum of the phonocardiogram [10]. Their suggested method has produced encouraging results compared with those obtained using the MFCC.

In this paper, the proposed approach is based on using the wavelet transform and Shannon energy techniques mentioned previously in combination with the heart rate estimates from Shannon energy to identify the first heart sound component S1.

In addition, to confirm the S1 results, the combination of MSWT and k-means clustering is executed on the original signal to extract and classify these heart sound components. Finally, the results obtained using these two methods are compared.

METHODOLOGY

Identification of Sounds of Interest (SOI)

It has been suggested in [2] that the PCG signal $S(n)$ can be modeled as

$$S(n) = F(n) + O(n) = F(n) + C(n) + N(n), \quad (1)$$

where $F(n)$ represents the fundamental components of the heart sounds S1 and S2 (SOI), and $O(n)$ represents other sounds which can be decomposed into $C(n)$, other heart sound components (such as murmurs, etc) and $N(n)$, the noise component.

The first step consists in isolating $F(n)$ by running the signal through an adaptive sublevel tracking module [2]. This module is based on a reiterative process involving wavelet filtering. The 4th order Daubechies wavelet (db4) is used with 7 levels of decomposition. The approximation and detail coefficients are passed through an adaptive threshold. The threshold in the j -level during the k th iteration is defined as

$$Th_{j,k} = |Mean_{j,k}| + f_{j,k} \cdot Std_{j,k}, \quad (2)$$

where $Mean_{j,k}$ is the mean value of the coefficients, $f_{j,k}$ is an adjustment factor which is varied between 2 and 3, and $Std_{j,k}$ is the standard deviation of the coefficients for a given level and iteration.

The larger signals (coefficients $> Th_{j,k}$) are kept as part of the SOI and the lower signals (coefficients $< Th_{j,k}$) are passed through the wavelet transform again. The minimum likelihood method is used to adjust the stopping criterion S_p .

$$S_p = \left| \frac{E(O_k^2) - E(O_{k-1}^2)}{E(O_k^2)} \right|, \quad (3)$$

where $E(O_k^2)$ is the expected value of square other signal set $O(n)$ at iteration k and $E(O_{k-1}^2)$ denotes the expected value at iteration $k-1$.

To extract the envelope of the signal, the Shannon energy is calculated according to

$$E_s = \frac{-1}{N} \sum_{i=1}^N H_{norm}^2(i) \cdot \log H_{norm}^2(i), \quad (4)$$

where,

$$H_{norm} = F(n) / \max(F(n)), \quad (5)$$

and N is the length of the selected window. This energy calculation emphasizes medium energy components and attenuates low intensity signals compared to high intensity signals [7]. The Shannon energy is calculated by using a 20ms window with a 10ms segment overlap. The significant sounds are then found through the zero crossing points of the normalized Shannon energy

$$E_{s_{norm}} = E_s - \langle E_s \rangle, \quad (6)$$

where $\langle \rangle$ represents the mean operator.

The second stage is the identification of SOI based on physiologically inspired properties. To validate the peaks in energy that are found we observe the following properties: sound lobe duration, time interval between sound lobes and the peak energy of the sound lobes. The following criterions are used to identify S1 and S2 [3].

- 1) All sound lobes have to be between 30ms and 250ms. This is valid for both healthy and cardiac patients. Any sound lobes outside of this range are discarded for further processing.
- 2) If the time interval between two sounds is smaller than 50ms, it is determined that the sound has been split. The sound with the greatest energy is kept for further processing and the other is discarded.
- 3) For auscultation done at the apex (5th intercostal space), the energy and length (time duration) of S1 is generally greater than S2. For auscultation in the aortic or pulmonary area the energy of S2 is greater than S1.

A final processing step in the preparation of segmentation is the utilization of the approximate heart rate of the patient to determine expected time intervals. The FFT of the Shannon energy is calculated and filtered using a low-pass filter. The peak frequency of this spectrum provides a useful approximation of the patient's heart rate. Based on this information and an error margin of $\pm 20\%$, the interval between S1 sounds is verified and errors due to missing S2 sounds are eliminated or reduced.

The sounds of interest are then compared based on the approximate heart rate intervals, peak energy and expected S1-S2-S1 pattern and identified for segmentation.

Mel-Scaled Wavelet Transform Validation

The mel-scaled cepstral coefficients (MFCC) are readily used in the voice identification field. The mel-scale provides a scaling of the frequency spectrum similar to the human ear's response. Coefficients are then extracted with a mel-scaled filter bank and used to characterize the sound. The dimensionality of the data is reduced by the use of the discrete cosine transform (DCT).

Wang et al. [10] have proposed a mel-scaled wavelet transform (MSWT) that serves the same purpose as the MFCC but helps reduce the impact of noise on the coefficients.

In order to provide a validation of the segmentation results obtained in the first part of the algorithm, the MSWT was implemented and k-means clustering on the coefficients was used to separate S1 from S2 sounds. This information, combined with the results of the first algorithm, results in a more accurate ultimate determination of S1 and S2 and segmentation of the PCG.

The MSWT is implemented by first blocking and windowing the data with a Hamming window. The FFT of each windowed section is then taken and multiplied by the mel-scaled filterbank. The discrete wavelet transform (DWT) is then used to reduce the dimensionality of the data.

The coefficients for each sound lobe identified in the first part of the algorithm are then summed to give a single set of coefficients for each sound of interest. K-means clustering then separates the sounds of interest into two groups by minimizing the Euclidian distance between each set of coefficients and two centroids. This results in a group of S1 sounds and a group of S2 sounds. The results from this step are used to validate the results from the first part of the algorithm.

RESULTS AND DISCUSSION

Testing method

PCG recordings were done at the 5th intercostal spacing on non-cardiac patients as this was deemed the position providing the most precise information for segmentation purposes. These were done at 44.1 kHz sampling rate. Pre-recorded pathological heart sounds were also used to further test the robustness of the algorithm to different pathologies. The results of the segmentation algorithm were then compared to the manually segmented data.

Preliminary results of the MFCC and MSWT algorithms were compared. The k-means clustering

technique for differentiating between S1 and S2 sounds was used on the MFCC and MSWT results.

Results

Results of S1 identification for the first part of the algorithm (without MSWT or MFCC) were generally successful as can be seen in Table 1.

Table 1: Statistical Results of S1 Identification from SOI

Samples	Correct S1 / Correct Other	False Positive	False Negative	Specificity/ Sensitivity
11 Samples (7 healthy, 4 pathological)	202 / 206	31	33	86.9% / 86.0%

A single pre-recorded example of a mitral regurgitation case significantly lowered the sensitivity and specificity. In this case, S2 sounds were identified as S1 because this pathology makes the S2 sounds longer and more energetic than S1 sounds. This accounts for 27 of the 31 false positives and 29 of the 33 false negatives. Without this sample, sensitivity and specificity are both 98.1%. However, the MSWT correctly identified the S1 and S2 sounds of this particular case. Thus, with the use of the MSWT S1 validation step, this error would have been accurately corrected. In this same case, replacing the MSWT algorithm with the traditional MFCC still provides errors and is thus not useful in correcting the first algorithm.

In figures 1 and 2 below, we can clearly see the attenuating effect of the MSWT on the noise peak located between 1.9 s and 2.1 s when compared to the MFCC. It can also clearly be seen from these figures that for the MSWT, all characteristics provide information about each sound lobe. However, with the MFCC, only one of the characteristics (the blue line in figure 2) provides information about the sound lobes. The other characteristics of the MFCC are similar for all parts of the sound and characterize heavily the noise components of the signal. This provides clear indication of the interest in the MSWT validation step which clearly reduces the impact of noise on the coefficients.

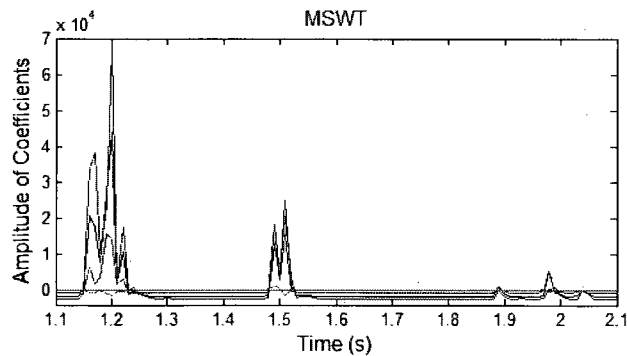


Figure 1: MSWT for single heart beat

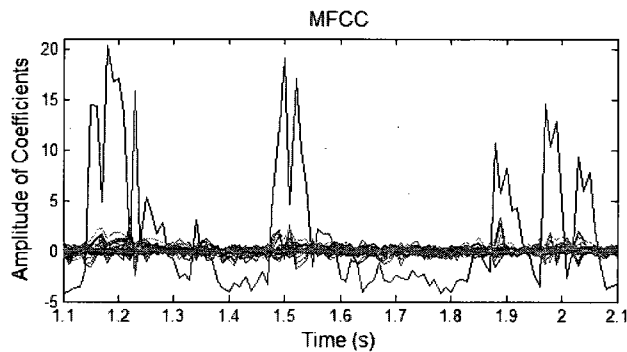


Figure 2: MFCC for single heart beat.

In only one of the samples was the MFCC method slightly more accurate than the MSWT. In 7 of the 11 samples, the MSWT was 100% correct in its distinction of S1 and S2 sounds. This shows that the MSWT is indeed more useful in distinguishing S1 from other sounds than the MFCC in most real life cases such as these where conditions are often not perfect and noise and artifacts do exist.

CONCLUSION

This article proposed the use of an adaptive threshold wavelet transform filtering technique used with Shannon energy, physiological factors and heart rate approximation to properly identify S1 sounds and segment the PCG. However, this method can still present some errors when faced with complex signals. Therefore, the addition of an MSWT validation step was proposed. Preliminary results indicate that the MSWT is less prone to noise than the MFCC and can distinguish S1 sounds from others when faced with complex signals. Future implementation of more robust clustering techniques such as various neural networks have the potential of making the use of the MSWT validation a successful technique to improve accuracy of S1 detection and PCG segmentation.

REFERENCES

- [1] S. Chauhan, P. Wang, C. Sing Lim, and V. Anantharaman, "A computer-aided MFCC-based HMM system for automatic auscultation," *Computers in Biology and Medicine*, vol. 38, pp. 221-233, 2008.
- [2] P. Wang, Y. Kim, L. H. Ling, and C. B. Soh, "First heart sound detection for phonocardiogram segmentation," in *Annual International Conference of the IEEE Engineering in Medicine and Biology - Proceedings*, Shanghai, 2005, pp. 5519-5522.
- [3] D. Kumar, P. Carvalho, M. Antunes, P. Gil, J. Henriques, and L. Eugénio, "A new algorithm for detection of S1 and S2 heart sounds," in *ICASSP, IEEE International Conference on Acoustics, Speech and Signal Processing - Proceedings*, Toulouse, 2006.
- [4] H. Nazeran, "Wavelet-based segmentation and feature extraction of heart sounds for intelligent PDA-based phonocardiography," 2007.
- [5] S. Choi and Z. Jiang, "Comparison of envelope extraction algorithms for cardiac sound signal segmentation," *Expert Systems with Applications*, vol. 34, pp. 1056-1069, 2008.
- [6] D. Kumar, P. Carvalho, M. Antunes, J. Henriques, L. Eugénio, R. Schmidt, and J. Habetha, "Detection of S1 and S2 heart sounds by high frequency signatures," in *Annual International Conference of the IEEE Engineering in Medicine and Biology - Proceedings*, New York, NY, 2006, pp. 1410-1416.
- [7] H. Liang, H. Liang, S. Lukkarinen, and I. Hartimo, "Heart sound segmentation algorithm based on heart sound envelopogram," in *Computers in Cardiology 1997*, 1997, pp. 105-108.
- [8] A. D. Ricke, R. J. Povinelli, and M. T. Johnson, "Automatic segmentation of heart sound signals using hidden Markov models," in *Computers in Cardiology*, Lyon, 2005, pp. 953-956.
- [9] P. Wang, C. S. Lim, S. Chauhan, J. Y. A. Foo, and V. Anantharaman, "Phonocardiographic signal analysis method using a modified hidden Markov model," *Annals of Biomedical Engineering*, vol. 35, pp. 367-374, 2007.
- [10] P. Wang, Y. Kim, and C. B. Soh, "Feature extraction based on mel-scaled wavelet transform for heart sound analysis," in *Annual International Conference of the IEEE Engineering in Medicine and Biology - Proceedings*, Shanghai, 2005, pp. 7572-7575.
- [11] L. G. Durand and P. Pibarot, "Digital signal processing of the phonocardiogram: Review of the most recent advancements," *Critical Reviews in Biomedical Engineering*, vol. 23, pp. 163-219, 1995.